KINEMATICS AND MECHANICS OF FAST-STARTS OF RAINBOW TROUT *Oncorhynchus mykiss* AND NORTHERN PIKE *Esox lucius*

by

DAVID GORDON HARPER

B.Sc., University of British Columbia, 1983

A THESIS SUBMITTED IN PARTIAL FULFILLMENT OF

THE REQUIREMENTS FOR THE DEGREE OF

DOCTOR OF PHILOSOPHY

in

THE FACULTY OF GRADUATE STUDIES

Department of Zoology

We accept this thesis as conforming

to the required standard

THE UNIVERSITY OF BRITISH COLUMBIA

May, 1990

08

In presenting this thesis in partial fulfilment of the requirements for an advanced degree at the University of British Columbia, I agree that the Library shall make it freely available for reference and study. I further agree that permission for extensive copying of this thesis for scholarly purposes may be granted by the head of my department or by his or her representatives. It is understood that copying or publication of this thesis for financial gain shall not be allowed without my written permission.

Department of Zoology

The University of British Columbia
Vancouver, Canada

Date 12 JANUARY 1991

ABSTRACT

Film is commonly used to estimate the fast-start performance of fish. An analysis of hypothetical, film-derived, and accelerometer-measured acceleration-time data of fish fast-starts indicates that the total error in film studies is the sum of the sampling frequency error (i.e., the error due to over-smoothing at low film speeds) and measurement error. The error in film based studies on the acceleration performance of fish is estimated to be about 33 to 100% of the maximum acceleration, suggesting that other methods of estimating acceleration should be employed.

The escape performance of rainbow trout *Oncorhynchus mykiss* and northern pike *Esox lucius* (mean lengths 0.32 m and 0.38 m, respectively) were measured here with subcutaneously implanted accelerometers. Acceleration-time plots reveal two types of escape fast-starts for trout and three for pike. Simultaneous high-speed ciné films demonstrate a kinematic basis for these differences. Trout performing *C*-shaped fast-starts produce a unimodal acceleration-time plot (type I), while during *S*-shaped fast-starts a bimodal acceleration-time plot (type II) results. Pike also exhibit similar type I and II fast-starts, but also execute a second *S*-shaped fast-start that does not involve a net change of direction. This is characterized by a trimodal acceleration-time plot (type III).

Intraspecific and interspecific comparisons of displacement, time, mean and maximum velocity, and mean and maximum acceleration rate indicate that fast-start performance is significantly higher for pike than for trout, for all performance parameters. This indicates that performance is related to body form. Overall mean maximum acceleration rates for pike were 120.2 ± 20 m s^{-2} ($x \pm 2$S.E.) and 59.7 ± 8.3 m s^{-2} for trout.

Performance values directly measured from the accelerometers exceed those previously reported. Maximum acceleration rates for single events reach 97.8 m s^{-2} and 244.9 m s^{-2} for trout and pike, respectively. Maximum final velocities of 7.06 m s^{-1} (18.95 L s^{-1}, where L is body length) were observed for pike and 4.19 m s^{-1} (13.09 L s^{-1}) for trout; overall mean maximum velocities were 2.77 m s^{-1} for trout and 3.97 m s^{-1} for pike.

The fast-start performance of pike during prey capture was also measured with subcutaneously implanted accelerometers. Acceleration-time plots and simultaneous high-speed ciné films reveal four behaviours with characteristic kinematics and mechanics. As for the escape data, fast-start types are identified by the number of large peaks that appear in the acceleration-time and velocity-time data.

Comparisons of mean performance were made between each type of feeding fast-start. Type I fast-starts were of significantly (i.e., $p < 0.05$) shorter duration (0.084 s) and displacement (0.132 m) than type III (0.148 s and 0.235 m) and type IV (0.189 s and 0.307 m) behaviours, and higher mean and maximum acceleration (38.6 and 130.3 m s^{-2}, respectively) than the type II (26.6 and 95.8 m s^{-2}), type III (22.0 and 91.2 m s^{-2}), and type IV (18.0 and 66.6 m s^{-2}) behaviours. The type II behaviours were also of shorter duration and displacement, and of higher mean acceleration than type IV fast-starts, and were of significantly shorter duration than the type III behaviours.

Prey capture performance was compared to escapes by the same individuals. When data are combined, regardless of mechanical type, mean acceleration (37.6 versus 25.5 m s^{-2}), maximum acceleration (120.2 versus 95.9 m s^{-2}), mean velocity (1.90 versus 1.57 m s^{-1}), and maximum velocity (3.97 versus 3.09 m s^{-1}) were larger, and duration shorter (0.108 versus 0.133 s) during escapes than during prey capture. No differences were found

through independent comparisons of the performance of feeding and escape types II and III, but type I escapes had significantly higher mean velocity (2.27 versus 1.58 m s^{-1}), maximum velocity (4.70 versus 3.12 m s^{-1}), and mean acceleration (54.7 versus 38.6 m s^{-2}) than the type I feeding behaviours.

Prey capture performance was also related to prey size, apparent prey size (defined as the angular size of the prey on the pike's retina), and strike distance (the distance from the pike to the prey at the onset of the fast-start). Mean and maximum acceleration increased with apparent size and decreased with strike distance, while the duration of the event increased with strike distance and decreased with apparent size. No relation was found between the actual prey size and any performance parameter.

Strike distance ranged from 0.087 to 0.439 m, and decreased as the apparent size increased from 2.6 to 9.9° (r^2 = 0.75). The type I behaviour was usually employed when the strike distance was small and the prey appeared large. As strike distance increased and apparent size decreased, there was a progressive selection of type II, then III, then IV behaviours.

TABLE OF CONTENTS

LIST OF TABLES

LIST OF FIGURES

AKNOWLEDGEMENTS

This study could not have been completed without the advice and support of many people. First, I would like to thank my father, Charles M. M. Harper, for providing unconditional moral, and personal financial support. I would like to thank my wife, Janis, for the love and patience she provided during the final stages of this work. Academically, there are several people who deserve my gratitude, in particular Dr. Boye Ahlborn and Dr. Tom Daniel, for their advice on earlier drafts of various chapters. Finally I would like to express my sincere thanks to Bob Blake. His guidance, support, wisdom, and sense of humour were an inspiration throughout. I am fortunate to have him as an academic advisor and friend.

Life is not without its misfortunes. During this study my Uncle Reg, a second father really, and Mike Serink, a dear friend, passed away. This work is dedicated to them.

CHAPTER 1

Introduction

Fish swimming can be grouped into three broad catagories based on the hydrodynamics and kinematics of their movements: steady forward swimming, unsteady swimming, and median and paired fin swimming (Blake, 1983). Fish use unsteady movements during high-speed turns and when executing fast-starts (sudden, high-energy, bursts of swimming activity, initiated from a still position). Fast-starts are of great biological importance because they are employed by most fish when escaping life-threatening situations, and by some fish as a means of attaining prey. Fish that do not execute fast-starts depend on other mechanisms (armour, spines, poisons, camouflage, etc.) of protection. This work assesses the methods used in previous studies to estimate the performance of fish during fast-starts, and employs miniature accelerometers in an investigation of the fast-start performance of trout and pike during feeding and escapes.

Early studies on fish fast-starts (Gero, 1952; Gray, 1953; Hertel, 1966; Fierstine and Walters, 1968; Weihs, 1973) qualitatively investigated kinematics and reported maximum acceleration rates of 40-50 m s^{-2}. Webb (1975) suggested that to evaluate fast-start performance properly, data for the duration of the event, mean and maximum accelerations, mean and maximum velocities, and the distance covered must all be reported. Since then, several studies (Eaton *et al.* 1977, 1988; Webb, 1978*a*,*b*,; Webb and Skadsen, 1980) have suggested that displacement alone is adequate to evaluate fast-start performance. However, some models estimating thrust and

energetics during fast-starts incorporate performance variables other than displacement (e.g., Weihs, 1973; Lighthill, 1975; Harper and Blake, 1988, Appendix).

High-speed cinematography is often employed in studies on fish swimming, particularly where performance is estimated (e.g., Wardle, 1975; Eaton *et al.* 1977; Webb, 1978*b*; Dorn *et al.* 1979; Videler, 1981). One commonly reported aspect of performance is the acceleration of fish during fast-starts (Weihs, 1973; Webb, 1975, 1976, 1977, 1978*a*,*b*, 1982, 1983, 1986; Rand and Lauder, 1981). Chapter 3 is a critical examination of the use of cinematography to estimate the maximum acceleration of fish during fast-starts.

High-speed (200-250 Hz) cinematography has also been employed to evaluate more specific aspects of fast-starts, such as predator and prey latency periods (Webb, 1984; Eaton *et al.* 1977, respectively) and the effects of size, median fin amputation, temperature, and body form on escape performance (Webb, 1976, 1977, 1978*a*,*b*, respectively). Rand and Lauder (1981), employing the same methodology, correlated feeding and locomotor behaviour, while Webb and Corolla (1981) investigated the burst swimming performance of larvae. All of these assume that film-derived estimates of performance are accurate.

When using film, accelerations must be derived from the distance-time data provided. This is accomplished by employing statistical methods that generate the second differential of distance with respect to time. In earlier studies, Webb (1975, 1976) differentiated the empirical equation derived from a simple linear regression, calculated for the distance-time data. Later studies (Webb, 1977, 1978*a*,*b*, 1982) employed a more sophisticated five point moving regression method (described in Chapter 3)

which was found to have significantly greater accuracy (Webb, 1977). This method provides instantaneous accelerations as opposed to averages, allowing for the peak performance during fast-starts to be reported as maximum acceleration.

The error involved in performing the differentiations has not been quantitatively analyzed. Webb (1975) argued that the error in calculating instantaneous accelerations as well as the over-smoothing error (the tendency for successive differentiations to smooth high frequency variations in acceleration) were small when the simple linear regression method was employed. As stated previously, this method was later abandoned for a more accurate one (Webb, 1977), and no further reference to the error inherent in film analysis was made.

Two independent sources of error are inherent in film analyses; that involved in measuring the distance moved from frame to frame and that related to the sampling frequency, in this case, film speed. The effects of each are summed to determine total error. Other sources of error, such as the condition of the fish, and the temperature and salinity of the water, have been suggested (Blaxter, 1969). These are deemed easily controllable and are not considered here.

Films provide accurate distance-time data, but instantaneous acceleration is highly dependent on framing rate. All accelerations derived from film assume that acceleration is piecewise constant in time (Rayner and Aldridge, 1985). This averaging, or over-smoothing, is referred to in Chapter 3 as sampling frequency error (SFE). As the interval between frames lessens, so does the difference between frame-averaged and actual instantaneous accelerations. This results in a lower SFE. The exact relation between film speed and SFE has not been previously reported; however, some

problems arising from low sampling rates have been identified (Eaton *et al.* 1977).

The error involved in measuring the frame to frame displacement is referred to, in Chapter 3, as measurement error (ME). The accuracy with which images on a screen can be transmitted to digital information will vary with the type of imaging system used and from person to person. The error should, however, remain relatively constant for the same individual using the same system. ME is also affected by other forms of distortion, such as image blurring and parallax. Though these sources of error can be significant, they were found here to be relatively small, and for the purposes of this analysis will be considered to be minimal.

In Chapter 3, I consider the practical limits of using cinematography to estimate accelerations during fast-starts of fish, and determine the sampling frequency and measurement error inherent in the procedure. This is addressed by using hypothetical acceleration-time data, and the simultaneous use of high-speed cinematography and subcutaneous accelerometers.

Few investigations have employed methodologies other than film analysis to study fast-start performance. DuBois *et al.* (1976) inserted a biaxial accelerometer into the stomach of a bluefish, *Pomatomus saltatrix*, and measured escape accelerations. Unfortunately they did not consider the location of their accelerometer relative to the combined centre of mass of the fish and accelerometer. In addition, the fish was "scared" shortly (5-20 min) after previous bouts of steady and unsteady activity, so it was probably performing sub-maximally.

Other studies on fast-starts include an investigation of caudal fin strains during escapes, using rosette strain guages (Lauder, 1982), and studies on the reticulospinal command mechanisms involved in escape

behaviour in fish (Eaton *et al.* 1984, 1988). None of these evaluated swimming performance.

In Chapter 4, the escape performances of trout and pike are determined by accelerometry and cinematography. Two species of fish, with different body forms, are observed to test the hypothesis that mean and maximum accelerations during fast-starts are independent of body form (Webb, 1978*b*). The northern pike *Esox lucius* is chosen because, in theory, it is morphologically adapted to maximize accelerative performance (Weihs, 1973). The rainbow trout *Oncorhynchus mykiss* is chosen because its body form is that of a generalist; morphologically adapted to allow considerable performance when employing any swimming strategy (Weihs and Webb, 1983).

Consideration is given to the classification of both escape fast-starts (Chapter 4) and feeding fast-starts (Chapter 5). Weihs (1973) defines three kinematic stages for fast-starts: a preparatory stage (stage 1), in which the straight-stretched fish bends into an *L*-shape, a propulsive stroke (stage 2), in which the fish executes a reverse bend, and a variable stage (stage 3), which may be one or more repititions of stage 2, steady swimming, or an unpowered glide. Webb (1976) describes *C*- and *S*-starts based on the body conformation at the end of stage 1. However, these classifications do not describe the kinematics of the entire fast-start, though they may tacitly imply involvement of certain reticulospinal command mechanisms (Eaton and Hacket, 1984; Eaton *et al.* 1988).

Fast-starts can also be classified on the basis of the shape of the path described by the centre of mass during the event. This accounts for the turns that often occur during the event, as well as body orientations. Although this does not relay information about neural control, it does provide a more dynamic description of the event. In Chapters 4 and 5, the

kinematics of the fast-starts are compared to previous studies based on this criteria, not on the shape of the fish at the end of stage 1.

Chapter 4 and 5 introduce a new system of classification of fast-starts based on mechanical information. Here the important criterion is the number of large peaks appearing in the acceleration-time and velocity-time plots. This allows fast-start type to be determined without relying on film data, though it does reflect the kinematics of the events. It also allows investigations of short term behaviour based on mechanical, rather than kinematic data. For example, this information is useful when considering the energetics of ambush predators (Harper and Blake, 1988, Appendix).

Much attention has been focused on piscivorous predator-prey interactions. Studies have investigated the behavioural (e.g., Crossman, 1959; Ware, 1971; Nursall, 1973), kinematic (e.g., Webb, 1976; Webb and Skadsen, 1980; Vinyard, 1982) and energetic (e.g., Isaacs and Wick, 1973; Ware, 1975; Kerr, 1982; Harper and Blake, 1988, Appendix) characteristics of these events. Others have focused on more specific feeding characteristics. Optimal prey size (Wankowski, 1979; Schmitt and Holbrook, 1984; Harper and Blake, 1988, Appendix), its relation to optimal foraging (Werner and Hall, 1974) and handling time (Werner, 1974), underlying sensory mechanisms (Ware, 1973; Vinyard and O'Brien, 1976; O'Brien *et al.* 1976; Morgan and Ritz, 1983), and prey response characteristics (Dill, 1973, 1974*a*,*b*; Webb, 1984) have all received considerable attention.

Few, however, have focused on the kinematics and mechanics of piscivorous feeding interactions. Studies correlating feeding and general locomotor behaviour (Webb, 1976, 1986; Webb and Skadsen, 1980; Rand and Lauder, 1981) and the specific behaviour, suction feeding (e.g., Lauder, 1979, 1980, 1983), have been conducted, employing high-speed film to

estimate performance. This is an effective method of analyzing the small scale movements observed in suction feeding, but comprehensive, whole-body performance estimated by film is subject to considerable error, particularly where acceleration is concerned, as shown in Chapter 3.

Chapter 5 combines accelerometry and high-speed ciné film in an investigation of the prey capture performance of *Esox lucius*, a piscivorous ambush predator. It is complementary to Chapter 4; documenting the mechanics and kinematics of the same individuals.

Prey capture performance is also related to predatory behaviour in Chapter 5. Prey of different sizes were offered at different distances to determine whether actual or apparent prey size (the angular size of the prey on the predator's retina) was the visual cue for predation.

CHAPTER 2

General Materials and Methods

A. FISH

Two species of fish were used in these studies, northern pike *Esox lucius* (n = 4, mass = 0.396 ± 0.058 kg, fork-length = 0.378 ± 0.019 m: throughout, means are reported as ±2 S.E.) and rainbow trout *Oncorhynchus mykiss* (n = 8, mass = 0.318 ± 0.063 kg, fork-length = 0.316 ± 0.020 m). The pike were seined from Baptiste Lake in northern Alberta; trout were obtained from a local (British Columbia) fish hatchery. These species were selected because their fast-start performance is well documented (Eaton *et al.* 1977; Webb 1975, 1976, 1977, 1978*a*,*b*, 1982, 1983, 1986). Healthy adults were held for 6-12 months in 1000 l circular outdoor holding tanks (2 m in diameter) which were flushed continuously with fresh water at 15-20°C. Fast-start performance is independent of temperature over this range (Webb, 1978*a*). Trout were fed trout chow daily and pike were fed live goldfish thrice weekly until ready for use.

B. THE EXPERIMENTAL ARENA

The experimental arena, made of glass and Plexiglas, measured 2.45 m × 1.22 m × 0.47 m, and was filled to a depth of approximately 0.30 m. A 0.02 m grid was placed on the bottom of the arena, and fresh water, from the same

supply as the outdoor holding tanks, was slowly circulated, except while filming. Fish were allowed 48 h to acclimate to the aquarium before experimentation and were not fed during that time.

C. CINEMATOGRAPHY

Accelerating fish were filmed with a 16 mm high-speed ciné camera (Locam model 51-0002) on Kodak 7250 400 ISO ciné film at 50-350 Hz. Fish were filmed as if from above by mounting a 2.45 m × 1.22 m mirror at 45° over the tank. When filming pike, illumination was provided by two Berkey Beam 800 spot/flood lights mounted in front of the arena and shone into the mirror. For trout, four Crown 650 video lights were directed through the sides of the arena, below water level.

Processed films were analyzed on an image analyzer (Photographic Analysis Limited Projection Analysis Unit, ZAE 76). The system includes a variable speed projector, ground glass viewing/digitizing tablet, and a digitizing computer. Images of the accelerating fish were directed onto the tablet where frame-by-frame tracings of the fish were made and digital recording of the movement of the centre of mass was attained. This position was easily identifiable due to the incision scar resulting from accelerometer implantation. These data were then transferred to an Olivetti M24 PC for further analysis.

Distance-time data from the film were differentiated to give velocity-time and acceleration-time curves. A five point moving regression (for a description, see Chapter 3) was used to perform the differentiations. The maximum instantaneous acceleration was then taken from the acceleration-time data.

D. MEASUREMENT OF ACCELERATION

Accelerations were directly measured with a Kistler 8616-A1000 low-impedance piezoelectric accelerometer (range ± 1000 g; frequency response 125 kHz; cylindrical dimensions 0.0058 m × 0.0051 m diameter; mass < 0.0005 kg). Acceleration-time data were stored in the mainframe memory of a Nicolet 4094 digital oscilloscope, transferred to floppy disk, and later to the computer. Accelerometer and film data were synchronized by a light beacon situated in the corner of the camera's field of view. This was linked to the oscilloscope trigger mechanism such that the beacon would be illuminated while the oscilloscope recorded acceleration.

Damping and linearity are not significant sources of error with the accelerometers used here. The high frequency response (125 kHz) precludes the possibility of phase shifts. The linearity of the response is reported to be ±1%, maximally, at 1000 g. Since the maximum accelerations recorded here are of the order of 25 g, the error arising from poor linearity is likely to be extremely small.

Fish were quickly anesthetized in 0.002 kg l^{-1} MS222 (Sandoz) buffered with 0.004 kg l^{-1} sodium bicarbonate. Once anesthetized, fish were transferred to a "wet" table where one-third strength anesthetic was flushed continuously over the gills by a recirculating pump. For a description of the anesthetizing procedure, see Richardson (1985).

The accelerometer was implanted subcutaneously. The incision was made above the centre of mass, parallel to the centre-line of the fish, just lateral to the vertebral column. Centre of mass was assumed to be 0.41 × fork length (measured from the nose to the middle of the caudal fin trailing

edge) for pike and at the leading edge of the dorsal fin for trout (Webb, 1978*b*). The small mass of the accelerometer (<0.2% of fish mass for the smallest specimen) eliminated the need to reconsider the location of the centre of mass after implantation. The incision was never longer or deeper than about 1 cm, involved no tissue removal, and no significant loss of blood. Once the accelerometer was implanted, the incision was tightly closed using Ethicon V-5 tapercut cardiovascular sutures. The shape of the incision and the tight closure prevented the accelerometer from altering its orientation in the fish during experiments.

Fish were then placed in a recovery tank where fresh water was flushed over the gills until normal opercular activity resumed. At this point the fish was re-introduced to the experimental arena and allowed to recover for 48 h. No deaths could be attributed to the incision or anesthetization.

When a fish was still, in the centre of the tank, it was startled by thrusting a wooden pole towards its head, perpendicular to its long axis. This produced a high-performance escape behaviour, because the startle response is an all-or-none maximum response (Eaton *et al.* 1977). A method for startling fish by electric shock (Webb, 1975) was employed in preliminary experiments but elicited less forceful fast-starts. A recovery period of several hours was allowed between test runs.

E. ACCELEROMETER CALIBRATION

The accelerometer was calibrated on a guillotine-like apparatus which provided constant free-fall acceleration. The apparatus (Fig. 2.1) consists of a brass bar (mass = 1 kg) which slides down parallel steel rods. Two sets

Figure 2.1. Schematic diagram of the accelerometer calibration apparatus. The time of the drop is measured as the bar travels from the upper to lower set of infrared timing lights (D). Other equipment includes the camera (A), lights (B), free-fall apparatus (C), accelerometer power source and amplifier (E), oscilloscope (F), and digital clock (G).

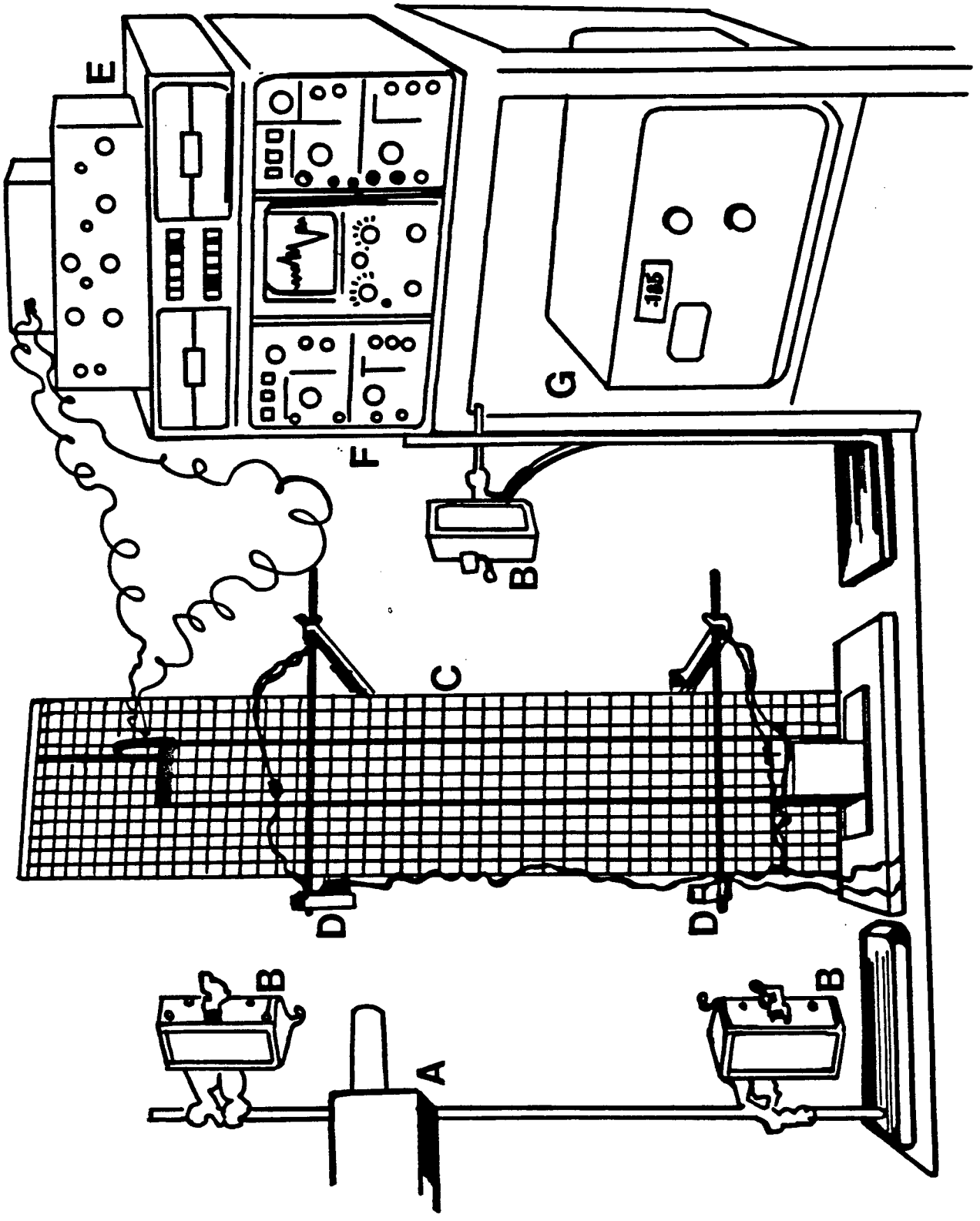
E
G
F
B
C
D
DE
B
B
A

of infrared lights and sensors were positioned 0.50 m apart near the top and bottom of the rods. These input to a digital clock which measured the time of the drop; the first set of sensors starting, and the second set stopping the clock. The elapsed time was used to determine the actual acceleration of the bar by employing the standard relation for free-falling objects:

$$a = 2\,\Delta d\,t^{-2} \tag{1}$$

(Tilley & Thumm, 1974), where a is acceleration, d is distance, and t is time. The time measured was that of the latter portion of the drop, corresponding to the position of the infrared sensors. These were set further down the rods so that interference with the start lever (which sets the bar into motion) could be neglected.

The total distance of the drop (Δd_T) is 0.68 m, of which the last 0.50 m (Δd_2) is timed; the initial 0.18 m (Δd_1) is not. The measured time (t_2) is the difference between total drop time (t_T) and the time to fall to the first set of sensors (t_1):

$$t_2 = t_T - t_1, \tag{2}$$

which was measured to be 0.185 ± 0.001 s (n = 40). Rearranging equation 1 and substituting values for Δd_T and Δd_1 gives:

$$t_T = \left(\frac{2 \times 0.68}{a} \right)^{1/2} \tag{3}$$

and

$$t_1 = \left(\frac{2 \times 0.18}{a}\right)^{1/2}. \quad (4)$$

Substituting equations 3 and 4 and the measured value for t_2 into equation 2 gives:

$$0.185 = \left(\frac{1.36}{a}\right)^{1/2} - \left(\frac{0.36}{a}\right)^{1/2}. \quad (5)$$

Solving for a gives a value of 9.37 m s^{-2}. The difference between this value and the standard gravitational constant (g = 9.81 m s^{-2}) can be attributed to the friction on the rods and air resistance.

The accelerometer was affixed to the brass bar with modelling clay, in the same orientation as in the fish. Accelerations from 40 further drops were then recorded on the oscilloscope. Figure 2.2 is an example of one such calibration. The raw accelerometer data is smoothed because vibrations in the apparatus created high frequency noise. This noise also accounts for the data points located below zero before the bar is dropped. The resulting curve (Fig. 2.2) indicates low frequency variations, which are due to instability (vibration) in the apparatus. In the still fish, flat line signals were recorded from the accelerometers.

The average signal strength was found to be 148 ± 6 m*V*, which translates to 155 mV g^{-1}, after accounting for frictional resistance. Subsequent trials, involving changes of orientation of the accelerometer, confirmed that it is equally sensitive in the reverse direction and insensitive when oriented sideways (parallel with the ground).

Figure 2.2. Example of an accelerometer calibration trace. Voltage is indicated on the left axis and the corresponding acceleration on the right. Open circles represent every 100th accelerometer data point. The solid line is the smoothed accelerometer data. The dashed line is the average acceleration of the timed portion.

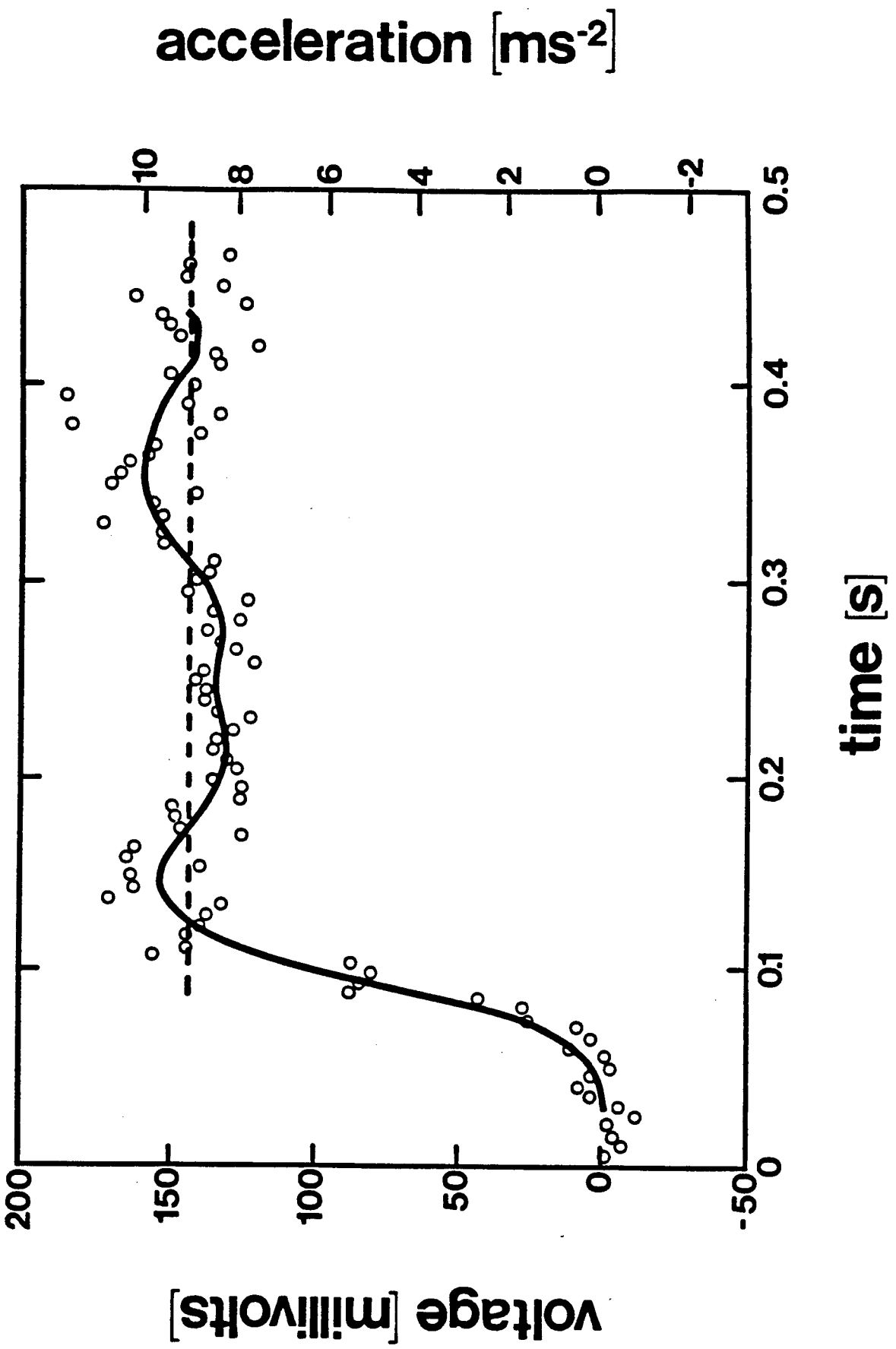
acceleration [ms-2]
10
8
6
4
2
0
-2
0.5
0.4
0.3
0.2
0.1
0
time [s]
200
150
100
50
0
-50
voltage [millivolts]

F. CORRECTION FOR ROTATIONAL ACCELERATION

The curvilinear nature of the escape trajectories introduce circumstantial accelerations that are detected by the accelerometer. This results from the fact that bodies accelerating along a curved trajectory realize, along with the acceleration directed towards the centre of rotation, a component parallel to the tangent of the trajectory (Meriam, 1975). This will be referred to as tangential acceleration, an artifact resulting from non-linear motion which must be subtracted from the accelerometer values. This is necessary when comparing complex motions (e.g. fish fast-starts) that involve varying degrees of curvature. Therefore it is important to note that the results reported in Chapters 3 and 4 are scalar values, not vector values.

Film data were used to determine the tangential acceleration, which is equal to the product of the angular acceleration and the radius of the curve. To determine these values, the position of the accelerometer (easy to locate from the incision scar) at each point in time was plotted, giving the trajectory traced-out during the escape. The centre of rotation was determined by locating the intercept of perpendicular lines drawn from tangents to the curve. The distance from the curve to the intercept is the radius.

The angular acceleration is given by the rate of change of the angular velocity, which is, in turn, equal to the velocity of the fish divided by the radius of the curve. Velocity was determined by differentiating the distance-time film data with respect to time, using the five point moving regression method (Lanczos, 1956).

CHAPTER 3

The Error Involved in High-Speed Film When Used to Evaluate Maximum Accelerations of Fish

A. INTRODUCTION

High-speed film is commonly used to estimate the performance of fish during fast-starts (see Table 3.4). Film gives accurate estimates of displacement; however, the error inherent in deriving maximum acceleration data from film has not been documented. Maximum accelerations are important because they represent the maximum level of performance that can be employed during life threatening situations; they are often reported in studies on fish fast-start performance (Table 3.4). This chapter addresses the issue of errors involved in deriving performance data from film.

Two independent sources of error are inherent in film analyses; that involved in measuring frame to frame displacements (measurement error), and that related to the sampling frequency (sampling frequency error), in this case, film speed. The percent effects of each can be summed to estimate total error.

Measurement error (ME) arises from electronic imperfections in the camera and from the mechanical imperfections associated with placing the digitizer cursor accurately over the data point of interest. There is no previous discussion of ME in the literature, as it relates to assessing the acceleration of fish.

Sampling rates in the earliest film studies on fast-starts were of the order of 60 Hz. Webb (1975, 1976) used film speeds of 64 Hz, which provided only five data points to calculate velocity and acceleration for a given fast-start. Later Webb (1977, 1978*a*,*b*, 1982) used film speeds of 250 Hz along with improved analysis techniques (Webb, 1977) to obtain better estimates of instantaneous maximum accelerations. The sampling frequency error (SFE), however, could not be evaluated because actual instantaneous accelerations were not directly measured.

It should be noted that many of these earlier studies focussed on criteria other than acceleration when estimating performance (Webb, 1976, 1977*a*,*b*, 1978), though acceleration data were included. In this light, they serve as a good starting point for more accurate measurements of acceleration, employing new technologies. More comprehensive techniques, such as over-sampling combined with statistical filtering, can also be employed to increase the signal-to-noise ratio, but are not considered here because this study assesses previous estimates of acceleration using the techniques employed at the time. Furthermore, over-sampling is not always possible in film studies of events of short duration and rapid change in force (e.g., fast-starts) due to the limited sampling rates of affordable cameras.

Here, subcutaneously implanted accelerometers are combined with ciné films to assess the error inherent in calculating the maximum accelerations of fish from filmed fast-starts.

B. MATERIALS AND METHODS

Data from the digitizer come in the form of *xy* coordinates for each frame of the film; the inverse of the film speed gives the corresponding time interval. The Pythagorean theorem is applied to these data to give distance-time data. The regression first calculates the slope of the line from the first point to the second (e.g., Δdistance/Δtime), second to third, etc. and then averages the first five values. Mathematically, this is the same as calculating an average slope for the first five values. This is then plotted against time at the centre point of the regression (the third value) in the velocity-time data set. The regression then "moves down" the data one point and averages the second to sixth values of the distance-time data. This continues until the end of the data set is reached. Lanczos (1956) describes a method for extrapolating to obtain the first two and last two data points for each regression. In this study these points were simply omitted, ensuring that the differentiated data points were consistently derived.

The acceleration-time data were derived in a similar manner, using the velocity-time data. These data were then plotted or analyzed, again omitting the first and last two points. For a discussion of moving point regressions and their applications see Lanczos (1956).

C. THEORETICAL ASSESSMENT OF SAMPLING FREQUENCY ERROR (SFE)

Fabrication of hypothetical acceleration-time data creates a controlled environment in which the effects of the sources of error can be explored. The acceleration curve (Fig. 3.1), hereafter referred to as 800norm, was created to simulate the rise-time and maximum acceleration typical of that recorded from the accelerometer (e.g., see Fig. 3.9). The curve consists of acceleration data plotted every 0.00125 *s* (1/800 *s*) forming a unimodal, symmetrical acceleration profile. The time interval was selected to provide sufficient data points to accurately describe the unimodal curve.

1. Calculation of Velocity and Distance

The derivation of velocity from acceleration data involves an integration with respect to time. Distance can then be obtained by a second integration, performed on the resultant velocity-time data. In the following procedure it is assumed that the acceleration between data points is such that the curve can be considered as a series of straight lines connecting these points. The small time interval (0.00125 s) between data points supports this assumption.

Since, by definition, fast-starts originate from an idle position, the velocity and acceleration at time T_0 are also zero ($V_0 = 0$; $a_0 = 0$). The velocity (V_i) at time T_i is approximated by numerical integration using the following formula:

Figure 3.1. Hypothetical acceleration-time plot (800norm; thin solid line) along with traces simulating the same data sampled at frequencies of 400 (short dash), 200 (long dash), 100 (thick solid), and 50 (medium solid) Hz. A full description is given in the text. Inset shows 800norm with data points (solid circles).

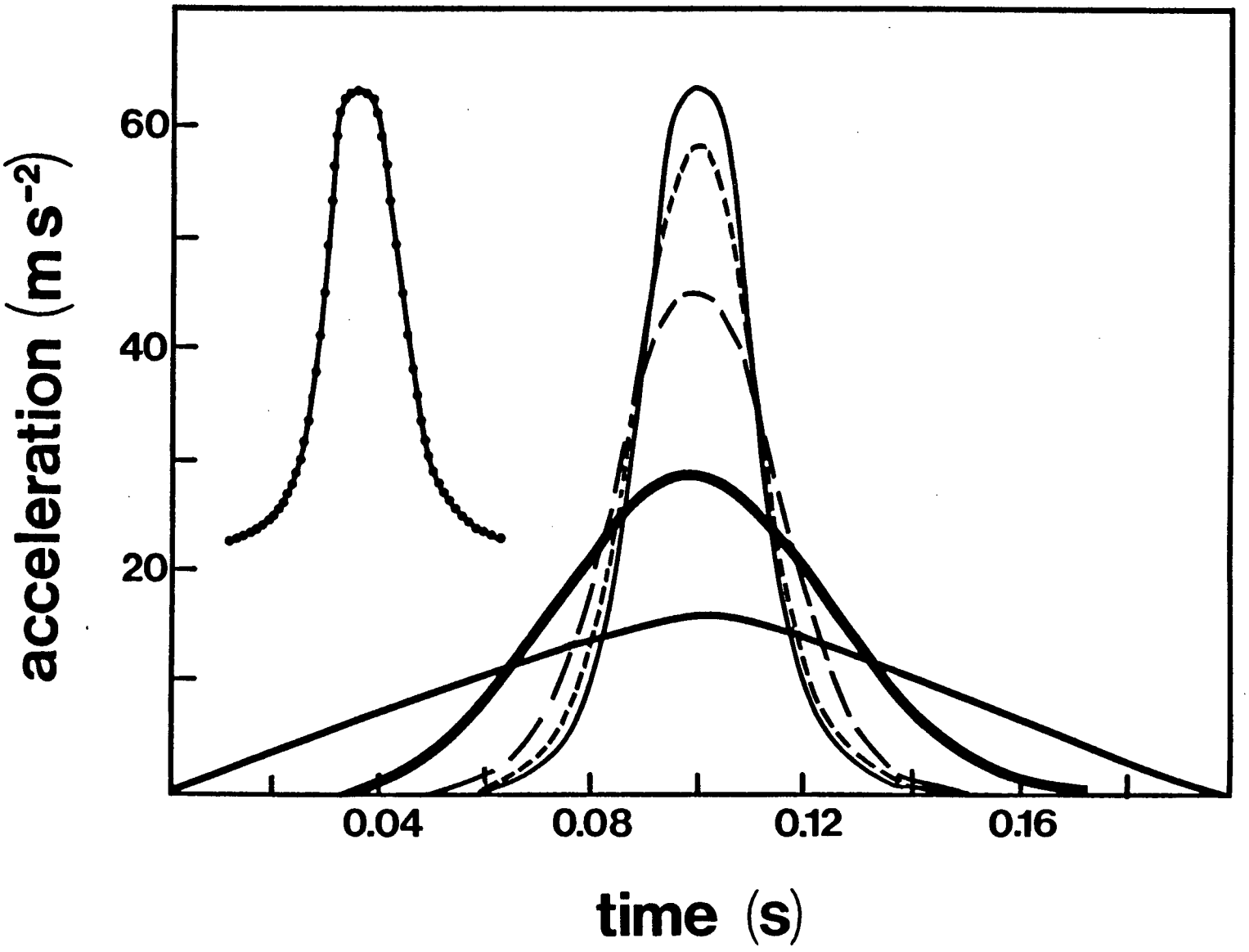
acceleration (m s-2)
60
40
20
0.04
0.08
0.12
0.16
time (s)

$$V_i = V_0 + \sum_{i=1}^{n} \frac{\left(a_{i-1} + a_i\right)}{2} \Delta t \quad . \tag{6}$$

The distance moved can be derived from the velocity data in the same way:

$$D_i = D_0 + \sum_{i=1}^{n} \frac{\left(V_{i-1} + V_i\right)}{2} \Delta t \quad . \tag{7}$$

Distance-time data were then generated from the acceleration data following the algorithm developed above. This provided the cumulative distance moved at a sampling frequency of 800 Hz, thus simulating the type of information that is accurately recorded by film (i.e., distance-time data). As a control, these data were then converted to instantaneous distance-time information and twice differentiated with the moving regression method. Some over-smoothing of the already smooth data did occur, but comparison to 800norm indicated that this error is less than 1%.

2. Estimate of Sampling Frequency Error

The 800norm cumulative distance-time data were then used at progressively lower sampling frequencies to estimate SFE. This was done by taking every second distance-time point to simulate a film speed of 400 Hz, every fourth point for 200 Hz, etc. The resulting data sets were twice-differentiated with the moving point regression method and compared with 800norm.

The effects of the simulated reduction of film speed to 400, 200, 100, and 50 Hz are plotted in Fig. 3.1. Two major departures from 800norm become apparent: the maximum accelerations become progressively smaller and the curve becomes less peaked and more broad.

SFE was determined using a simple method of comparison where the difference between the maximum acceleration of 800norm and the test case is presented as a percentage of the 800norm value. For example, the calculation for the test case at 400 Hz is:

$$SFE = \frac{|A_{800} - A_{400}|}{A_{800}} \times 100 \qquad (8)$$

SFE for maximal accelerations is plotted against film speed in Fig. 3.2. The equation for this line was determined from a regression analysis to be:

$$SFE = 10^{(-0.00279 \times FS + 2.019)}, \qquad (9)$$

where FS is the film speed in Hz. Maximum acceleration (A_{max}) is the chosen point of interest because this value is often reported in the literature (e.g., Weihs, 1973; Webb, 1975, 1976, 1977, 1978*a*,*b*, 1983). It is also of biological relevance because it represents the maximum level of performance that can be employed during life threatening situations. Figure 3.2 shows that SFE increases exponentially with decreasing film speed. It should be noted that SFE will always cause underestimations of actual accelerations because of over-smoothing.

Figure 3.2. Sampling frequency error (SFE; long dash), measurement error (ME; short dash), and total error (TE; solid line) as a percentage of the maximum acceleration rate (A_{max}) in Fig. 3.1. The errors are plotted against film speed.

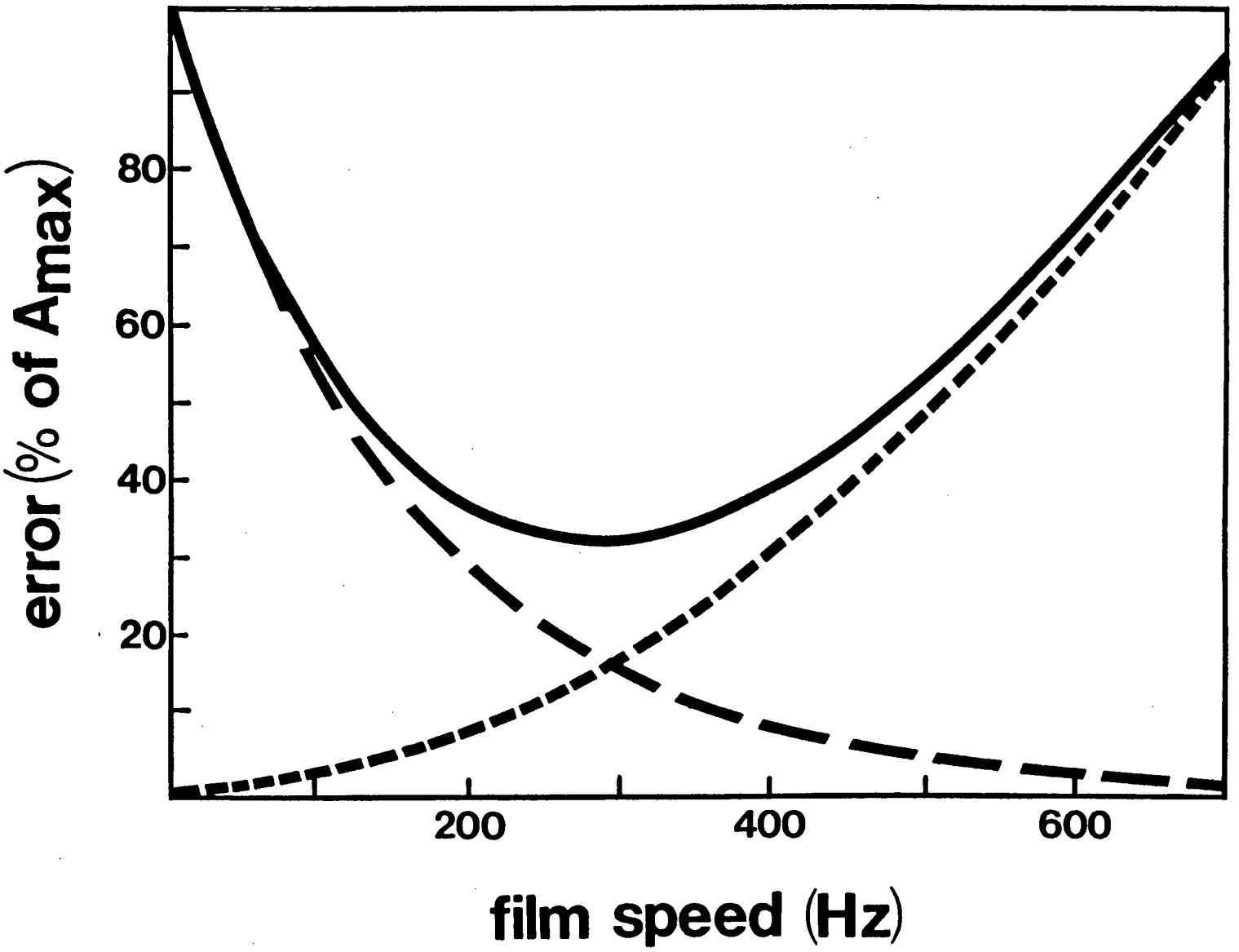
error (% of Amax)
80
60
40
20
200
400
600
film speed (Hz)

D. THEORETICAL AND EXPERIMENTAL ASSESSMENT OF MEASUREMENT ERROR (ME)

The effect of random measurement error (ME), will be to over- or under-estimate actual accelerations. ME arises from small mechanical and electrical imperfections in the camera and digitizing system. The camera used in this study has a maximum error of ±1%, translating to a fractional uncertainty of ± 0.01 Hz. The error in the digitizing system, determined by repeated relocations of the cursor to predetermined locations (thereby accounting for both human and system error), was found to be ±2% in both the x and y directions. This may vary with the system used, but will not likely be less than 2%. Because the uncertainties in x and y are independent and random, the total error in determining any distance (δD) is given by Taylor (1982):

$$\delta D = \pm \sqrt{(\delta x)^2 + (\delta y)^2} \quad , \tag{10}$$

where δx and δy are the uncertainties in x and y, respectively. This gives a total distance uncertainty of 2.83%. Since acceleration is determined by twice-differentiating the distance data with respect to time, the distance and time uncertainty will be propagated and smoothed during this procedure.

Because ME arises during digitizing of each frame of the film, it will also increase with film speed. As film speed increases, the distance moved per frame decreases, so the digitizing error becomes a greater proportion of the measured distance. To present ME as a proportion of acceleration, it is necessary to multiply the fractional uncertainty for acceleration by film

speed squared, since distance is twice divided by time in the double differentiation. Therefore, ME for the acceleration-time data, at any film speed (FS), is given by:

$$ME = 0.000125 \times (FS)^2. \quad (11)$$

This gives an absolute value for the uncertainty in derived accelerations. To determine actual ME values, the magnification of the image on the digitizing tablet must be considered. For example, if the image on the tablet is actual size, then every centimetre measured will correspond to 1 cm of movement and the uncertainty will be given directly from equation 11, in units of metres per square second (e.g., at a film speed of 200 Hz the uncertainty in acceleration will be ± 5.0 m s^{-2}). To present this in the same way as SFE, ME must be calculated as a percentage of A_{max}. However, because ME is constant for any combination of film speed and magnification, presenting it in this way makes ME dependent on A_{max}:

$$ME = \frac{100^{[\log (FS)]}}{80 \times A_{max}}. \quad (12)$$

Increasing image size has the same effect on ME as decreasing the film speed in equal proportion. For example, if the film speed is halved, the fish will move twice as far on the tablet, from one frame to the next. It is easily shown that the same will occur if image size is doubled. Likewise, if image size is reduced, the effect will be similar to increasing the film speed. In this way, departures from actual-size magnifications can be accounted for by adjusting film speed. ME is calculated using the A_{max} from

the SFE analysis and plotted against film speed in Fig. 3.2, demonstrating that ME increases exponentially with film speed.

ME was measured experimentally, employing the same guillotine apparatus used to calibrate the accelerometer (Chapter 2). As the accelerometer was dropped, it was filmed at speeds ranging from 50 to 400 Hz. Film distance-time data were then twice-differentiated giving acceleration-time values. The constant acceleration rate (9.37 m s^{-2}) during the drop eliminated the effects of SFE because there were no major peaks or valleys in the acceleration-time data. Therefore, any discrepancy between the film-derived and known acceleration is due to ME alone. Figure 3.3 is a plot of error (expressed as a percentage of A_{max}) for various film speeds. The theoretical curve is derived from equation 12, using appropriate values for A_{max} and image magnification. Note that the vast majority of error values fall beneath the theoretical line, indicating that the relation described in equation 12 accounts for almost all of the error observed.

Figure 3.3. Measurement error (ME) as a function of film speed. The theoretical prediction for ME is shown by the dashed line. Box-plots show experimental values for ME at 50, 100, 200, and 400 Hz. Boxes represent 50% of the data points and the bisecting line represents the mean. Open circles represent experimental error values deviating by more than 25% from the mean.

error (% of Amax)
50
150
250
film speed (Hz)
100
200
300
400

E. EFFECTS OF IMAGE SIZE AND MAXIMUM ACCELERATION RATE ON TOTAL ERROR (TE)

The total error (TE) results from the additive effects of SFE and ME (Fig. 3.2). Because SFE is inversely proportional to film speed, and ME is positively proportional, the curve for total error is U-shaped, resulting in optimal film speed for minimal error. The optimal speed predicted for the hypothetical example, 800norm, at actual image size, is approximately 280 Hz (Fig. 3.2). Note that the minimum total error at this film speed is about 33%.

Figure 3.4 shows the effects of image magnification and reduction on total error at various film speeds. As the image is progressively magnified, three important changes become evident: minimum error is reduced, optimal film speed is increased, and the increase in total error due to a given increase in film speed above the optimum is reduced. The minimal errors from the curves in Fig. 3.4 are plotted against log(magnification) in Fig. 3.5, which also includes a curve indicating optimal film speeds for magnifications ranging from × 1/20 to × 20.

Figure 3.6 shows the effect of varying the magnitude of acceleration on the error versus film speed curves. Because ME is an absolute value, it will decrease proportionally with increasing A_{max}, becoming a progressively smaller proportion of that value. Figure 3.6 shows the effect on error of varying the magnitude of acceleration from 20 to 100 m s^{-2}. As with the magnification curves, minimum errors and optimal film speeds from these curves are plotted against acceleration rate in Fig. 3.7.

Figure 3.4. Effect of image size on total error (TE) curves. Curves are for image sizes of 1/5× (long dash), 1/2× (short dash), actual size (solid), 2× (dash wtih solid circles), and 5× (medium dash).

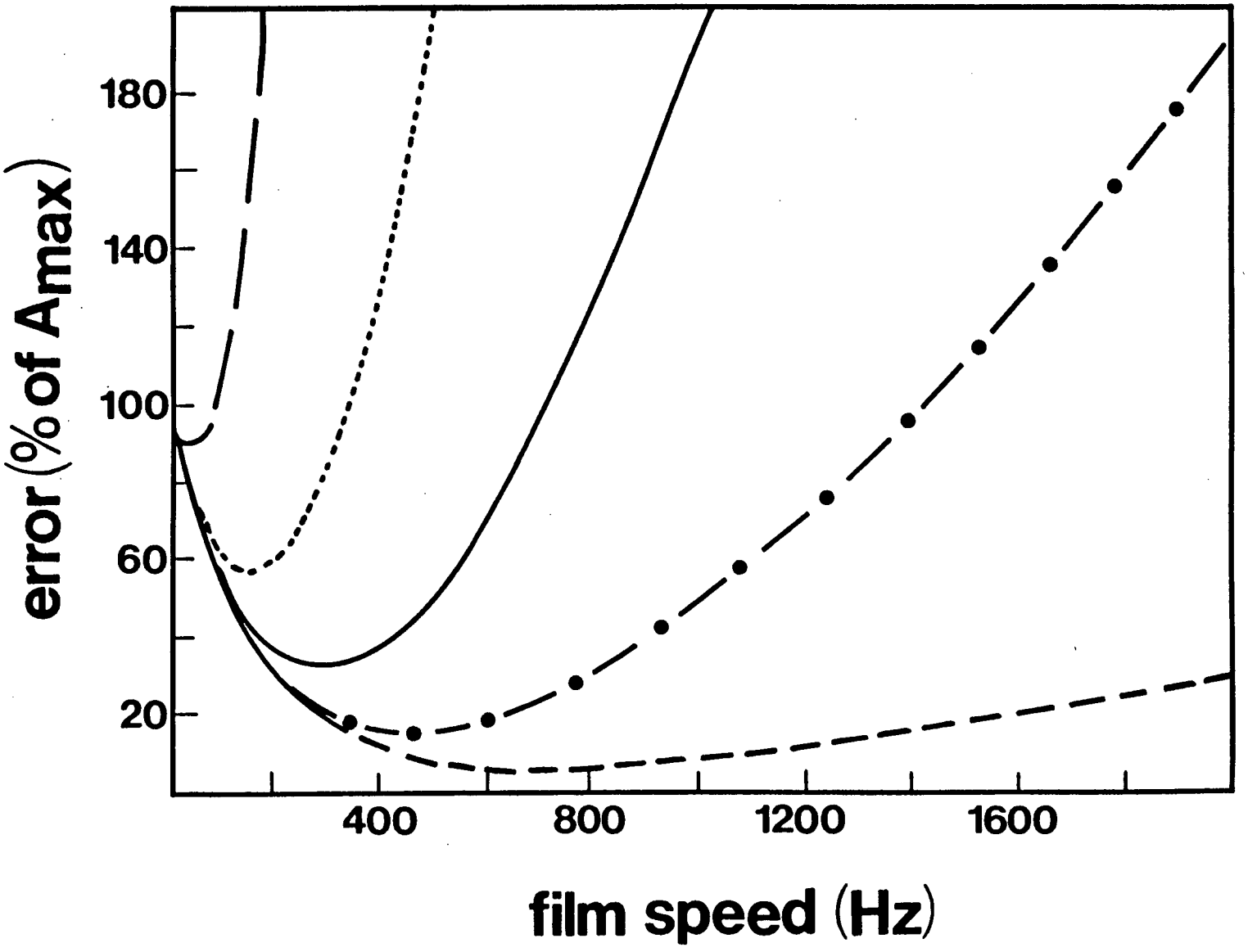
180
140
100
60
20
error (% of Amax)
400
800
1200
1600
film speed (Hz)

Figure 3.5. Minimum error (dashed line) and optimal film (solid line) speed for a range of image sizes. The left side of the figure represents image reductions and the right side, image magnifications.

error (% of Amax)
140
100
60
20
800
600
400
200
film speed (Hz)
-1.5
-1.0
-0.5
0
0.5
1.0
1.5
log (image size)

Figure 3.6. Effect of maximum acceleration rate (A_{max}) on total error (TE) curves. Curves are for A_{max} of 20 m s^{-2} (long dash), 40 m s^{-2} (short dash), 60 m s^{-2} (solid), 80 m s^{-2} (dash with solid circles), and 100 m s^{-2} (medium dash).

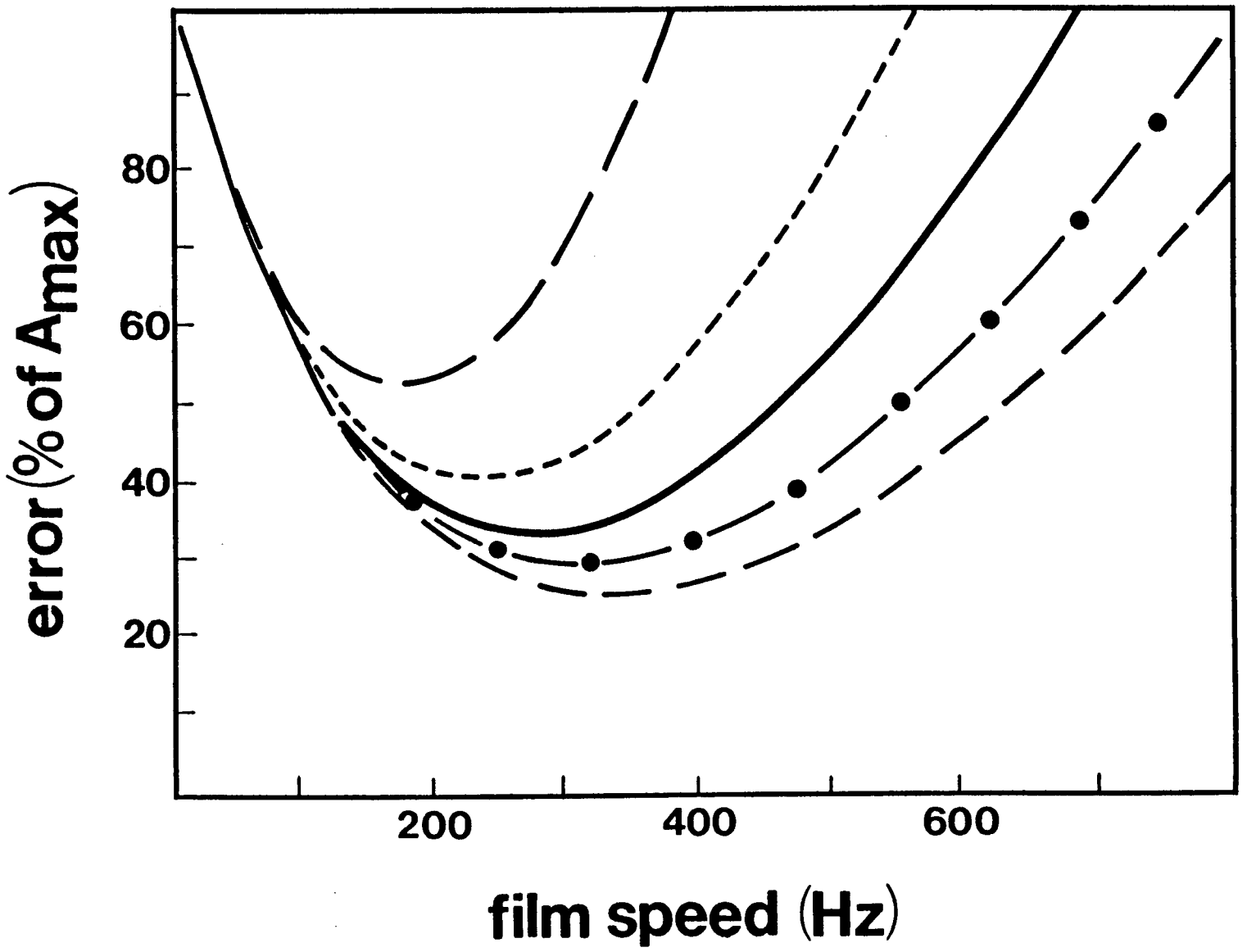
error (% of A_{max})
80
60
40
20
200
400
600
film speed (Hz)

Figure 3.7. Minimum error (dashed line) and optimal film speed (solid line) for maximum acceleration rates (A_{max}) ranging from 20 to 100ms^{-2}.

film speed (Hz)
300
200
100
acceleration (m s-2)
80
60
40
20
error (% of Amax)
60
40
20

To consider the combined effects of changes in image magnification and the magnitude of acceleration, a series of error versus magnification curves are generated for accelerations of various magnitudes (Fig. 3.8). A second series of curves shows optimal film speeds for the same accelerations.

Figure 3.8 shows that the effects of image magnification on minimal error and optimal film speed override those of acceleration. Even though the accelerations considered vary by a factor of five, there is relatively little difference between the curves. This reinforces the importance of maximizing image, and digitizing tablet, size to reduce error.

Figure 3.8. Combined effects of image size and maximum acceleration rate (A_{max}) on minimum error (decreasing) and optimal film speeds (increasing). Curves are for A_{max} ranging from 20 to 100 m s^{-2}. Symbols are the same as in Fig. 3.6.

160
120
80
40
error (% of Amax)
1000
600
200
film speed (Hz)
-1.5
-1.0
-0.5
0
0.5
1.0
1.5
log (image size)

F. DISCUSSION

The experiments conducted provided both film, at a range of speeds, and accelerometer data for fish executing fast-starts. The film data provided acceleration-time plots. Direct measurements for the same events were simultaneously recorded with the accelerometer and converted to the same units as the film-derived data using the calibration relation. This allowed both the accelerometer and film-derived data to be plotted together. Examples for film speeds of 100, 200, 250, and 350 Hz are shown in Fig. 3.9.

Trout and pike peak accelerations (A_{max}) from the film-derived data were compared with directly measured accelerations using equation 8. Differences between the two were assumed to be attributable to SFE and ME. This difference was calculated as a percentage of the actual (accelerometer) maximum acceleration. Theoretical error values were calculated from equations 9 and 12, after correcting for image magnification. The theoretical and experimental errors were compared by dividing the latter into the former and plotting against film speed in Fig. 3.10. The error quotients do not form a consistent pattern, primarily due to the variability of A_{max} in the experimental trials. Arguably, it can be concluded from Fig. 3.10 that the theoretical values approximate those derived experimentally, indicating that discrepancies between film-derived and accelerometer-measured accelerations can be attributed to the effects of SFE and ME.

Figure 3.9. Acceleration-time plots for both film-derived (lines with closed squares) and accelerometer (solid lines) data. Vertical axes are accelerations in units of m s^{-2} and horizontal axes are times in seconds. Film speeds are 100 Hz for 3.9A, 200 Hz for 3.9B, 250 Hz for 3.9C, and 350 Hz for 3.9D.

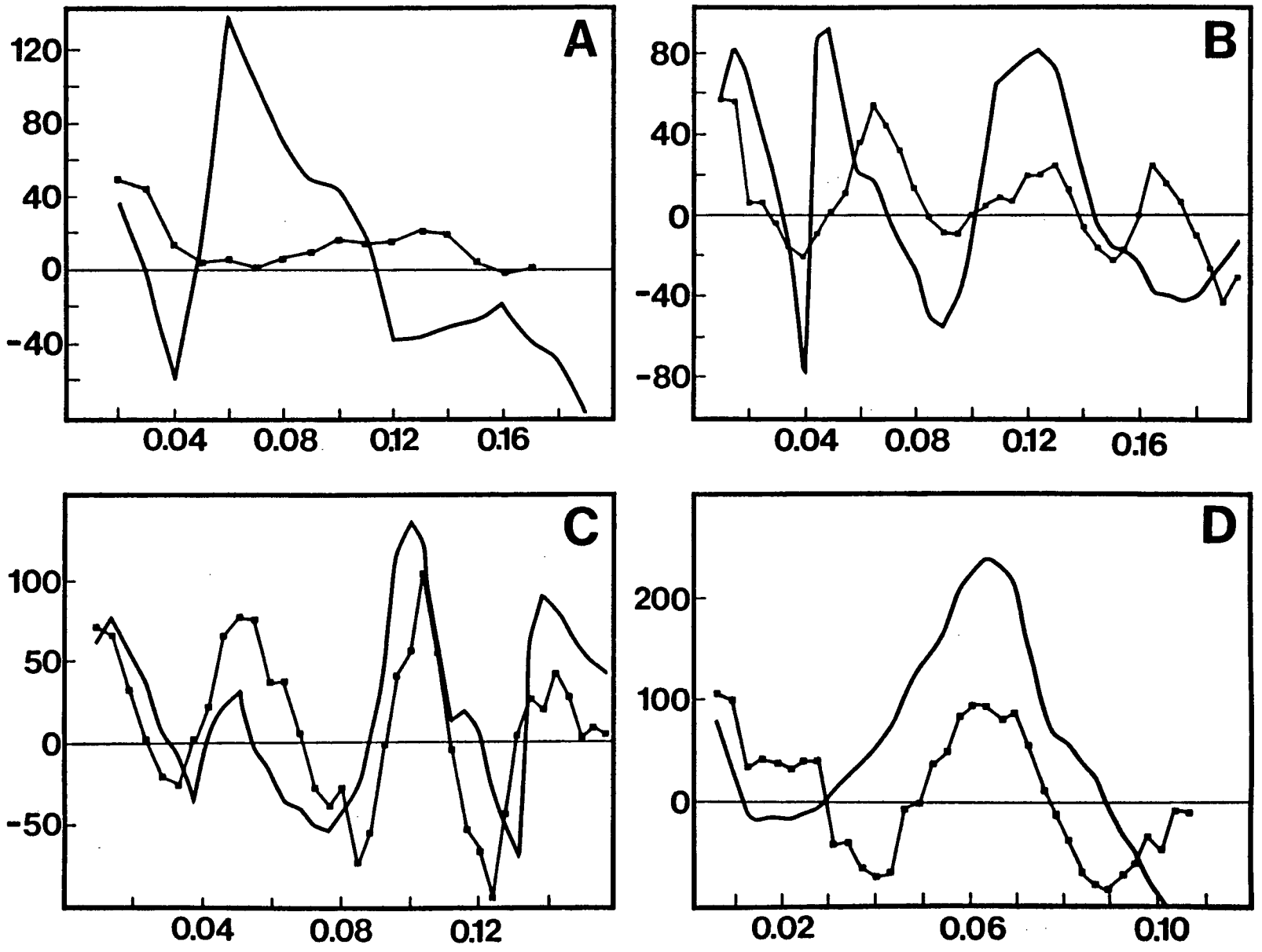
A
120
80
40
0
-40
0.04
0.08
0.12
0.16
B
80
40
0
-40
-80
0.04
0.08
0.12
0.16
C
100
50
0
-50
0.04
0.08
0.12
D
200
100
0
0.02
0.06
0.10

Figure 3.10. Quotient of theoretical total error and experimentally determined error for a range of film speeds. A discussion is given in the text.

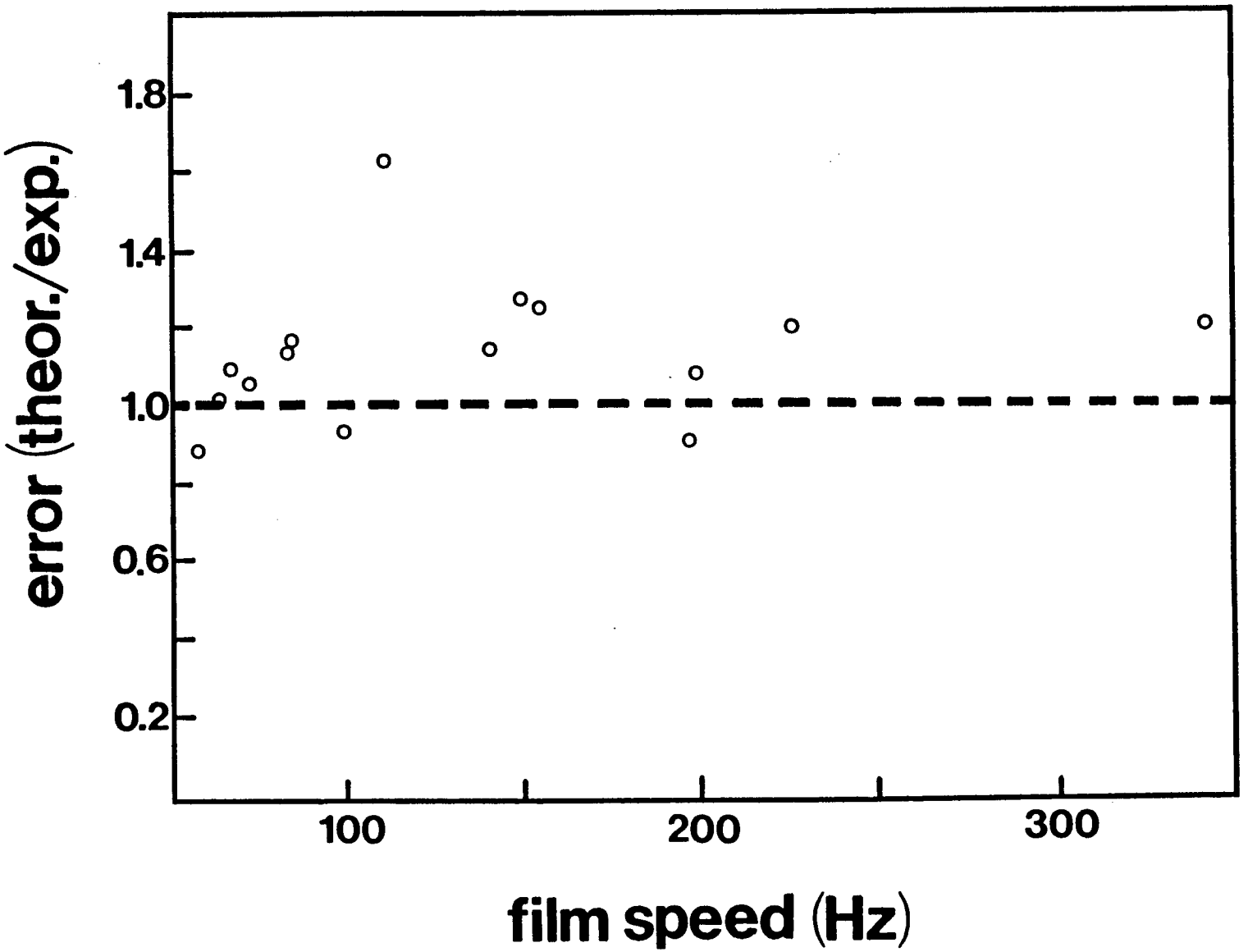
error (theor./exp.)
1.8
1.4
1.0
0.6
0.2
100
200
300
film speed (Hz)

This study clearly demonstrates the need to consider sources of error when deriving accelerations from film. This is shown to be particularly important when using a reduced image size (Fig. 3.5). Because image magnification has not been reported in the literature, it is not possible to estimate the error for the maximum accelerations reported. However, Fig. 3.2 shows that the accelerations derived from films taken at less than 100 Hz are unreliable. This side of the total error curve is driven by SFE, which is not dependent on magnification or the magnitude of acceleration, as discussed earlier.

Many adult fish, including pike and trout, are large enough to accommodate implantations of accelerometers. Therefore, using film to determine accurate accelerations during fast-start studies must be questioned. Even when distance-time data are statistically smoothed before each differentiation, it is still common for small amplitude noise in the distance-time data to be amplified and distort the acceleration-time trace substantially, rendering it useless (Rayner and Aldridge, 1985). The principal assumption made when employing these statistical methods is that there are no sudden changes in force and therefore acceleration (Lanczos, 1956). The accelerometer data in Fig. 3.9 indicate that, in reference to fast-starts of fish, this is a rash assumption. Rates of change of acceleration found here are of the order of 100 m s^{-2} in about 0.02 s.

Miniature accelerometers make direct measurements of acceleration practical and reliable. This argument cannot, however, be extended to all biomechanical analyses of accelerations. For very small animals (e.g., insects, larval fish) or those that cannot be readily tethered (e.g., birds), film studies remain one of the few practical methods available. Film also allows kinematic analyses of accelerative events, so it should be used

where possible.

When film must be used, error can be limited by maximizing image magnification (Fig. 3.5) and selecting the corresponding optimal film speed. Figure 3.2 shows that simply increasing film speed does not necessarily improve the reliability of the derived accelerations, because ME increases exponentially with film speed. Webb (1977, 1978*a*,*b*, 1982) employed film speeds as high as 250 Hz. At this film speed, the minimum total error for images of actual size is of the order of 40% (Fig. 3.2). At extreme magnification (×20) and very high film speeds (>1000 Hz), the practical lower limit of total error approaches zero (Fig. 3.5). Modern high-speed ciné cameras can run at speeds of the order of 10,000-12,000 Hz, so the limiting factor in reducing this error is the magnification of the image which, in turn, is partly dependent on the size of the digitizing tablet. The digitizing tablet should be as large as practically possible.

Magnification is also limited by the behaviour of the specimen. If the direction of the fast-start is unpredictable (e.g., startle response of fish) space must be left on all sides of the specimen in the camera viewfinder. If the behaviour is more predictable, as in predation studies, the camera should be "zoomed-in" on the specimen, leaving space only in the predicted direction of motion.

Experimental evidence for the occurrence of both SFE and ME are presented in Fig. 3.10. The average ratio of theoretical to experimental error is 1.12. The actual average experimental and theoretical errors are 58 and 65%, respectively. It is not surprising that the theoretical error is, in most cases, slightly higher than the the experimental error, because equations 9 and 12 describe the maximal total error expected for any given combination of film speed, image size, and magnitude of acceleration.

Therefore experimentally derived values are expected to fall somewhere below theoretical values. The close relation between the experimentally-derived and theoretical error in Fig. 3.10 indicates that SFE and ME account for a large proportion of the variability between film-derived and direct measurements of acceleration.

Figure 3.9 shows the effect of film speed on the "fit" of film-derived to accelerometer data. Figure 3.2 indicates that the best fit (i.e., lowest error) of the film data will occur at speeds of about 280 Hz. This is supported by the relatively good fit of the data in Fig. 3.9C. The film-derived data in Figs. 3.9A and 3.9D (recorded at 100 and 350 Hz, respectively) indicate the departure from actual values predicted by the total error curve in Fig. 3.2.

The directly measured (accelerometer) data for pike, in Fig. 3.9D, are of particular importance. The maximum acceleration rate of this fast-start, as measured by the accelerometer, was 244.9 m s^{-2}, much higher than the highest previously reported A_{max} of 110 m s^{-2} determined by Webb (1983) for bass (*Micropterus dolomieu*), using film at 60 Hz. The highest previously reported A_{max} for pike was 39.5 m s^{-2} (Webb, 1978*b*), again using film, but at a much higher rate (250Hz). Fig. 3.9A-C indicate that the fast-start acceleration of pike regularly reaches peak rates of 80 to 100 m s^{-2}. Arguably, the escape behaviour analyzed in Fig. 3.9 would maximize fast-start performance. The values reported here indicate that pike are capable of acceleration performance far higher than previously thought.

This Chapter presents one of the first works to use direct measurements of acceleration to estimate the performance of fast-starts of fish. Acceleration-time plots for fish during fast-starts (Fig. 3.9) have never before been presented for either film-derived or accelerometer data.

The acceleration-time plots in Fig. 3.9 were chosen because they are of the same fish (a pike) executing the same behaviour, an escape. However, film showed that the escapes were kinematically different, and this is reflected in the acceleration traces. Figures 3.9A and 3.9D are examples of *C*-shaped escapes, which involve a curved trajectory, whereas Figs. 3.9B and 3.9C represent *S*-shaped escapes where the trajectory is straightaway (the kinematics of fast-starts are discussed in Chapter 1). The accelerometer data show that for pike, the *C*-shaped and *S*-shaped fast-starts produce unimodal and trimodal plots, respectively. A more thorough analysis of this, and comparisons of pike and trout escapes, assessed by accelerometers, are investigated in Chapter 4.

CHAPTER 4

Fast-start Performance of Rainbow Trout *Oncorhynchus mykiss* and Northern Pike *Esox lucius*, During Escapes

A. INTRODUCTION

Weihs (1973) applied the large-amplitude elongated body theory (Lighthill, 1971) to the analysis of fish fast-starts. The optimal body shape, maximizing total thrust force for given energy expenditure at the highest possible rate, was shown to have a rigid front, and flexible rear portion with a large tail; posteriorly located dorsal and anal fins were also found to be beneficial. Therefore fish like northern pike *Esox lucius* have body forms that should maximize acceleration capabilities. However, Webb (1978*b*) measured the fast-start performance of seven species of fish with different morphologies (including pike) and found no significant differences in acceleration performance. It was suggested that the similarities were due to "trade-offs" in body form (e.g., smaller percent muscle mass in laterally compressed fish).

Chapter 3 shows that the method Webb (1978*b*) used to determine acceleration, high-speed ciné film, is subject to considerable error. Here, the escape performances of trout and pike are determined by accelerometry and cinematography. Two species of fish, with different body forms, are observed to test the hypothesis that mean and maximum accelerations during fast-starts are independent of body form.

B. RESULTS

1. Kinematics and Mechanics

Film analysis of escapes reveal that both fish employ the three kinematic stages described by Weihs (1973): preparatory, propulsive and variable. *C* and *S* patterns similar to those described by Webb (1976) are also observed, although the mechanics of *E. lucius* suggests two forms of *S*-shaped fast starts.

Figures 4.1 - 4.5, which have been corrected for tangential acceleration, indicate that there is a functional relation between the mechanics of the escapes, revealed by the accelerometer, and kinematics of these patterns, shown by film. These figures show acceleration, velocity, and distance travelled (after correcting for tangential acceleration) over the same period. It is assumed that the fast-start terminates when the fish reaches its maximum velocity. Comparisons of escape times with those from previous studies which evaluate performance to the end of stage two (e.g., Webb, 1978*b*), indicate that this is valid. Insets show traces from simultaneous film records of the same events. Although these traces are to scale, they have been realigned on the grid and, as such, they represent the orientation of the fish's body with reference to its original position, not the actual distance travelled.

Trout fast-starts can be categorized into two different mechanical types. During type I fast-starts (Fig. 4.1) the fish bends into an *S*, then a *C* shape (numbers 1 and 3 in Fig. 4.1, respectively) and turns considerably more than 90° from its original orientation. Maximum acceleration occurs

Figure 4.1. Mechanical and kinematic data for the type I fast-start of *Oncorhynchus mykiss* (mass = 0.488 kg, fork-length = 0.370 m), corrected for tangential acceleration, showing acceleration, velocity and distance travelled versus time. Numbers on the tracings correspond to those on the acceleration plot. The scale for the grid is 10 cm.

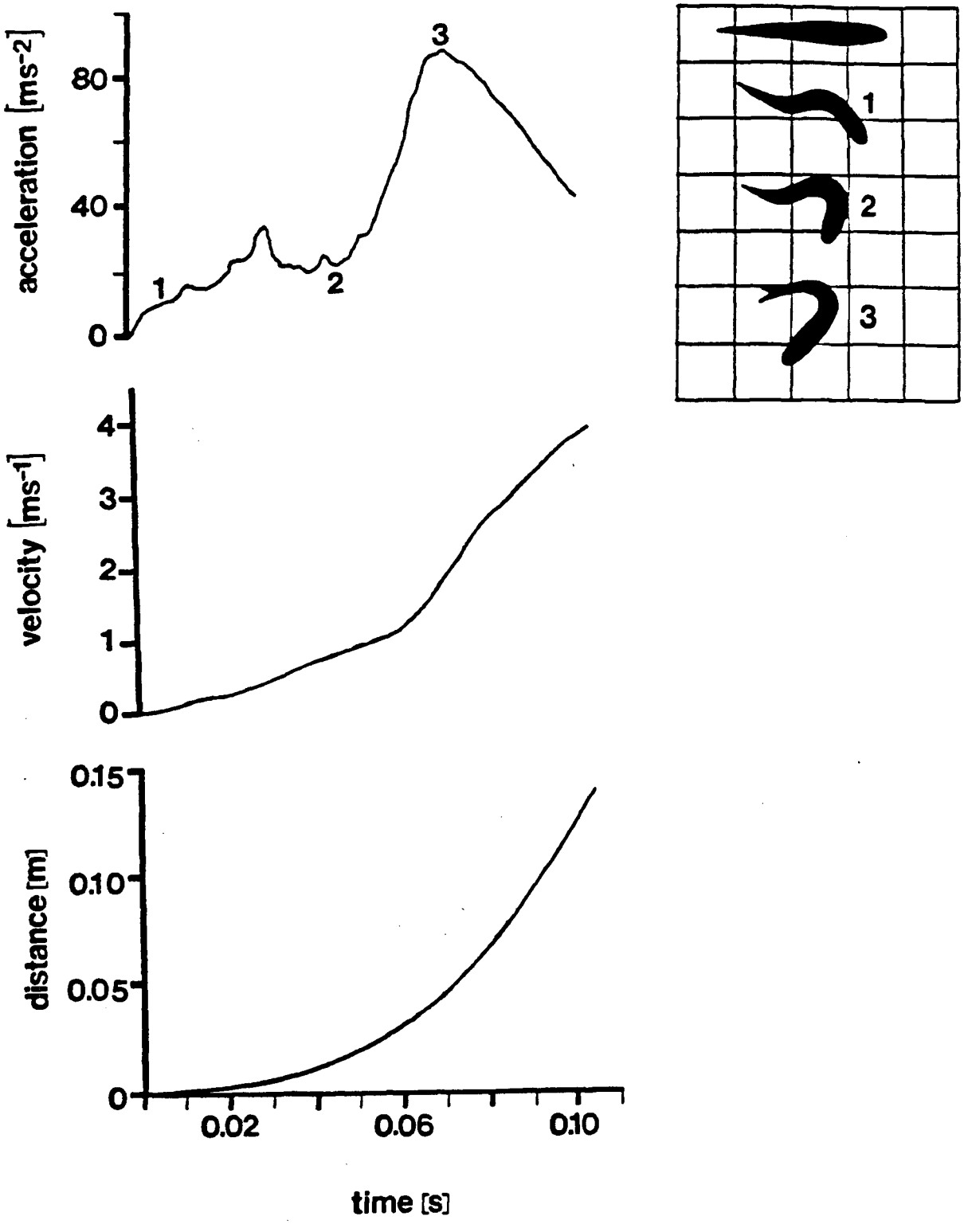
acceleration [ms-2]
80
40
0
1
2
3
velocity [ms-1]
4
3
2
1
0
distance [m]
0.15
0.10
0.05
0
0.02
0.06
0.10
time [s]
1
2
3

Figure 4.2. Mechanical and kinematic data for the type II fast-start of *Oncorhynchus mykiss* (mass = 0.488 kg, fork-length = 0.370 m).

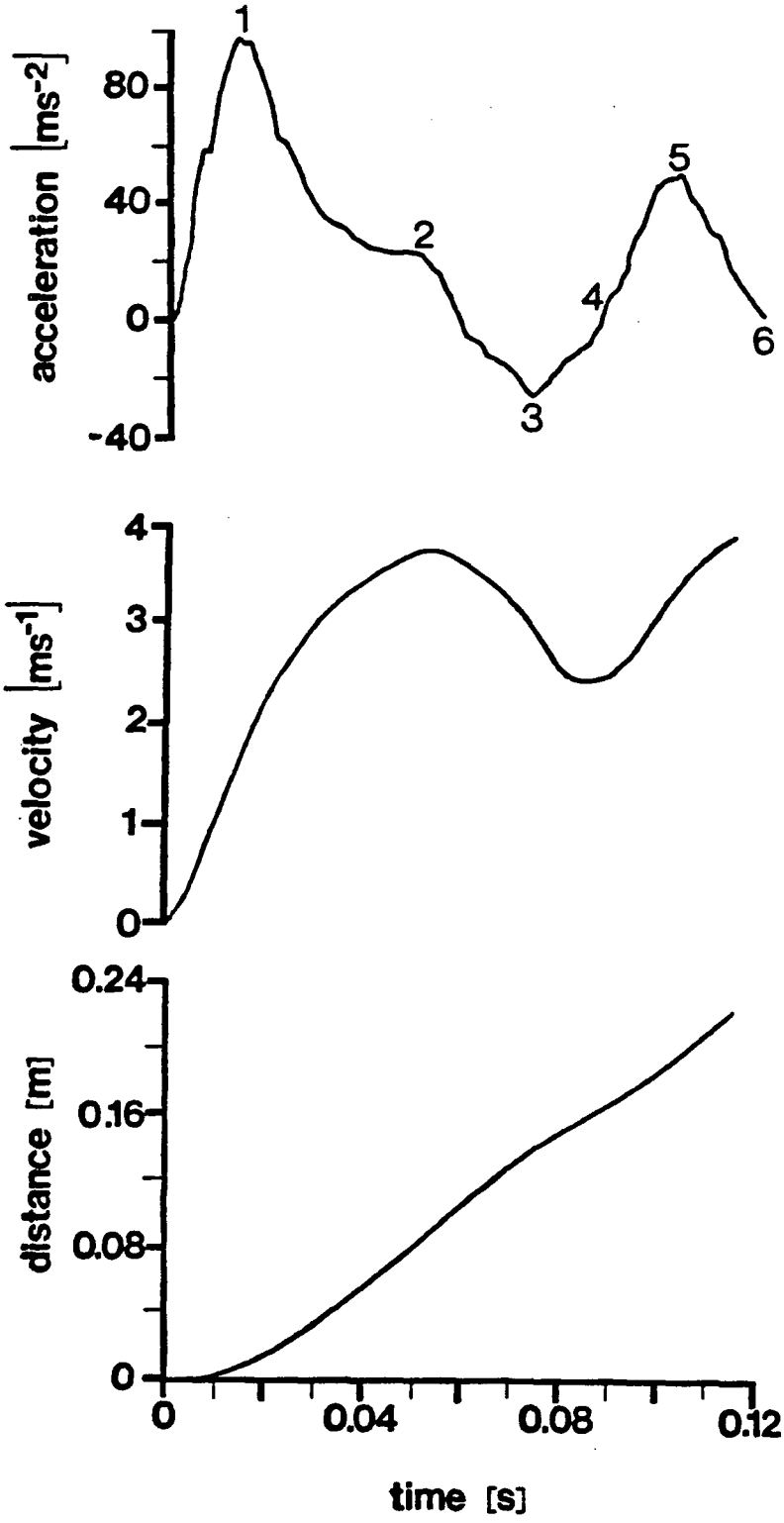
acceleration [ms-2]
80
40
0
-40
1
2
3
4
5
6
velocity [ms-1]
4
3
2
1
0
distance [m]
0.24
0.16
0.08
0
0
0.04
0.08
0.12
time [s]

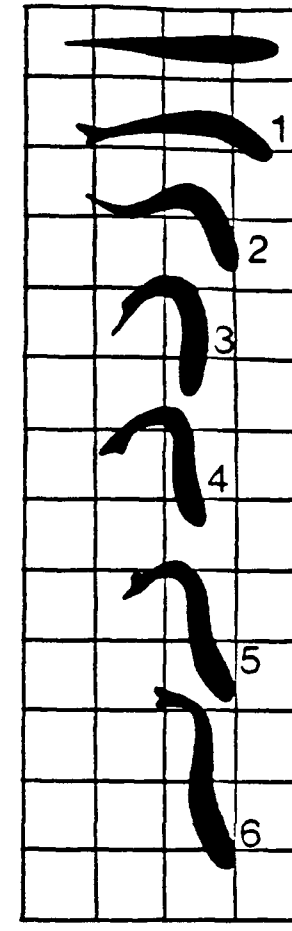
1
2
3
4
5
6

when the head is oriented towards the direction of escape. The acceleration plot for this behaviour is unimodal, rising to one significant peak, then declining. Fig. 4.2 shows a *O. mykiss* escape response characteristic of a type II fast-start. Note that both acceleration and velocity plots are bimodal. Kinematically, the fish again bends into an *S* shape (2), but then turns its head back in the direction of original orientation (4). As its body forms a *C* shape (3), the fish reaches maximal deceleration. Type II escapes involve a turn of about 90° and reach maximum acceleration during the preparatory stage. Relative to the type I escape, a greater distance is covered in the first half of the event, though the total distance travelled is about the same.

Figure 4.3 shows the unimodal acceleration plot typical of a type I fast-start for *E. lucius*. There are similarities with *O. mykiss* type I escapes, other than this unimodal shape. For example, *E. lucius* also bends into an *S* (2), then *C* shape (4). Again, the maximum acceleration is recorded when the head is oriented towards its final destination which, as with *O. mykiss*, is much greater than 90° from its original orientation. The main difference between the two is the magnitude of the performance. The higher acceleration exhibited by *E. lucius* results in a higher final velocity, moving the fish a greater distance in less time.

The type II fast-start of *E. lucius* (Fig. 4.4) is also similar to that of *O. mykiss*. The bimodal shapes of the acceleration and velocity plots are similar, though the point of maximum acceleration is, consistently, at the peak of the second mode rather than the first, as is the case for *O. mykiss*. This, and the earlier decelerative phase, make the peak velocity at the first mode lower. In type II starts, *E. lucius* - unkike *O. mykiss* - never actually bends into a *C* shape; at maximum deceleration (2) a small degree of

Figure 4.3. Mechanical and kinematic data for the type I fast-start of *Esox lucius* (mass = 0.377 kg, fork-length = 0.376 m).

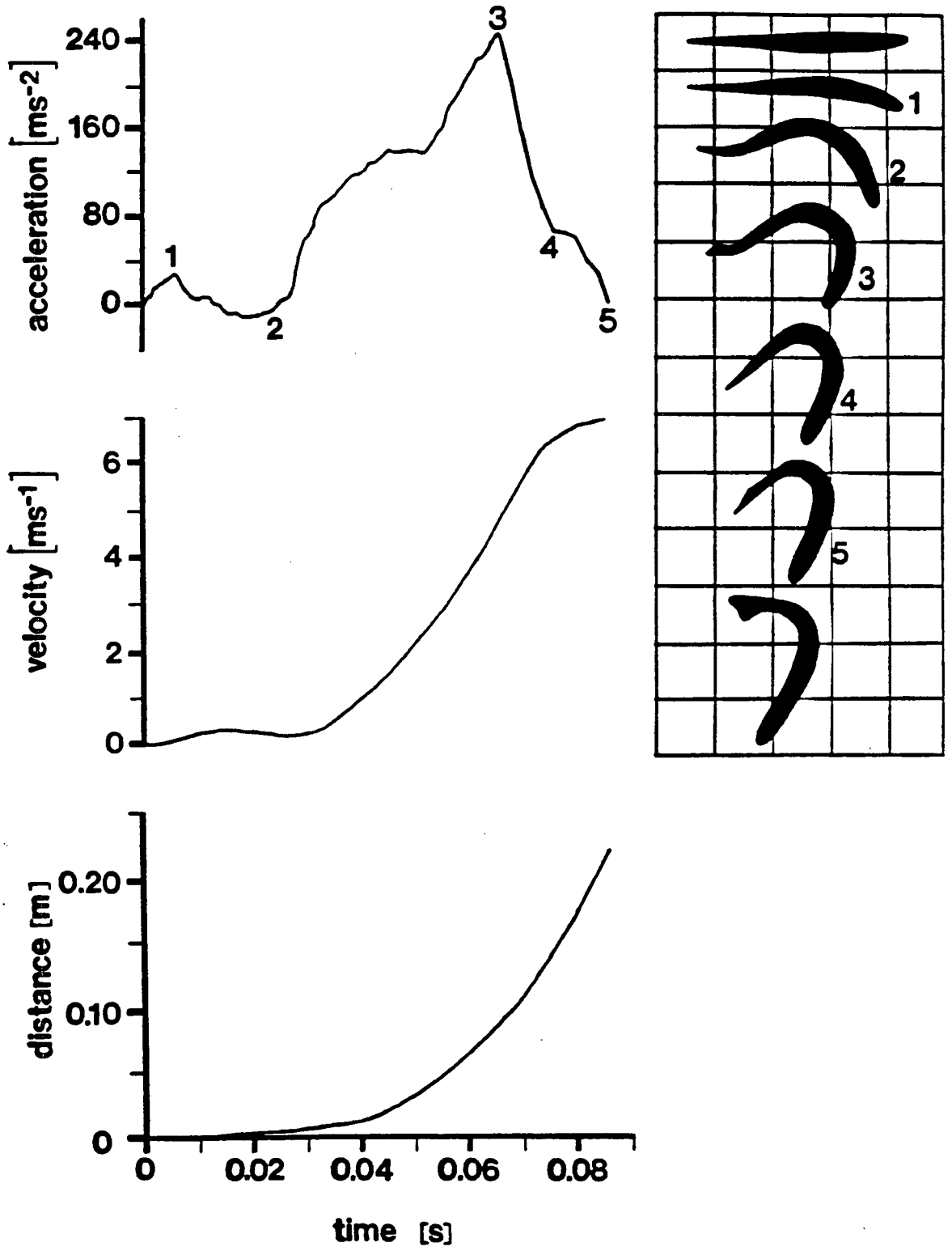
acceleration [ms-2]
240
160
80
0
1
2
3
4
5
velocity [ms-1]
6
4
2
0
distance [m]
0.20
0.10
0
0
0.02
0.04
0.06
0.08
time [s]

Figure 4.4. Mechanical and kinematic data for the type II fast-start of *Esox lucius* (mass = 0.372 kg, fork-length = 0.363 m).

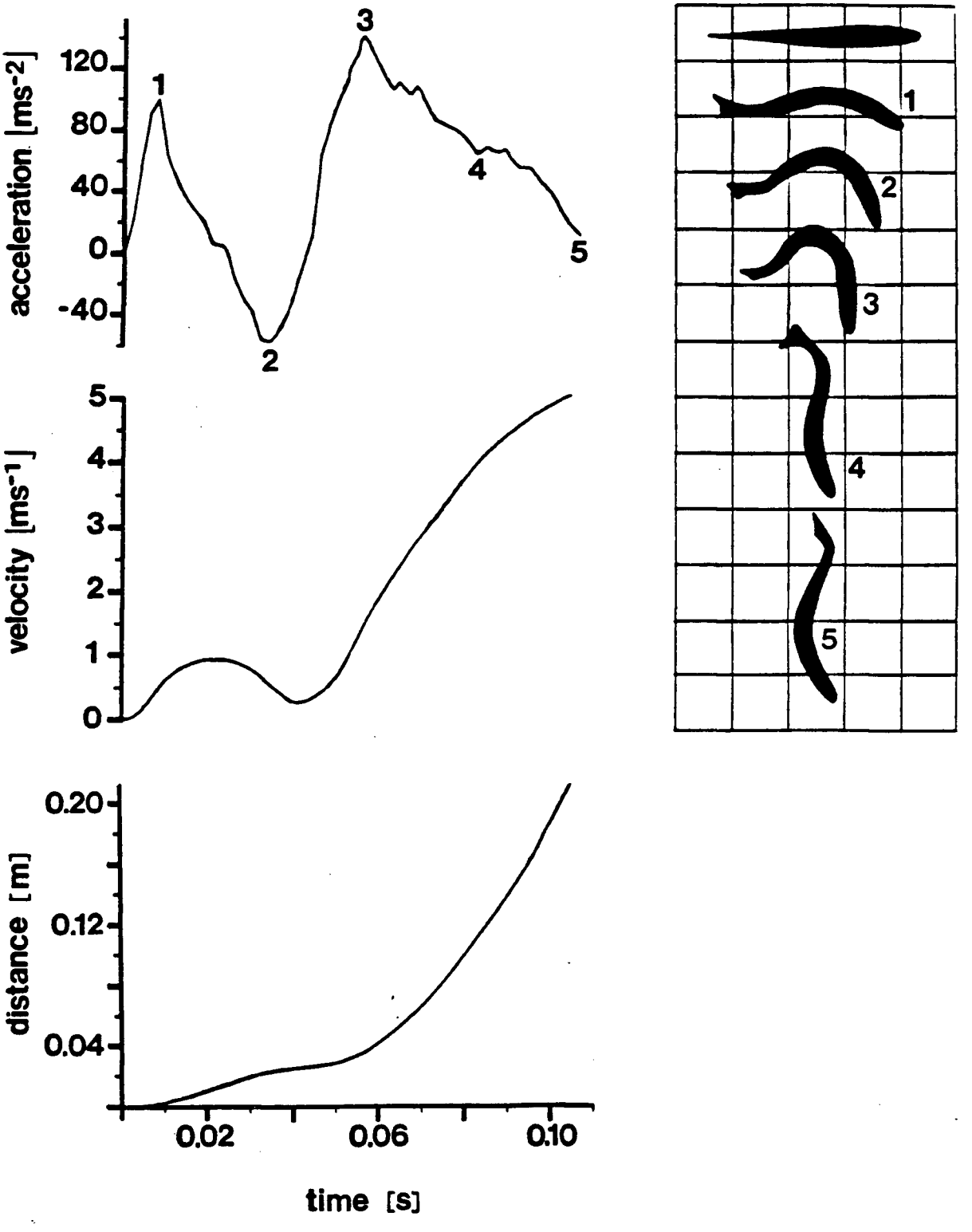
acceleration [ms-2]
120
80
40
0
-40
1
2
3
4
5
velocity [ms-1]
5
4
3
2
1
0
distance [m]
0.20
0.12
0.04
0.02
0.06
0.10
time [s]

Figure 4.5. Mechanical and kinematic data for the type III fast-start of *Esox lucius* (mass = 0.322 kg, fork-length = 0.356 m).

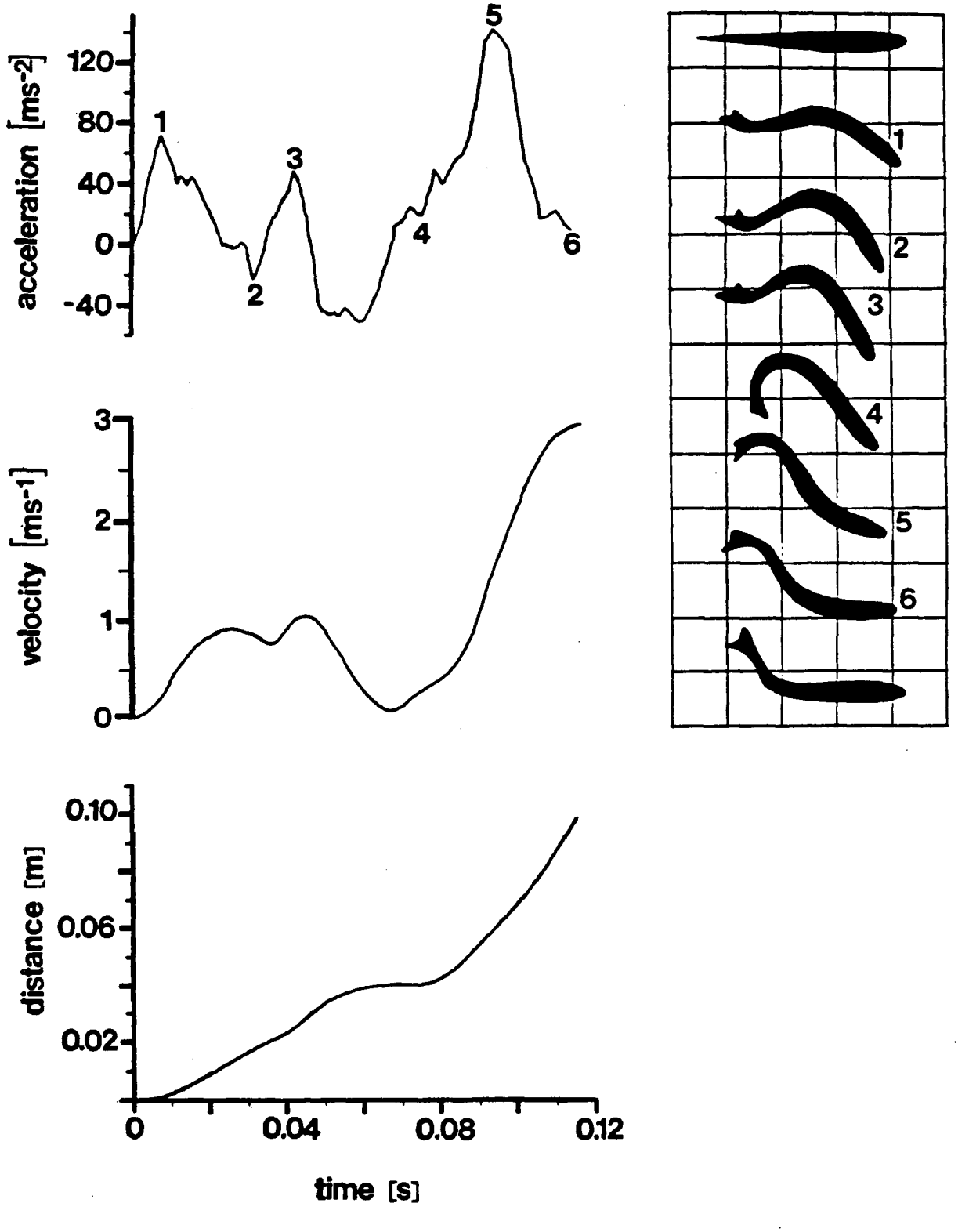
acceleration [ms-2]
120
80
40
0
-40
1
2
3
4
5
6
velocity [ms-1]
3
2
1
0
distance [m]
0.10
0.06
0.02
0
0.04
0.08
0.12
time [s]

reverse curvature is seen at the tail. As with *O. mykiss*, the final orientation is about 90° from the original one.

Type III fast-starts (Fig. 4.5), have characteristic trimodal acceleration and velocity plots and are observed during escapes of *E. lucius*. In Fig. 4.5, the fish almost stops before the third increase in acceleration. Arguably, the objective of this type of fast-start is to maintain directional stability and orient in the same direction as originally aligned. From a still position to orientation (2), the acceleration and kinematics are similar to a type II escape. After this point, a second, reverse *S* shape is produced by the body which changes course back to the original orientation.

Fifty-five escapes were analyzed; 30 by *O. mykiss* and 25 by *E. lucius*. The mechanical types described here are representative of each species because all individuals exhibited the behaviour patterns characteristic of its species and no other behaviour patterns were observed. *O. mykiss* employed type I escapes 60% and type II 40% of the time. Since *C*- and *S*-starts are kinematically similar to type I and II escapes, respectively, these results can be compared to, and are in agreement with, values reported by Webb (1976) for *O. mykiss* of this size. *E. lucius* exhibited type II escapes 44% of the time; the remaining fast-starts being divided evenly between type I and III (28% each).

2. Effect of Tangential Acceleration

The magnitude of the tangential acceleration is presented as percent changes to the accelerometer data in Table 4.1. The effect on the performance records from the trout is significant; reductions in all

Table 4.1. Mean effect of tangential acceleration on performance data, expressed as percent changes to accelerometer values. Combined data, disregarding mechanical types, for each species are presented as totals. Errors are given in brackets as ± 2 S.E. Data includes samples from all eight trout and four pike.

		n	Distance	Mean Velocity	Mean Maximum Velocity	Mean Acceleration Rate	Mean Maximum Acceleration
	Type I	9	-32.6	-34.1	-24.1	-22.3	-6.6
			(±2.1)	(±3.8)	(±3.4)	(±3.0)	(±2.5)
Salmo	Type II	4	-28.4	-28.6	-18.8	-17.6	-8.8
			(±3.6)	(±3.7)	(±3.8)	(±3.8)	(±3.6)
	Total	13	-31.1	-32.4	-22.5	-20.8	-7.3
			(±2.0)	(±3.2)	(±3.2)	(±2.8)	(±2.0)
	Type I	3	-18.8	-6.8	-9.2	-10.9	10.3
			(±2.6)	(±5.6)	(±4.7)	(±4.4)	(±4.6)
Esox	Type II	6	-11.1	-8.5	-3.8	-3.7	4.0
			(±2.9)	(±2.8)	(±2.4)	(±2.4)	(±4.2)
	Type III	3	-10.9	-10.5	-9.0	-11.3	7.1
			(±2.8)	(±2.8)	(±2.6)	(±3.0)	(±3.2)
	Total	12	-12.5	-8.5	-6.5	-7.4	6.4
			(±2.6)	(±2.7)	(±2.0)	(±2.2)	(±2.8)

performance parameters, apart from mean maximum acceleration, range from about 20-30%. Pike performance records are affected to a lesser degree, amounting to reductions in the order of 5-10%. It is of interest that the mean maximum acceleration of pike, as measured by the accelerometer, actually underestimates the true value by 6.4%. This is due to a tendancy for the fish to reach maximum acceleration near the end of the curved portion of the escape trajectory. At this point the rate of change of angular velocity, and therefore tangential acceleration, is negative. The effect of tangential acceleration on each mechanical fast-start type is also presented in Table 4.1. It would appear that this factor is of greatest influence during type I fast-starts, because angular velocities are higher.

3. Escape Performance

Escape performance, measured here with subcutaneously implanted accelerometers, is presented in Table 4.2. Performance values are grouped into mechanical types, and are also presented as totals, combining types, for both *O. mykiss* and *E. lucius*. The duration of the escapes ranges from 0.085 s for *E. lucius* type I, to 0.134 s for *O. mykiss* type I fast-starts. Distance travelled is greatest for *E. lucius* type III (0.223 m) and least for *O. mykiss* type I (0.141 m) escapes. The remaining ranges of performance are all least for *O. mykiss* Type I and greatest for *E. lucius* Type I behaviours. Mean velocities range from 1.16 to 2.27 m s^{-1}; mean maximum velocities are 2.79 and 4.70 m s^{-1}. Mean acceleration rates from 21.4 to 57.4 m s^{-2} were observed; mean maximum accelerations range from 56.6 $^{-2}$ to 157.8 m s^{-2}.

Table 4.2. Results of escape performance for *Oncorhynchus mykiss* and *Esox lucius* determined by accelerometry. Errors are given in brackets as ± 2 S.E. Totals combine data, regardless of mechanical type, for each species. In total, eight trout and four pike were used.

		n	Total Time (s)	Distance (m)	Mean Velocity (ms^{-1})	Mean Maximum Velocity (ms^{-1})	Mean Acceleration Rate (ms^{-2})	Mean Maximum Acceleration (ms^{-2})
	Type I	18	0.134	0.141	1.16	2.79	21.4	56.6
			(±0.019)	(±0.020)	(±0.19)	(±0.35)	(±4.0)	(±10.1)
Salmo	Type II	12	0.110	0.142	1.29	2.74	24.1	64.7
			(±0.015)	(±0.043)	(±0.27)	(±0.63)	(±3.6)	(±14.3)
	Total	30	0.125	0.141	1.21	2.77	22.4	59.7
			(±0.014)	(±0.020)	(±0.15)	(±0.31)	(±2.8)	(±8.3)
	Type I	7	0.085	0.194	2.27	4.70	57.4	157.8
			(±0.005)	(±0.044)	(±0.28)	(±0.52)	(±7.0)	(±37.3)
	Type II	11	0.110	0.192	1.76	3.69	33.2	107.9
Esox			(±0.013)	(±0.032)	(±0.18)	(±0.46)	(±5.0)	(±16.4)
	Type III	7	0.132	0.223	1.72	3.61	25.1	91.4
			(±0.013)	(±0.027)	(+0.31)	(±0.68)	(±6.6)	(±22.8)
	Total	25	0.108	0.201	1.90	3.97	37.6	120.2
			(±0.010)	(±0.020)	(±0.17)	(±0.36)	(±6.1)	(±20.0)

Table 4.3. Descriptive statistics for comparison of escape performance both within and between species. Probabilities are indicated; NS denotes comparisons that are not significantly different. Where a significant difference is indicated, reference to Table 4.2 will reveal which is the larger. Tukey's test is used for all comparisons except where combined data, regardless of mechanical type, are compared using the two-sample Student's *t*-test.

Comparison		Time (s)	Distance (m)	Mean Velocity (ms^{-1})	Maximum Velocity (ms^{-1})	Mean Acceleration Rate (ms^{-2})	Mean Maximum Acceleration (ms^{-2})
Salmo	**Type I vs. II**	NS	NS	NS	NS	NS	NS
	Type I vs. II	NS	NS	$P < 0.05$	NS	$P < 0.001$	$P < 0.01$
Esox	**Type I vs. III**	$P < 0.025$	NS	NS	NS	$P < 0.001$	$P < 0.005$
	Type II vs. III	NS	NS	NS	NS	NS	NS
	*S*I vs. *E*I	$P < 0.001$	NS	$P < 0.001$	$P < 0.001$	$P < 0.001$	$P < 0.001$
	*S*I vs. *E*II	NS	NS	$P < 0.001$	$P < 0.05$	$P < 0.005$	$P < 0.001$
Salmo (S)	*S*I vs. *E*III	NS	$P < 0.025$	$P < 0.025$	NS	NS	NS
versus	*S*II vs. *E*I	NS	NS	$P < 0.001$	$P < 0.001$	$P < 0.001$	$P < 0.001$
Esox (E)	*S*II vs. *E*II	NS	NS	$P < 0.05$	NS	NS	$P < 0.05$
	*S*II vs. *E*III	NS	$P < 0.05$	NS	NS	NS	NS
	Total	$P < 0.05$	$P < 0.001$	$P < 0.001$	$P < 0.001$	$P < 0.001$	$P < 0.001$

Statistical analyses (Table 4.3) employ the Student's *t*-test to identify differences in performance between species, when all escapes are considered, indicating significant differences for all performance parameters. The data sets were then considered according to mechanical type, for both species. One-way analysis of variance again showed strong significant differences between means for all parameters. Finally Tukey's test was used to indicate where robust differences between means were to be found, considering all possible comparisons.

Table 4.3 shows no significant difference between the type I and II escapes exhibited by *O. mykiss*. From Figs 3 and 4, it is evident that the maximum rate of acceleration is reached more quickly in the type II fast-start. From Table 4.3, it is also evident that no significant differences exist in comparisons of *E. lucius* type II and III fast-starts, nor is there any difference for within-species comparisons of distance or mean maximum velocity. When *E. lucius* type I fast-starts are compared to types II and III, significant differences in performance are identified, particularly with respect to mean and maximum acceleration. In all such comparisons it is the type I behaviour that exhibits the highest performance.

Comparisons of *E. lucius* and *O. mykiss* escapes reveal an array of significant differences, particularly where *O. mykiss* and *E. lucius* type I escapes are compared. In contrast, when compared to *E. lucius* type III escapes, neither of the *O. mykiss* behaviour patterns (types I and II) were found to have significantly different mean or maximum acceleration, maximum velocity, or duration. When the type II behaviours for each species are compared, similar levels of performance are exhibited, except with reference to mean velocity and maximum acceleration. Where differences are identified, Table 4.2 indicates that *E. lucius* displays the higher performance.

C. DISCUSSION

1. Sources of Error

Criticism of the use of accelerometry centres around three major points; the introduction of rotational accelerations due to the curvilinear trajectory, the possibility that transient motion may occur between the body of the fish and the accelerometer, and consideration of the orientation of the instrument with respect to the centre of mass.

Point-by-point analysis of film shows that the trajectory along which the centre of mass travels during a fast-start is not linear, but forms a series of alternating, left- and/or right-hand curves. In fact, any point along the centre-line of the fish will follow these curves, though amplitudes increase with distance from the centre of mass. Since the accelerometer used in this study is firmly implanted parallel to the centre-line of the fish, it will also follow a curved trajectory. The accelerometers employed here are sensitive only along the long axis of the instrument, so they record only in the forward (and rearward) direction, at any time. They will, however, detect rotational accelerations tangent to the curved trajectory. Tangential accelerations can be calculated, and accelerometer values corrected, assuming film data are available. Table 4.1 shows that this correction is not consistant for all performance parameters and that it varies between species. The relative changes in performance values (except maximum acceleration) for *O. mykiss* are about three times those of *E. lucius*. This is primarily due to two factors; *O. mykiss* escapes have curvatures of smaller radii and longer duration and, though the

absolute values for tangential acceleration are similar, they represent proportionally lower values in *E. lucius*, owing to the higher levels of performance.

Because of tangential accelerations, the use of accelerometry requires simultaneous film data when trajectories are curved. However, for stereotypic events this component of acceleration, and its effect on predicted velocities and distances, can be detertmined initially, then factored into subsequent events measuring performance by accelerometry alone. Table 4.1 also shows that studies evaluating only maximum accelerations would be much less influenced by tangential accelerations.

The orientation of the accelerometer with respect to the centre of mass is important because misalignment would cause the instrument to detect a component of centripetal acceleration, which is directed perpendicular to the tangent of the curved trajectory (and is not, therefore, normally realized by the directionally biased accelerometer). A worst-case scenario, where the accelerometer was oriented 10° from the tangent to the curve, was investigated. Several escapes were re-evaluated in this manner, considering all components of acceleration. Comparisons to accelerations assuming perfect alignment showed that the net effect was maximally less that 5%.

Another important consideration when employing accelerometry is that tissue flexibility could introduce transient motions between the musculature of the fish and the accelerometer. With respect to this problem, and that of accelerometer orientation, it is worth reiterating the importance of ensuring proper implantation by following the procedure described in Chapter 2. To estimate the effect of both transient motion and orientation on accelerometer data, values for displacement, as predicted by film and accelerometry, were compared (Fig. 4.6). Had these two factors produced

Figure 4.6. Predicted escape displacements compared to film data. The solid line represents film data versus themselves, for comparison to accelerometer predictions of distance (open circles) and corrected predictions (closed circles) once tangential accelerations have been considered. Regression lines have r^2 values of 0.68 for accelerometer data (long-dashed line) and 0.94 for corrected data (short-dashed line).

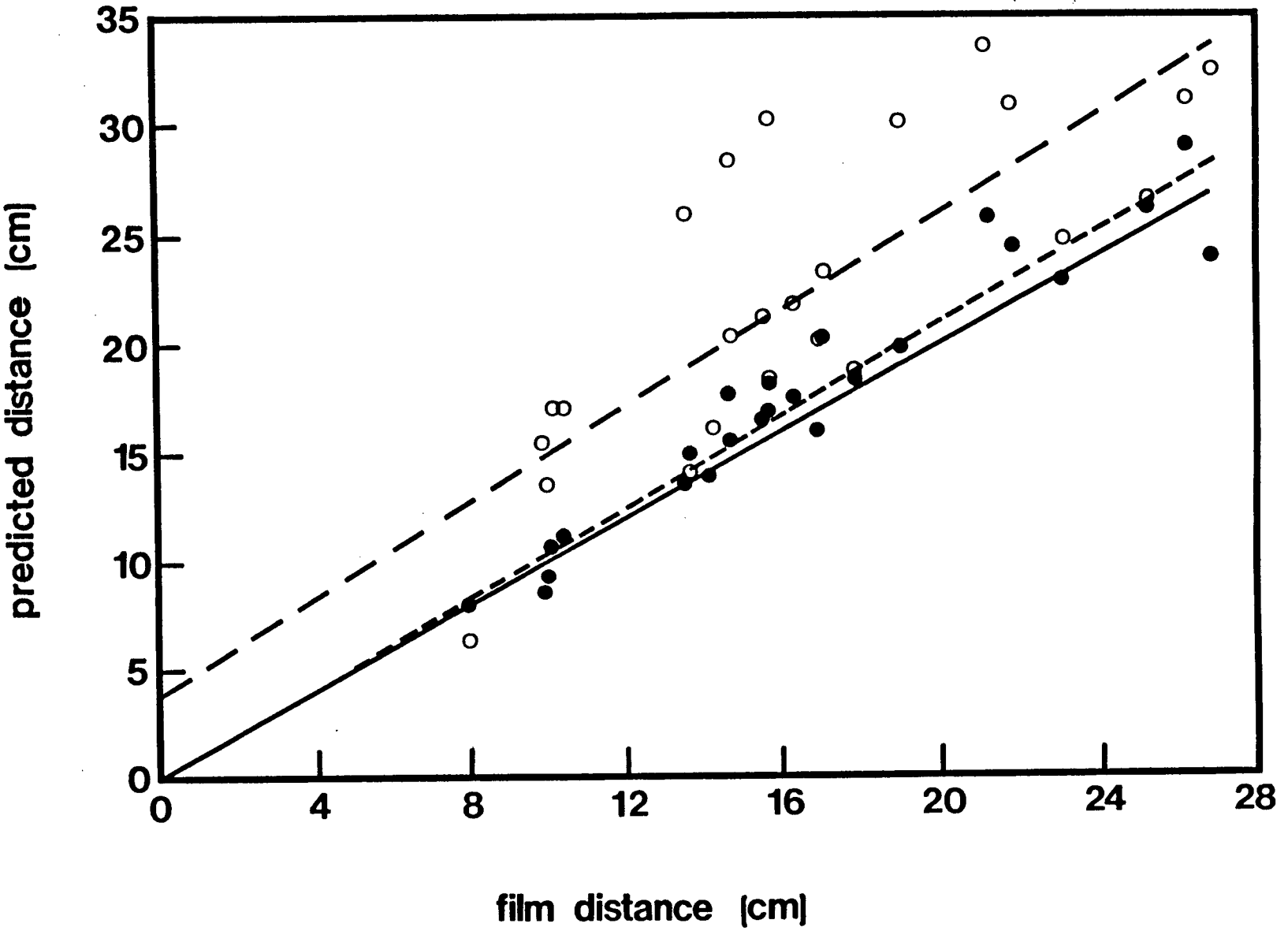
predicted distance [cm]
film distance [cm]
0
5
10
15
20
25
30
35
0
4
8
12
16
20
24
28

significant effects on acceleration, this would be propagated through the integrations giving velocity and distance data. Fig. 4.6 shows that once tangential acceleration is considered, the difference between film and accelerometer estimation of displacement is small. Incidently, this comparison would also account for any other sources of error in the accelerometer data.

Another potential problem is the calibration of the accelerometers. The accelerometers used here are calibrated using a back-to-back comparison technique against a reference standard. They were also calibrated in the laboratory to determine how output voltage translates to actual accelerations (Chapter 2).

2. Comparison With Previous Studies

Results of previous studies are presented, in chronological order, in Table 4.4. Since all performance parameters were rarely reported, some of the data in Table 4.4 had to be calculated from that given, or from given formulae. Research evaluating only displacements are not included because this study focuses on other aspects of performance, particularly acceleration. Data from Eaton *et al.* (1977) are also omitted, because their performance was measured with respect to the rostral tip of the nose. Webb (1978*b*) explains why such comparisons are unjustified. Therefore Table 4.4 is not comprehensive, but does reflect the bulk of previous performance data of the sort measured here.

Previous reports of mean maximum acceleration during escapes are as high as 50 m s^{-2} for pike *Esox lucius* (Weihs, 1973). Webb (1978*b*) found values of 40 m s^{-2} for teleosts, with 95% confidence limits of ±25% of the

Table 4.4. Chronological review of comprehensive fast-start performance data reported in the literature. Studies reporting displacements only, or those evaluating performance with respect to points other than the centre of mass are omitted. Symbols are: † calculated from data, †† calculated from formulae, ‡ read from figures, * single event, ** larval fish, 1 *S*-start, and 2 *C*-start.

		Mean Maximum Acceleration (ms^{-2})	Mean Acceleration Rate (ms^{-2})	Mean Maximum Velocity (ms^{-1})	Mean Velocity (ms^{-1})	Distance (m)	Time (s)	Species	Common Name	Length (m)	Method	Rate (Hz)
Weihs	1973	40.0	-	-	-	-	-	*Salmo trutta*	Trout	-	film	-
		50.0	-	-	-	-	-	*Esox*	Pike	-	film	-
		25.5	20.6	-	0.57†	0.113‡	0.200‡	*Oncorhynchus mykiss*	Rainbow trout	0.330	film	40
Webb	1975	42.1	12.1	1.21	0.72†	0.056	0.078	*Oncorhynchus mykiss*	Rainbow trout	0.143	film	64
		15.7	8.1	0.67	0.36†	0.029	0.079	*Lepomis cyanellus*	Green sunfish	0.080	film	64
		95.0	-	-	-	-	-	*Oncorhynchus mykiss*	Rainbow trout	- *	film	64
Dubois *et al.*	1976	23.5	-	2.80	-	-	0.210	*Pomotamus saltatrix*	Bluefish	0.630*	accelerometer	
Webb	1976	40.6	17.6	2.85	1.63†	0.163	0.100	*Oncorhynchus mykiss*	Rainbow trout	0.387	film	64
Webb	1977	26.6	8.6	1.44	0.70†	0.076	0.109	*Oncorhynchus mykiss*	Rainbow trout	0.174	film	250
Webb	1978*a*	41.0	-	1.71	1.13†	0.113	0.100	*Oncorhynchus mykiss*	Rainbow trout	0.136	film	250
Webb	1978*b*	39.5	10.4	1.56	0.73	0.084‡	0.115‡	*Esox sp.*	Tiger musky	0.217	film	250
		32.6	10.6	1.58	0.75	0.085‡	0.114‡	*Oncorhynchus mykiss*	Rainbow trout	0.195	film	250
		23.9	9.3	1.15	0.50	0.051‡	0.103‡	*Perca flavescens*	Yellow perch	0.155	film	250
		28.8	12.3	1.30	0.67	0.059‡	0.088‡	*Lepomis macrochirus*	Bluegill	0.153	film	250
		28.7	11.0	1.14	0.49	0.038‡	0.078‡	*Notropis cornutus*	Common shiner	0.107	film	250
		22.7	6.1	0.77	0.43	0.035‡	0.081‡	*Cottus cognatus*	Slimy sculpin	0.082	film	250
		32.3	10.3	0.89	0.43	0.024‡	0.056‡	*Etheostoma caeruleum*	Rainbow darter	0.062	film	250
Rand and Lauder	1981	-	21.1†	2.47†	1.08†	0.100†	0.092	*Esox niger*	Chain pickerel	0.273	film	200
Webb and Corolla	1981	-	-	0.38†	0.21†	0.068†	0.323	*Engraulis mordax*	Northern anchovy	0.013**	film	250
Webb	1982	-	-	-	1.01†	0.147††	0.146	*Oncorhynchus mykiss*	Rainbow trout	0.298	film	240
Webb	1983	80.0	-	2.50	-	-	-	*Oncorhynchus mykiss*	Rainbow trout	0.257*	film	60
		110.0	-	2.50	-	-	-	*Micropterus dolomieu*	Smallmouth bass	0.236*	film	60
Webb	1986	-	19.0‡	1.36	-	-	-	*Esox sp.*	Tiger musky[1]	0.065	film	60
		-	16.0‡	-	-	-	-	*Esox sp.*	Tiger musky[2]	0.065	film	60
		-	15.0‡	0.96	-	-	-	*Micropterus salmoides*	Largemouth bass	0.051	film	60
		-	14.5‡	1.01	-	-	-	*Lepomis macrochirus*	Bluegill	0.064	film	60
		-	11.5‡	0.81	-	-	-	*Pimephales promelas*	Fathead minnow	0.058	film	60

mean, though an individual smallmouth bass was reported to have accelerated at 110 m s^{-2} (Webb, 1983). Mean acceleration rates for rainbow trout *O. mykiss*, chain pickerel *Esox niger*, and tiger musky *Esox* sp. are, maximally, about 20 m s^{-2} (Weihs, 1973; Rand and Lauder, 1981; Webb, 1986, respectively). Maximum velocities range up to 2.85 m s^{-1} for *O. mykiss*, with mean velocities for the same species of 1.63 m s^{-1} (Webb, 1976). Fast-start durations range from about 0.056 s for *Etheostoma caeruleum* (Webb, 1978*b*) to 0.323 s for larvae of the northern anchovy, *Engraulis mordax* (Webb and Corolla, 1981).

Comparisons of results reported here employing accelerometry (Table 4.2), to film based studies (Table 4.4) demonstrate that, while most performance parameters for *O. mykiss* fall near the high range of previous results (with the exception of maximum acceleration), the values for *E. lucius* greatly exceed previously reported data for any species. The reason for the large disparity of mean maximum accelerations for both species is probably the large degree of error inherent in evaluating accelerations from double-differentiated, film-generated, distance-time data. Chapter 3 shows that, when determined from film, maximum accelerations incorporate errors of 35-100 % of reported values, for the range of sampling rates in Table 4.4. Only one previous study (Webb, 1978*b*) assesses a member of the genus *Esox* in a comprehensive manner. It is possible that the fish used in that study were performing sub-maximally. Table 4.4 indicates that high levels of escape performance are exhibited by *E. lucius*. It is therefore not suprising to find higher levels of performance in this species, considering the advanced methodology.

3. Maximum Performance

Except for escape duration (given accurately by film), the performance values reported in Table 4.2 are the highest yet reported for *E. lucius*. These are mean values, however, averaged for a number of specimens, each executing a number of fast-starts. This is necessary when making the statistical comparisons summarized in Table 4.3. It is also important when using this information in ecological models, such as those that predict feeding energetics or daily energy budgets.

The limits of performance (single, maximum performance, fast-starts) are also of interest because such information is useful in assessing the energetic cost of unsteady swimming, optimal behaviour during predator-prey interactions, and feeding efficiency of ambush predators, to name but a few applications. Also, since fish are stimulated artificially, under laboratory conditions, it is likely that they do not always react maximally, as they would to a predator, and may habituate to the stimulus. Reporting maximum values (Table 4.3), therefore, is important because it reveals the fish's capability under extreme conditions. Table 4.2 shows that *E. lucius* employ escape behaviour patterns other than that which would maximize performance. This implies that the fish are, at times, performing sub-maximally under experimental conditions.

Table 4.5 lists the maximum levels of performance for both species, for each type of escape. Performance values are much higher than any previously reported for *O. mykiss* and *E. lucius*. In fact, the absolute values reported here for the *E. lucius* type I escape are the highest reported for any fish. Webb (1975, 1978*b*, respectively) does report single maximum accelerations of

Table 4.5. Maximum levels of performance for all escape types exhibited by *Oncorhynchus mykiss* (mass = 0.488 kg, fork-length = 0.370 m) and *Esox lucius* (mass = 0.377 kg, fork-length = 0.376 m).

		Distance (m)	Maximum Mean Velocity (ms^{-1})	Maximum Final Velocity (ms^{-1})	Maximum Mean Acceleration (ms^{-2})	Maximum Acceleration Rate (ms^{-2})
Salmo	Type I	0.149	1.87	4.19	32.6	95.7
	Type II	0.223	1.93	3.94	32.0	97.8
	Type I	0.213	2.50	7.06	80.3	244.9
Esox	Type II	0.289	2.26	4.70	47.4	141.2
	Type III	0.227	2.14	4.50	35.5	130.5

95 m s^{-2} for *O. mykiss* and 110 m s^{-2} for *Micropterus dolomieu*, but this was derived from film recorded at 64 and 60 Hz, respectively, which Chapter 2 shows to involve an error of about 100%.

4. Comparison Between Species

This is the first study to demonstrate conclusive differences in mean and maximum accelerations for fish of different body forms. Webb (1978*b*) concluded that these performance parameters were independent of body form. In a later study relating escape behaviour to body form for teleost prey, Webb (1986) claims that tiger musky, *Esox* sp., had the highest mean acceleration rates, followed by bluegill *Lepomis macrochirus*, largemouth bass *Micropterus salmoides* and fathead minnow *Pimephales promelas*. However, the study used 60 Hz video film to determine acceleration which, as stated previously, is subject to large error. In the same study Webb derives an acceleration coefficient - a dimensionless factor relating the product of motor (muscle) and propellor (body and tail) thrust to the mass accelerated. This indicates that fish forms such as *E. lucius* have the highest acceleration coefficients, while those with morphologies like *O. mykiss* have lower coefficients.

Fish morphologies have evolved, in part, as a response to two functionally different hydrodynamic requirements: one specialized for long distance swimming, the other for rapid lunges (Weihs and Webb, 1983). Results here indicate that *E. lucius* are capable of much higher escape (lunging) performance than are *O. mykiss* of similar size. This supports previous suggestions (Weihs, 1973; Lighthill, 1975; Weihs and Webb, 1983; Webb, 1986) that the body form of *E. lucius* is well adapted to this type of

behaviour. The body form of *O. mykiss* is considered to be that of a generalist, displaying some characteristics that enhance steady swimming and some that benefit fast-starts (Webb 1978*b*).

5. Fast-Start Types

The integration of mechanics and kinematics (Figs 4.1 - 4.3) affords more detailed insight into fish fast-starts. In addition to simple kinematic categorizations, such as *C* and *S* patterns (Webb, 1976), it is clear that a mechanical basis underlies the kinematic observations. Accelerometer plots reveal that at least three different types of fast-starts exist: uni-, bi-, and trimodal. Dubois *et al.* (1976, Fig. 4) also provides acceleration-time plots which indicate type I and type II escapes in a bluefish *Pomatomus saltatrix*. However, because the elapsed time of this event is much longer than the events here, and because the correlation with kinematics is not as clear, a direct comparison is not possible.

CHAPTER 5

Prey capture and the fast-start performance of northern pike *Esox lucius*

A. INTRODUCTION

Many fish use fast-starts to escape predators, while some employ fast-starts to attain prey. Pike are "ambush" predators because they stalk prey and use rapid lunges during feeding. It is reasonable to assume that body forms like the pike's have adapted to maximize acceleration during these feeding lunges. This may, in turn, affect their escape performance.

Here, subcutaneously implanted accelerometers and simultaneous high-speed ciné film are used to investigate the feeding performance of the northern pike *Esox lucius*. The results are compared to escapes by the same individuals to determine whether the fast-start performance is compromised during feeding, since directional control is important. The kinematics and mechanics of the feeding behaviours are documented and their relation to the size and distance of the prey is investigated.

B. MATERIALS AND METHODS

Preliminary trials involved introducing one, then several goldfish into the experimental arena. This method was rejected, primarily because the goldfish tended to huddle in the corners of the tank, which greatly limited the performance of the pike. It was also evident that performance was not inhibited by the lights, but pike were sensitive to the presence of the investigators.

A blind was erected about 3 m in front of the tank and a system of pulleys and remote controls allowed manipulation of the camera and oscilloscope. The goldfish were maintained in the centre of the tank by a fine thread attached to their lower lip, which was affixed to an overhead lever. Ample slack in the thread allowed normal swimming behaviour near the centre of the tank. The position of the prey ensured that the walls of the tank would not interfere with the event. The goldfish ranged in size (fork-length) from 0.024 to 0.053 m.

Early observations also indicated that pike initiate strikes following sudden movements of their prey. A gentle tug on the overhead lever (from behind the blind) elicited an escape response from the goldfish which, in turn, initiated the attack, thereby affording some control over the approximate start-time of the event.

The field of view provided by the camera allowed only one-half of the tank to be filmed when maximizing the image size of the pike. Since the camera was in front of the blind, it was necessary to predetermine the view from a given orientation of the camera. This allowed the camera to be aligned to film the entire feeding event.

C. RESULTS

1. Predator-Prey Behaviour

Pike remained stationary in the arena while the prey was secured to the overhead lever arm. The goldfish were distressed upon introduction to the tank, but this subsided after a few seconds. The distress attracted the attention of the pike, which would orient head-long towards the prey. Goldfish movements consisted of small darting motions; pike tracked the prey axially, powered by median and paired fins.

Feeding events usually followed cessation of prey activity. Pike often moved slowly towards the goldfish, maintaining a straight-stretched posture. Occasionally sudden erections of the median fins, were observed independently from accelerative movements. Because median fins are erected prior to acceleration as part of the fast-start routine (Eaton *et al.* 1977; Webb, 1977), these actions may be strikes aborted at a very early stage. Goldfish did attempt escapes in most cases. These consisted of *C*-starts similar to those observed by Weihs (1972). This was rarely successful; prey were usually engulfed before executing the propulsive stage of their escape.

2. Kinematics and Mechanics

Films of feeding events show that *E. lucius* employs the preparatory, propulsive, and variable stages described by Weihs (1973). Kinematics were similar to the *S*-shaped patterns described by Webb and Skadsen (1980) for the tiger musky, *Esox* sp.

Figures 5.1 - 5.4 show acceleration, velocity, and distance travelled over the duration of the behaviour. As in Chapter 4, it is assumed that the event terminates when the fish reaches its maximum velocity. For all but one of the behaviours, pike reach maximum velocity at or beyond the position of the prey. Insets are traces from simultaneous film records. Although these traces are to scale, they have been realigned on the grid, and as such they represent the orientation of the fish's body with respect to its original position, not the actual distance travelled. These figures indicate that, as observed for escapes, there is a functional relation between the mechanics of feeding fast-starts (strikes), revealed by the accelerometer, and the kinematics of these events, shown by film.

The strikes of *E. lucius* can be categorized into four different mechanical types. During type I strikes (Fig. 5.1), the fish bends into an *S*-shape and makes a change in directional orientation. Maximum acceleration occurs after the head is oriented in the direction of the prey. The acceleration-time plot for this behaviour is unimodal, rising to one significant peak, then declining. This behaviour was only exhibited when the prey was particularly close to the pike and positioned at an angle relative to the longitudinal axis of the pike.

Types II, III, and IV strikes (Figs 5.2 - 5.4, respectively) involve no change in directional orientation; pike had manoeuvred head-long towards the prey. These three behaviours also differ from type I strikes in that the acceleration data tends to be more consistent and less "noisy". This is likely due to the directional stability. Types II-IV vary in the number of peaks apparent in the acceleration-time and velocity-time plots, which are the basis for the categories. Kinematically, an *S* shape is formed at the start of each behaviour. Differences arise from the number of half-cycles of

Figure 5.1. Kinematic and mechanical data for a representative type I feeding fast-start of *Esox lucius* (mass = 0.372 kg, fork-length = 0.363 m), corrected for tangential acceleration. Acceleration, velocity and distance data are shown. Numbers on the tracings correspond to those on the acceleration plot; The grid scale is 10 cm.

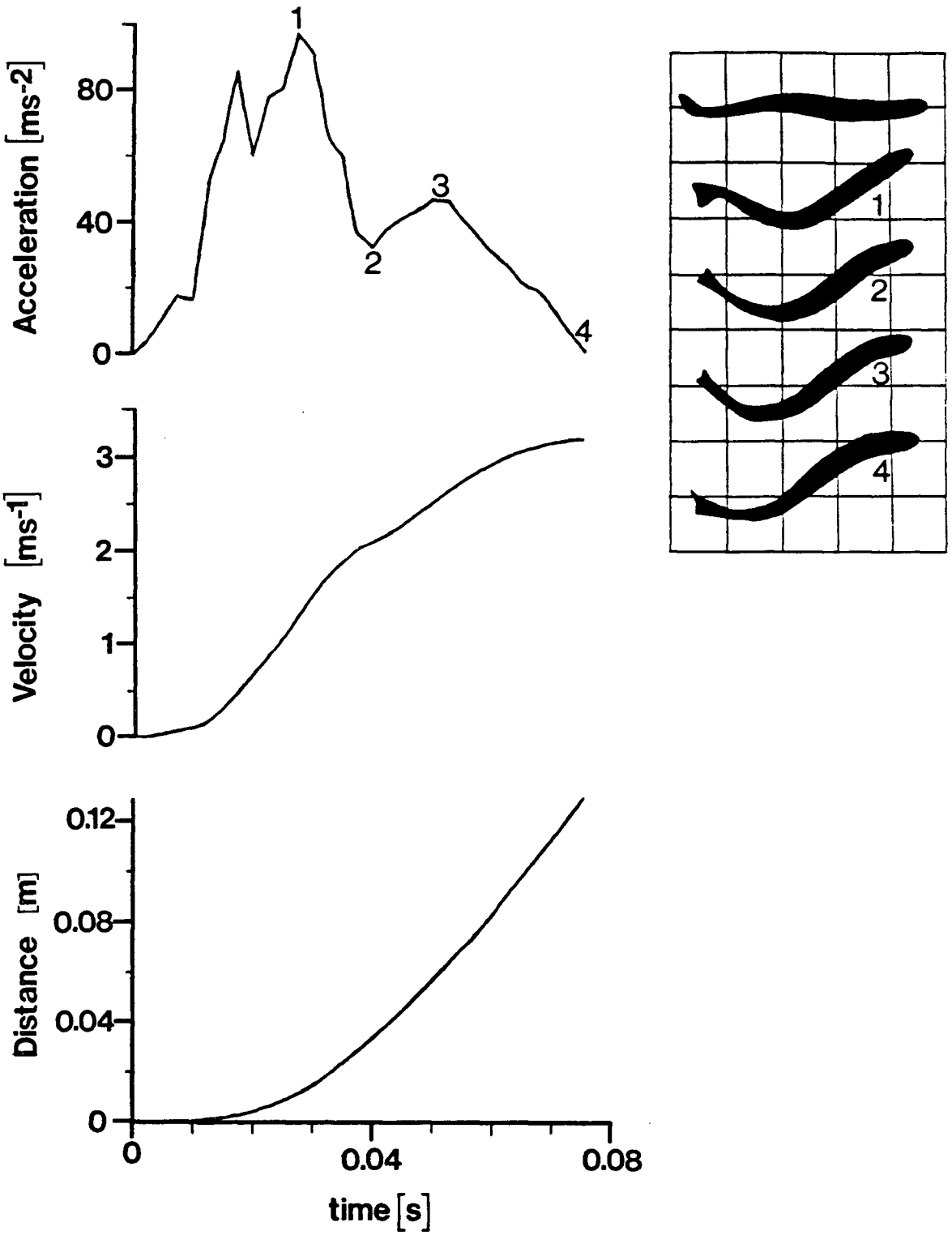
Acceleration [ms-2]
80
40
0
1
2
3
4
Velocity [ms-1]
3
2
1
0
Distance [m]
0.12
0.08
0.04
0
0
0.04
0.08
time [s]
1
2
3
4

Figure 5.2. Kinematic and mechanical data for a representative type II feeding fast-start of *Esox lucius* (mass = 0.377 kg, fork-length = 0.376 m).

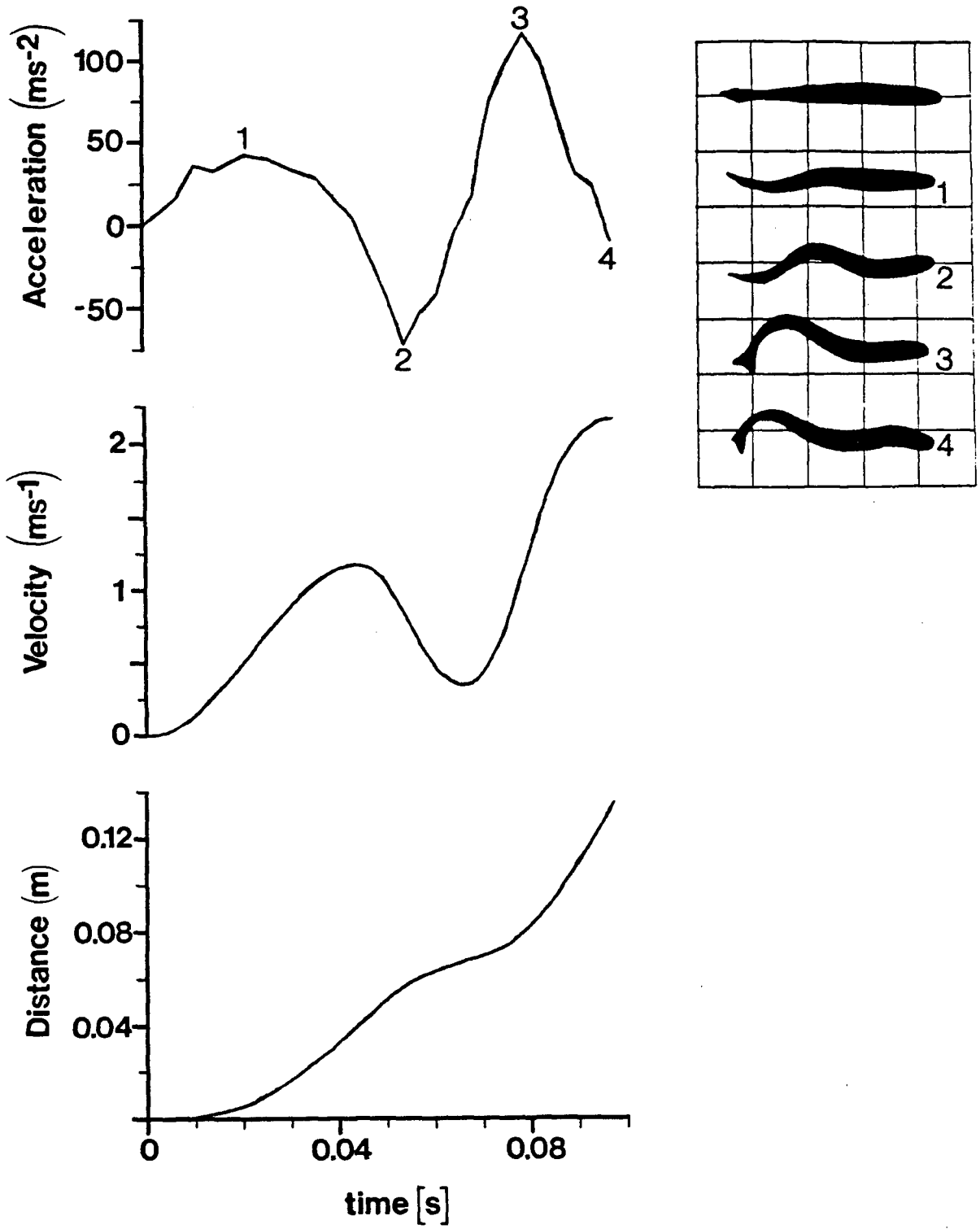
Acceleration (ms-2)
100
50
0
-50
1
2
3
4
Velocity (ms-1)
2
1
0
Distance (m)
0.12
0.08
0.04
0
0.04
0.08
time [s]

Figure 5.3. Kinematic and mechanical data for a representative type III feeding fast-start of *Esox lucius* (mass = 0.377 kg, fork-length = 0.376 m).

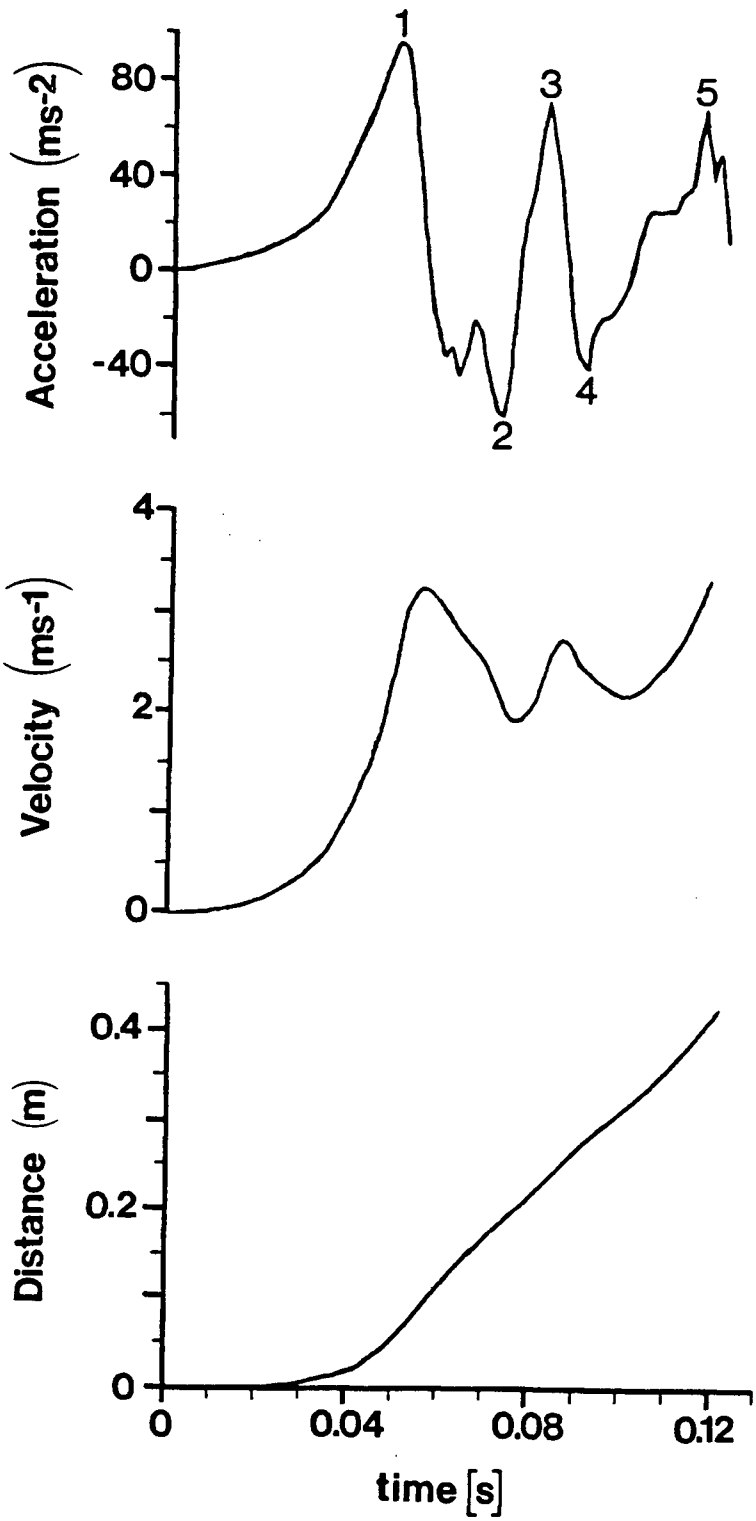
Acceleration (ms-2)
80
40
0
-40
1
2
3
4
5
Velocity (ms-1)
4
2
0
Distance (m)
0.4
0.2
0
0
0.04
0.08
0.12
time [s]

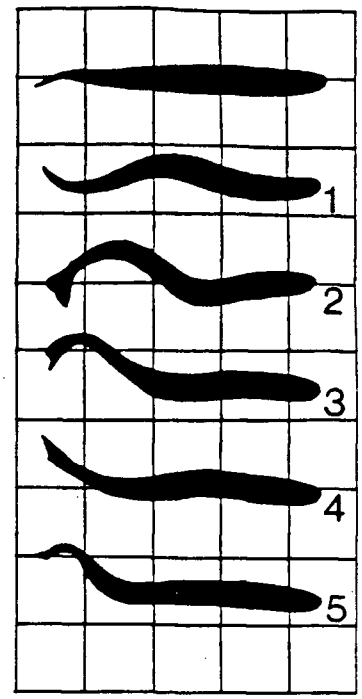
1
2
3
4
5

Figure 5.4. Kinematic and mechanical data for a representative type IV feeding fast-start of *Esox lucius* (mass = 0.372 kg, fork-length = 0.363 m).

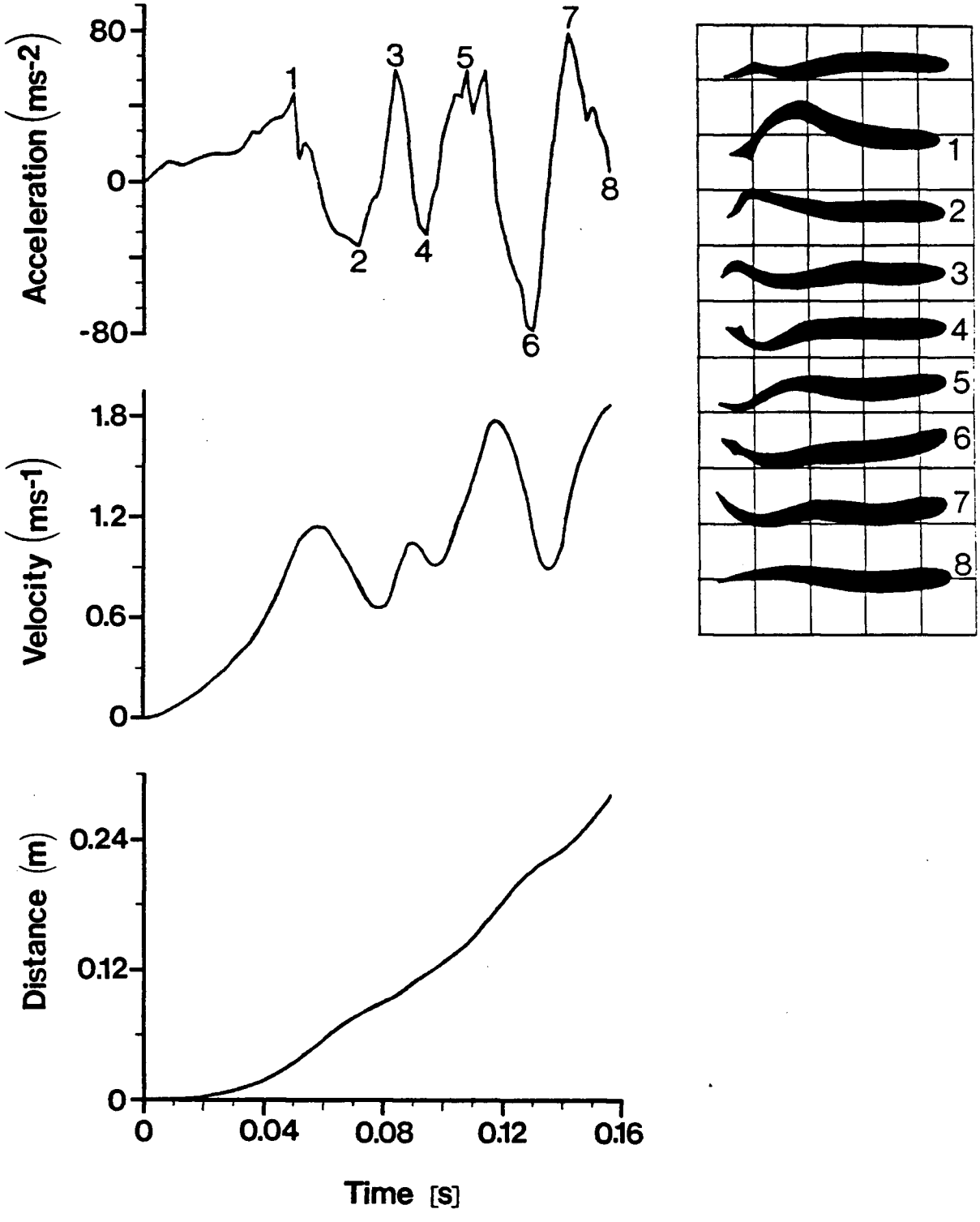
Acceleration (ms-2)
80
0
-80
1
2
3
4
5
6
7
8
Velocity (ms-1)
1.8
1.2
0.6
0
Distance (m)
0.24
0.12
0
0
0.04
0.08
0.12
0.16
Time [s]

the periodic tail motion. The frequency of this motion is relatively constant, ranging from about 11-12.5 Hz (durations of 0.08 to 0.09 s). The maximum acceleration is characteristically found at the first peak of the type III behaviour, and at the last peak for both types II and IV.

A total of 41 predator-prey interactions were analyzed. All fish exhibited all four behaviours (except for one pike which did not exhibit a type I behaviour) and the behaviours are considered characteristic of *E. lucius*. Type III behaviours were most common, occurring in 46% of the events. Type II behaviours were exhibited in 29% of the events. Type I and IV strikes were less common, occurring in 15% and 10% of the events, respectively.

The locomotor performance of *E. lucius* during feeding, measured by accelerometry, is presented in Table 5.1. Mean values for duration, displacement, and mean and maximum velocity and acceleration are given. Performance for each mechanical type is included, as well as a total, combining fast-start types. Data from fast-start escapes (Chapter 4), by the same individuals, are also presented for comparison.

The duration of the events increased from 0.084 s for type I, to 0.115 s for type II, to 0.148 s for type III, to 0.189 s for type IV. Displacement is greatest for type IV (0.307 m), and least for type I (0.132 m) strikes. Mean velocity varied only slightly, ranging from 1.50 m s^{-1} for type II to 1.63 m s^{-1} for type IV strikes. The Type IV strikes also exhibited the highest values for mean maximum velocity (3.24 m s^{-1}), and lowest values for mean (18.0 m s^{-2}) and maximum (66.6 m s^{-2}) acceleration. The latter two variables are highest for the type I strikes (38.6 and 130.3 m s^{-2}, respectively). The type II strike had the lowest mean maximum velocity (3.01 m s^{-2}).

Table 5.1. Feeding performance of *Esox lucius* determined by accelerometry. Values in brackets indicate error as ± 2 S.E. Totals combine data, regardless of mechanical type, for both feeding and escape (from Chapter 4) responses. Total time is the elapsed time to V_{max}.

		n	Total Time (s)	Distance (m)	Mean Velocity (ms^{-1})	Mean Maximum Velocity (ms^{-1})	Mean Acceleration Rate (ms^{-2})	Mean Maximum Acceleration (ms^{-2})
Feeding	Type I	6	0.084	0.132	1.58	3.12	38.6	130.3
			(±0.016)	(±0.028)	(±0.31)	(±0.13)	(±6.5)	(±21.7)
	Type II	12	0.115	0.173	1.50	3.01	26.6	95.8
			(±0.017)	(±0.028)	(±0.12)	(±0.37)	(±1.9)	(±7.9)
	Type III	19	0.148	0.235	1.60	3.11	22.0	91.2
			(±0.021)	(±0.064)	(±0.09)	(±0.32)	(±2.3)	(±9.7)
	Type IV	4	0.189	0.306	1.63	3.24	18.0	66.6
			(±0.042)	(±0.100)	(±0.44)	(±1.05)	(±8.3)	(±6.2)
	Total	41	0.133	0.209	1.57	3.09	25.5	95.9
			(±0.010)	(±0.022)	(±0.11)	(±0.29)	(±1.9)	(±7.8)
Escape	Type I	7	0.085	0.194	2.27	4.70	54.7	157.8
			(±0.005)	(±0.044)	(±0.28)	(±0.52)	(±7.0)	(±37.3)
	Type II	11	0.110	0.192	1.76	3.69	33.2	107.9
			(±0.013)	(±0.032)	(±0.18)	(±0.46)	(±5.0)	(±16.4)
	Type III	7	0.132	0.223	1.72	3.61	25.1	91.4
			(±0.013)	(±0.027)	(±0.31)	(±0.68)	(±6.6)	(±22.8)
	Total	25	0.108	0.201	1.90	3.97	37.6	120.2
			(±0.010)	(±0.020)	(±0.17)	(±0.36)	(±6.1)	(±20.0)

Statistical analyses (Table 5.2) first employed the Student's *t*-test to identify differences between escape and feeding performance when fast-start types are totalled, regardless of mechanical type. This indicated that the escapes incorporated significantly higher mean velocity (1.90 versus 1.57 m s^{-1}; $p < 0.001$), maximum velocity (3.97 versus 3.12 m s^{-1}; $p < 0.001$), mean acceleration (37.6 versus 25.5 m s^{-2}; $p < 0.001$), and maximum acceleration (120.2 versus 95.9 m s^{-2}; $p < 0.01$) over a shorter duration (0.108 versus 0.133 s; $p < 0.05$). One way analysis of variance of individual types of feeding and escape behaviours showed that the type I escapes were of significantly higher mean velocity (2.27 versus 1.58 m s^{-1}; $p < 0.005$), maximum velocity (4.70 versus 3.12 m s^{-1}; $p < 0.005$), and mean acceleration (54.7 versus 38.6 m s^{-2}; $p < 0.005$), than the type I feeding behaviours.

A second ANOVA was conducted on the feeding behaviours, indicating significant differences between means for duration, displacement, and mean and maximum acceleration (Table 5.2). Tukey's test was then used to indicate robust differences between means, considering all possible comparisons.

Table 5.2 shows that the type I behaviour is of significantly higher mean (38.6 versus 26.6 m s^{-2}; $p < 0.001$) and maximum acceleration (130.3 versus 95.8 m s^{-2}; $p < 0.01$) than the type II behaviour, and of significantly higher mean and maximum acceleration, and shorter duration and displacement than the type III and IV behaviours ($p < 0.001$ for all comparisons; see Table 5.1 for values). The type II behaviour is of shorter duration than the type III (0.115 versus 0.148 s; $p < 0.025$), and has higher mean acceleration (26.6 versus 18.0 m s^{-2}; $p < 0.005$), and shorter duration (0.115 versus 0.189 s; $p < 0.005$) and displacement (0.173 versus 0.307 m; $p < 0.01$) than the type IV behaviour. There was no significant difference in mean or maximum velocity for any comparison.

Table 5.2. Statistics for feeding performance, and comparing feeding fast-starts to escapes of *Esox lucius*. Probabilities are indicated (NS denotes no significant difference; i.e., $p > 0.05$). Where a difference is indicated, Table 5.1 identifies the larger. Total combines data, regardless of mechanical type. Tukey's test is used except for total, where the Student's *t*-test was employed.

	Comparison	Time (s)	Distance (m)	Mean Velocity (ms^{-1})	Mean Maximum Velocity (ms^{-1})	Mean Acceleration Rate (ms^{-2})	Mean Maximum Acceleration (ms^{-2})	Distance to Prey (m)	Apparent Size of Prey (degrees)
	Type I vs. II	NS	NS	NS	NS	$P < 0.001$	$P < 0.01$	NS	NS
	Type I vs. III	$P < 0.001$	$P < 0.001$	NS	NS	$P < 0.001$	$P < 0.001$	$P < 0.05$	$P < 0.025$
Feeding	Type I vs IV	$P < 0.001$	$P < 0.001$	NS	NS	$P < 0.001$	$P < 0.001$	$P < 0.001$	$P < 0.005$
	Type II vs. III	$P < 0.025$	NS	NS	NS	NS	NS	NS	NS
	Type II vs. IV	$P < 0.005$	$P < 0.01$	NS	NS	$P < 0.05$	NS	$P < 0.005$	$P < 0.01$
	Type III vs. IV	NS	NS	NS	NS	NS	NS	$P < 0.05$	NS
Feeding	Type I	NS	NS	$P < 0.005$	$P < 0.005$	$P < 0.005$	NS		
vs.	Type II	NS	NS	NS	NS	NS	NS		
Escapes	Type III	NS	NS	NS	NS	NS	NS		
	Total	$P < 0.05$	NS	$P < 0.001$	$P < 0.001$	$P < 0.001$	$P < 0.01$		

3. Effect of Prey Size and Strike Distance on Performance

Measurements of prey size and the distance from predator to prey at the start of the feeding behaviour (strike distance) were related to mechanical types and performance. Prey size was a linear measurement (fork-length); strike distance was determined from film by measuring from the centre of a straight line bisecting the eyes of the pike to the centre of mass of the goldfish (assumed to be about one-third of the length measured from the nose, Weihs, 1972). The relation between the two is presented in Fig. 5.5. The poor correlation (r^2 = 0.06) indicates that these two variables act independently in the interaction. However, strike distance does seem to be related to the type of fast-start employed. Fig. 5.6 supports this; generally, as strike distance increases, pike progressively select the type I, then II, then III, then IV behaviour.

Figure 5.7 demonstrates a relation between feeding behaviour and performance. As prey distance increases, the mean and maximum acceleration decrease, and duration increases. Velocity is not related to prey distance. Similar relations to performance are found as the behaviour changes from type I, to II, to III, to IV.

A significant relation (r^2 = 0.75) is found when strike distance is plotted against apparent prey size (Fig. 5.8). This variable differs from actual prey size in that it represents the angular size of the prey's image on the retina of the predator, in degrees (O'brien *et al.* 1976). Previous studies indicate that fish are particularly sensitive to apparent prey size (Ware, 1973; Dill, 1974*b*; O'brien *et al.* 1976). From Fig. 5.8 it is evident that mechanical type is related to apparent size. Fig. 5.6 demonstrates that

Figure 5.5. Prey distance (m) upon initiation of the feeding fast-start (strike distance) related to prey length (m). No correlation was found (r^2 = 0.06). Fast-start type is indicated for each event (type I, solid circles; type II, solid squares; type III, open squares; type IV, open circles).

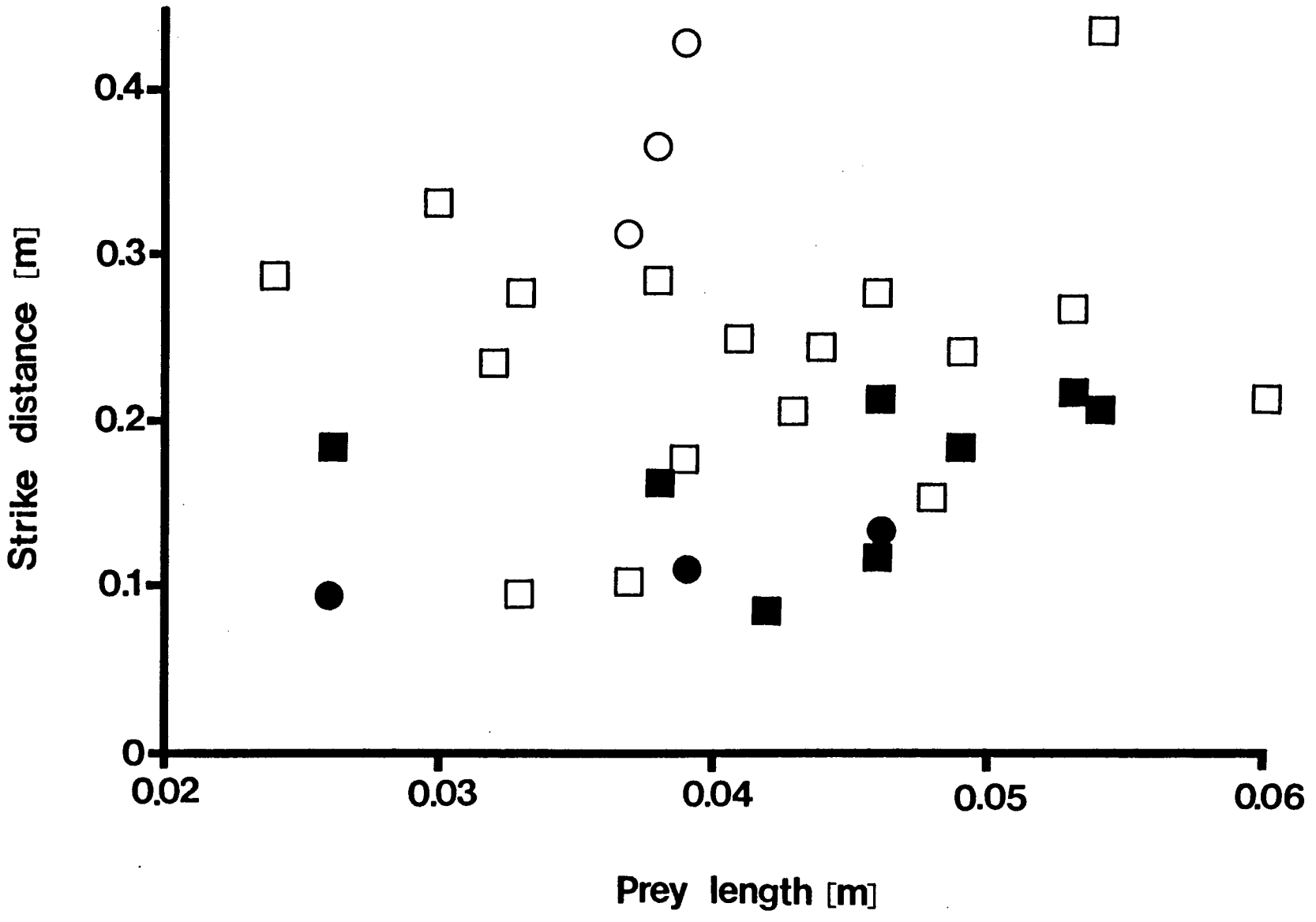
Strike distance [m]
0.4
0.3
0.2
0.1
0
0.02
0.03
0.04
0.05
0.06
Prey length [m]

Figure 5.6. Mean strike distance (solid diamonds) and apparent size (solid circles) for the four feeding types. Errors are indicated as ± 1 S.E.

Strike distance [m]
0
0.1
0.2
0.3
0.4
n
type I
type II
type III
type IV
0
2
4
6
8
10
Apparent prey size [degrees]

Figure 5.7. Relations of mean (A_{mean}) and maximum (A_{max}) acceleration, and event duration (Time), to strike distance. r^2: A_{mean} = 0.59 (y = -64.1x + 38.2), A_{max} = 0.45 (y = -166x + 130), and Time = 0.50 (y = 0.38x + 0.06). For clarity, individual data points for event duration are not included. Fast-start types for each event are indicated (type I, solid circles; type II, solid squares; type III, open squares; type IV, open circles).

Acceleration [ms-2]
0
20
40
60
80
100
120
140
Amean
Time
Amax
160
Strike distance [m]
0
0.1
0.2
0.3
0.4
0
0.05
0.10
0.15
0.20
0.25
Time to Vmax [s]

Figure 5.8. Relation of strike distance (m) to the apparent size (degrees) of the prey. r^2 for the regression line is 0.75 ($y = 0.034x + 4.30$). Fast-start types for each event are indicated (type I, solid circles; type II, solid squares; type III, open squares; type IV, open circles).

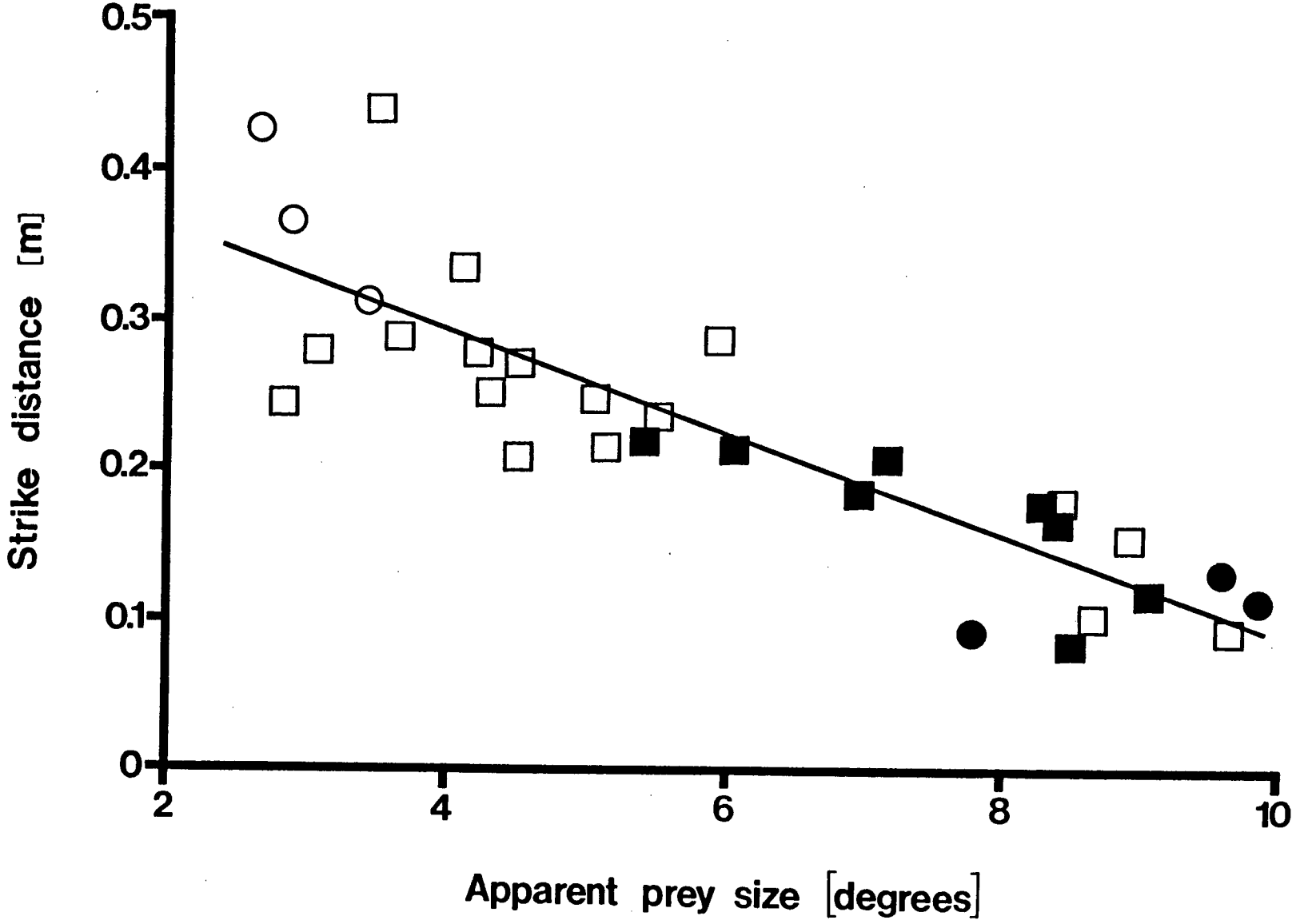
0.5
0.4
0.3
0.2
0.1
0
Strike distance [m]
2
4
6
8
10
Apparent prey size [degrees]

as apparent prey size decreases, pike progressively select the type I, then II, then III, then IV behaviour. Statistical support for this relationship is found in Table 5.2.

Figure 5.9 shows the relations between performance, mechanical type, and apparent size. As apparent size increases, mean acceleration, maximum acceleration, and duration decrease. Velocity is not related to apparent prey size. Similar relations to performance are found as the mechanical type selected changes from IV, to III, to II, to I.

Figure 5.9. Relations of mean (A_{mean}) and maximum (A_{max}) acceleration, and event duration (Time), to the apparent size of the prey. r^2: A_{mean} = 0.79 (y = 2.92x + 6.10), A_{max} = 0.65 (y = 7.81x + 45.0), and Time = 0.63 (y = -0.017x + .240). For clarity, individual data points for event duration are not included. Fast-start types for each event are indicated (type I, solid circles; type II, solid squares; type III, open squares; type IV, open circles).

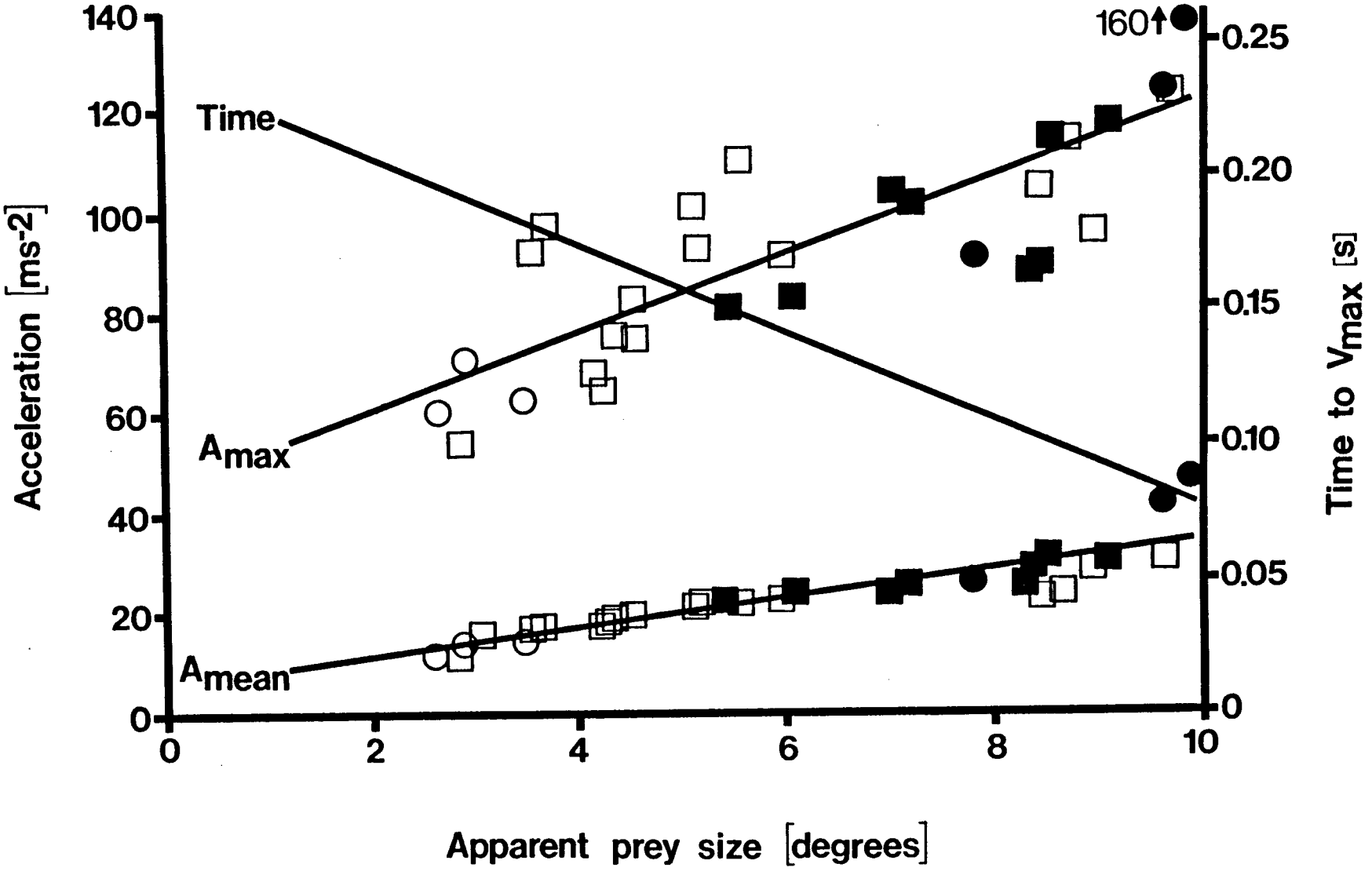
Acceleration [ms-2]
Time to Vmax [s]
Apparent prey size [degrees]
Time
Amax
Amean
140
120
100
80
60
40
20
0
160↑
0.25
0.20
0.15
0.10
0.05
0
0
2
4
6
8
10

D. DISCUSSION

1. Sources of Error

The most significant source of error inherent in accelerometry is the tangential error arising from curved trajectories (Chapter 2). Feeding fast-start types II-IV were not significantly affected by tangential error, due to their directional stability. However, the type I behaviours did involve significant tangential accelerations, which affected the predicted displacements. Therefore corrections to these data were made, following the procedure described in Chapter 4.

2. Comparison to Previous Studies

Mean maximum accelerations during strikes averaged 95.9 ± 7.8 m s^{-2}, lower than values recorded for escapes 120.2 ± 20.0 m s^{-2} (Chapter 4), but much higher than values previously reported from film based studies (40 m s^{-2} ± 25%, Webb, 1978*b*). Mean accelerations were of the order of those found for chain pickerel, *Esox niger* feeding fast-starts (Rand and Lauder, 1981) and tiger musky *Esox* sp. escape fast-starts (Webb, 1986), and significantly less than escape fast-starts of the same individuals (Tables 5.1 and 5.2). Mean durations were significantly longer than for escapes (Tables 5.1 and 5.2), but within the range of previous reports (Table 4.4). The mean and maximum velocities were also found to be significantly lower during feeding than during escapes, but higher than values previously reported (Webb, 1978*b*). The reason for the disparity of mean maximum accelerations between

this and other studies is likely due to the large degree of error inherent in evaluating accelerations from double-differentiated, film-generated, distance-time data, as explained in Chapter 3.

Types I and II feeding fast-starts were found to be kinematically different from escape types I and II, respectively. The difference arises from the directional stability inherent in the feeding behaviours. However, type III fast-starts were kinematically and mechanically similar. From Tables 5.1 and 5.2, it is evident that pike escapes are of shorter duration and higher mean and maximum acceleration and velocity than feeding events. This is reasonable since fish should maximize performance during escapes to avoid capture; failure to capture prey is not catastrophic. However, the overwhelming similarity of the kinematics and mechanics of the type III escapes and feeding strikes (the most common feeding behaviour) infers that the same neural pathways are being employed in both behaviours.

3. Strike Performance

Performance during feeding fast-starts appears to maximize and maintain velocity to the point of contact with the prey. Because tail beats involve periodic accelerations and decelerations, mean acceleration declines during longer strikes (Table 5.1), and because the distance travelled is related to the number of tail beats, the pike executes a given number of tail beats to attain its prey. This does not appear to be a predetermined behaviour for directionally stable strikes (Fig.s 2-4). Type I strikes cannot be directly compared in this manner because of the inherent directional change. In general, the pike executes one full-cycle tail beat, then continues to add half-cycle beats until the prey is captured. Therefore it can be concluded

that *E. lucius* maximizes performance, while maintaining directional stability, throughout the feeding fast-start.

Single event, maximum performance data are reported in Table 5.3. As for mean performance, maximum performance is higher for pike escapes than for feeding strikes. In particular, the maximum acceleration during escapes (244.9 m s^{-2}) is considerably higher than during strikes (159.6 m s^{-2}). Maximum performance data are important because they demonstrate locomotor capability under extreme conditions. This is useful in assessing the energetic cost and efficiency of ambush predation. Harper and Blake (1988, Appendix) have shown that the strike portion of a piscivorous predator-prey interaction accounts for up to 80% of the total energy expended by the predator.

4. Effect of Prey Size and Strike Distance on Behaviour

Strike distance is not dependent on prey size (Fig. 5.5), but is related to its apparent size (Fig. 5.8). This relation arises because apparent prey size is a function of the actual size of the prey and its distance from the predator (O'Brien *et al.* 1976). *E. lucius* interprets fish of apparently smaller size as being at a greater distance, and initiates strikes from further away. Types III and IV fast-starts are then employed to travel this distance. The opposite is true of apparently larger prey, where types I and II are commonly used (Fig. 5.6). This contradicts the previous suggestion that fast-start type is not predetermined. Fig.s 5.6 and 5.8 indicate that strike type is determined before the event is initiated, based on the apparent size of the prey. This suggests that pike disregard actual

Table 5.3. Maximum performance for all feeding and escape (from Chapter 4) types exhibited by *Esox lucius*.

		Distance (m)	Maximum Mean Velocity (ms^{-1})	Maximum Final Velocity (ms^{-1})	Maximum Mean Acceleration (ms^{-2})	Maximum Acceleration Rate (ms^{-2})
Feeding	Type I	0.158	2.17	3.35	47.7	159.6
	Type II	0.221	1.96	3.80	31.6	118.6
	Type III	0.311	2.13	4.61	31.6	136.0
	Type IV	0.429	2.21	4.75	30.4	72.9
Escape	Type I	0.213	2.50	7.06	80.3	244.9
	Type II	0.289	2.26	4.70	47.4	141.2
	Type III	0.227	2.14	4.50	35.5	130.5

prey size, and use apparent size to determine strike distance and feeding behaviour. This would be appropriate if available prey were of similar size, which may be true in Baptiste Lake. "Assuming" prey to be one size is an effective strategy for an ambush predator. If the prey turns out to be smaller than expected, it is still practical to capture it to compensate for the energy expended during the fast-start. If the prey is too large to consume, it will be too distant to capture.

Figures 5.7 and 5.9 demonstrate that acceleration performance is related to both strike distance and apparent size. Performance is maximal for small strike distance and large apparent size. This is directly related to the selection of feeding behaviour (Table 5.2), suggesting that if pike predetermine strike type, they also predetermine acceleration performance.

CHAPTER 6

Summary

This work has shown that accelerometers should be used to attain the most accurate measurements of acceleration during fast-starts in fish. Where this is not possible and film becomes the only source from which to determine acceleration, special attention should be given to sources of error arising from the use of film. This study has demonstrated that error due to sampling frequency and measurement act independently, but can be summed (using equations 9 and 12) to determine the total error arising. Fig. 3.5 is particularly useful in that it gives optimal film speeds for known image magnifications, which can be employed to limit the error associated with film-derived accelerations.

Levels of performance of northern pike *Esox lucius* and rainbow trout *O. mykiss* are shown to be both significantly different from each other and, for *E. lucius*, higher than previously reported from studies employing film analysis. In this light, it can be concluded that the fast-start performance of fish is dependent on body form. Furthermore, analysis of escape performance, through accelerometry, demonstrates a mechanical basis on which to catagorize this behaviour.

Feeding performance of the northern pike *Esox lucius*, determined by accelerometry, is shown to be significantly lower than escape performance by the same individuals when mean and maximum acceleration and velocity, and duration are considered. Displacement values, however, are similar. Four mechanical types of feeding strikes are identified; they are predetermined for use, depending on the apparent size of the prey.

REFERENCES

BLAKE, R.W. (1983). *Fish Locomotion.* Cambridge: Cambridge University Press.

BLAXTER, J.H.S. (1969). Swimming speeds of fish. *FAO (Food and Agricultural Organization of the United nations) Fisheries* **62**, 69-100.

CROSSMAN, E.J. (1959). A predator-prey interaction in freshwater fish. *J. Fish. Res. Bd. Can.* **16**, 269-281.

DILL, L.M. (1973). An avoidance learning submodel for a general predation model. *Oecologia (Berl.)* **13**, 291-312.

DILL, L.M. (1974*a*). The escape response of the zebra danio (*Brachydanio rerio*) I. the stimulus for escape. *Anim. Behav.* **22**, 711-722.

DILL, L.M. (1974*b*). The escape response of the zebra danio (*Brachydanio rerio*) II. the effect of experience. *Anim. Behav.* **22**, 723-730.

DORN, P., JOHNSON, L., and DARBY, C. (1979). The swimming performance of nine species of common California inshore fishes. *Trans. Amer. Fish. Soc.* **108**, 366-372.

DUBOIS, A.B., CAVAGNA, G.A., and FOX, R.S. (1976). Locomotion of bluefish. *J. exp. Zool.* **195**, 223-226.

EATON, R.C., BOMBARDIERI, R.A., and MEYER, D.L. (1977). The Mauthner-initiated startle response in teleost fish. *J. exp. Biol.* **66**, 65-81.

EATON, R.C., and HACKETT, J.T. (1984). The role of the Mauthner cell in fast-starts involving escape in teleost fishes. In: *Neural Mechanisms of Startle Behavior.* (ed. R.C. Eaton), pp. 213-266. New York: Plenum.

EATON, R.C., NISSANOV, J. and WIELAND, C.M. (1984). Differential activation of Mauthner and non-Mauthner startle circuits in the zebrafish: implications for functional substitution. *J. Comp. Physiol. A.* **155**, 813-820.

EATON, R.C., DIDOMINECO, R., and NISSANOV, J. (1988). Flexible body dynamics of the goldfish C-start: implications for reticulospinal command mechanisms. *J. Neurosci.* **8,** 2758-2768.

FIERSTINE, H.L. and WALTERS, V. (1968). Studies of locomotion and anatomy of scombroid fishes. *Mem. Southern Calif. Acad. Sci.* **6,** 1-31.

GERO, D.R. (1952). The hydrodynamic aspects of fish propulsion. *Am. Mus. Novit.* **1601,** 1-32.

GRAY, J. (1953). The locomotion of fishes. In: *Essays in Marine Biology.* Elmhirst Memorial Lectures (eds. S.M. Marshall and P. Orr), pp. 1-16. Edinburgh: Oliver and Boyd.

HARPER, D.G. and BLAKE, R.W. (1988). Energetics of piscivorous predator-prey interactions. *J. theor. Biol.* **134,** 59-76.

HERTEL, H. (1966). *Structure, Form and Movement.* New York: Reinhold.

ISAACS, J.D. and WICK, G.L. (1973). Optimized tactics for open-water marine predators. In: *Marine Biological Association of India Special Publication dedicated to Dr. N.K. Panikar.* Cochin, India: S.T. Reddiar and Sons, pp. 192-199.

KERR, S.J. (1982). Estimating the energy budgets for actively predatory fishes. *Can. J. Fish. Aquat. Sci.* **39,** 371-379.

LANCZOS, C. (1956). *Applied Analysis.* Englewood Cliffs: Prentice Hall.

LAUDER, G.V. (1979). Feeding mechanics in primitive teleosts and in the halecomorph fish *Amia calva. J. Zool., Lond.* **187,** 543-578.

LAUDER, G.V. (1980). Evolution of the feeding mechanism in primitive actinopterygian fishes: a functional anatomical analysis of *Polypterus, Lepisosteus,* and *Amia. J. Morph.* **163,** 283-317.

LAUDER, G.V. (1982). Structure and function in the tail of the Pumpkinseed sunfish *Lepomis gibbosus. J. Zool. Lond.* **197,** 483-495.

LAUDER, G.V. (1983). Prey capture hydrodynamics in fishes: experimental tests of two models. *J. exp. Biol.* **104,** 1-13.

LIGHTHILL, M.J. (1971). Large-amplitude elongated body theory of fish locomotion. *Proc. Roy. Soc. Lond. (B).* **179,** 125-138.

LIGHTHILL, M.J. (1975). *Mathematical Biofluiddynamics.* Philadelphia: Society for Industrial and Applied Mathematics.

MERIAM, J.L. (1975). *Dynamics: Second Edition - SI Version.* Toronto: John Wiley & Sons, Inc.

MORGAN, W.L. and RITZ, D.A. (1983). Sensory cues and mechanisms involved in the capture of euphausiids by the Australian salmon, *Arripis trutta. J. Fish. Biol.* **23,** 489-493.

NURSALL, J.R. (1973). Some behavioural interactions of spottail shiners *Notropis hudsonius*, yellow perch *Perca flavescens*, and northern pike *Esox lucius. J. Fish. Res. Bd. Can.* **30,** 1161-1178.

O'BRIEN, W.J., SLADE, N.A. and VINYARD, G.L. (1976). Apparent size as the determinant of prey selection by bluegill sunfish *Lepomis macrochirus. Ecology.* **57,** 1304-1310.

RAND, D.M. and LAUDER, G.V. (1981). Prey capture in the chain pickerel, *Esox niger*: correlations between feeding and locomotor behaviour. *Can. J. Zool.* **59,** 1072-1078.

RAYNER, J.M.V. and ALDRIDGE, D.J.N. (1985). Three-dimensional reconstruction of animal flight paths and the turning flight of microchiropteran bats. *J. exp Biol.* **118,** 247-265.

RICHARDSON, S.C. (1985). Effects of sampling on blood parameters in the rainbow trout. *J. Fish. Biol.* **26,** 725-732.

SCHMITT, R.J. and HOLBROOK, S.J. (1984). Gape-limitation, foraging tactics and prey selectivity of two microcarnivorous species of fish. *Oecologia* **63,** 6-12.

TAYLOR, J.R. (1982). *An introduction to error analysis: The study of uncertainties in physical measurements.* Mill Valley: University Science Books.

TILLEY, D. E. and THUMM, W. (1974). *Physics for College Students with Applications to the Life Sciences.* Menllo Park, CA: Cummings Publishing Company.

VIDELER, J.J. (1981). Swimming movements, body structure, and propulsion in cod *Gadus morhua.* In: *Vertebrate Locomotion.* (ed. M.H. Day), Symp. Zool. Soc. Lond. **48,** 1-27. Academic Press, London.

VINYARD, G.L. (1982). Variable kinematics of Sacramento perch (*Archoplites interruptus*) capturing evasive and nonevasive prey. *Can. J. Fish. Aquat. Sci.* **39,** 208-211.

VINYARD, G.L and O'BRIEN, W.J. (1976). Effects of light and turbidity on the reactive distance of bluegill (*Lepomis macrochirus*). *J. Fish. Res. Board Can.* **33,** 2845-2849.

WANKOWSKI, J.W.J. (1979). Morphological limitations, prey size selectivity, and growth response of juvenile atlantic salmon, *Salmo salar. J. Fish Biol.* **14,** 89-100.

WARDLE, C.S. (1975). Limit of fish swimming speed. Nature, Lond. **255,** 725-727.

WARE, D.M. (1971). Predation by rainbow trout (*Salmo gairdneri*): the effect of experience *J. Fish. Res. Bd. Can.* **28,** 1847-1852.

WARE, D.M. (1973). Risk of epibenthic prey to predation by rainbow trout (*Salmo gairdneri*). *J. Fish. Res. Bd. Can.* **30,** 787-797.

WARE, D.M. (1975). Growth, metabolism, and optimal swimming speed of a pelagic fish. *J. Fish. Res. Bd. Can.* **32,** 33-41.

WEBB, P.W. (1975). Acceleration performance of rainbow trout *Salmo gairdneri* and green sunfish *Lepomis cyanellus. J. exp. Biol.* **63,** 451-465.

WEBB, P.W. (1976). The effect of size on the fast-start performance of rainbow trout *Salmo gairdneri*, and a consideration of piscivorous predator-prey interactions. *J. exp. Biol.* **65,** 157-177.

WEBB, P.W. (1977). Effects of median-fin amputation on fast-start performance of rainbow trout *Salmo gairdneri*. *J. exp. Biol.* **68,** 123-135.

WEBB, P.W. (1978*a*). Temperature effects on acceleration of rainbow trout *Salmo gairdneri*. *J. Fish. Res. Board Can.* **35,** 1417-1422.

WEBB, P.W. (1978*b*). Fast-start performance and body form in seven species of teleost fish. *J. exp. Biol.* **74,** 211-226.

WEBB, P.W. (1982). Fast-start resistance of trout. J. exp. Biol. **96,** 93-106.

WEBB, P.W. (1983). Speed, acceleration, and manoeuvrability of two teleost fishes. *J. exp. Biol.* **102,** 115-122.

WEBB, P.W. (1984). Chase response latencies of some teleostean piscivores. *Comp. Biochem. Physiol. A.* **97,** 45-48.

WEBB, P.W. (1986). Effect of body form and response threshold on the vulnerability of four species of teleost prey attacked by largemouth bass *Micropterus salmoides*. *Can. J. Fish. Aquat. Sci.* **43,** 763-771.

WEBB, P.W. and COROLLA, R.T. (1981). Burst swimming performance of northern anchovy, *Engraulis mordax*, larvae. *Fish. Bull.* **79,** 143-150.

WEBB, P.W. and SKADSEN, J.M. (1980). Strike tactics of Esox. *Can. J. Zool.* **58,** 1462-1469.

WEIHS, D. (1972). A hydromechanical analysis of fish turning manoeuvres. *Proc. Roy. Soc. Lond. (B).* **182,** 59-72.

WEIHS, D. (1973). The mechanism of rapid starting of slender fish. *Biorheology.* **10,** 343-350.

WEIHS, D. and WEBB, P.W. (1983). Optimization of locomotion. In: *Fish Biomechanics* (eds. P.W. Webb and D. Weihs), pp. 339-371.

WERNER, E.E. (1974). The fish size, prey size, handling time relation in several sunfishes and some implications. *J. Fish. Res. Bd. Can.* **31,** 1531-1536.

WERNER, E.E. and HALL, D.J. (1974) Optimal foraging and the size selection of prey by the bluegill sunfish *Lepomis macrochirus*. *Ecology* **55,** 1042-1052.

APPENDIX

Energetics of piscivorous predator-prey interactions

by David G. Harper and Robert W. Blake

Department of Zoology, University of British Columbia

Vancouver V6T 2A9 Canada

From the Journal of Theoretical Biology (1988) **134,** 59-76

ABSTRACT

Information on fish swimming mechanics and feeding behaviour are combined in an energetic model of the feeding efficiency of a simple piscivorous predator-prey interaction. The intent is to make quantitative assessments of actual energies expended and gained in the interaction, and to determine the optimal prey size for a piscivorous predator. Feeding efficiency is defined here as "the energy input through feeding divided by the energy output required to catch and consume the prey". This is also referred to as the relative energetic benefit.

The variables in the model include the size of the prey relative to the predator, length of predator, its fineness ratio (length/maximum depth of section), a visual threshold angle at which the predator initiates an interaction, and a variable reflecting prey experience. The prey size that maximizes feeding efficiency is the largest available. Feeding efficiency is

also high when predator length and threshold angle are small, fineness ratio is high, and the prey is naive.

The model focuses on a three-staged interaction involving an approach, chase, and strike. When the size of the prey is small relative to the predator, the accelerative energy of the strike dominates the energy output. When this term is large, the drag force during the approach is important. Other predatory strategies (ambush, constant-velocity foraging, and high speed attacks on schools) are discussed with respect to optimal prey size and feeding efficiency. Constant-velocity foraging provides the greatest relative energetic benefit, but is restricted to small prey. The relative energetic benefit for the ambush strategy exceeds that for high speed attacks when the size of the prey relative to the predator is greater than about 0.4.

NOTATION

A_c: wetted surface area of predator

a_c: acceleration rate of predator

C: length of predator/length of prey

C_D: coefficient of drag

D_{pred}: reaction distance of predator

D_{prey}: reaction distance of prey

D_{str}: strike distance of predator

E: number of exposures to predators

e: gram caloric value of prey

F_{app}: approach force (steady)

F_{cha}: chase force (steady)

F_{str}: strike force (unsteady)

f_c: fineness ratio of predator

η_m: efficiency of muscular work

η_p: mechanical (Froude) efficiency

$\eta_{p_{st}}$: Froude efficiency of steady swimming

$\eta_{p_{unst}}$: Froude efficiency of unsteady swimming

K: optical constant determining predator reaction distance

k: rate of change of reaction angle of prey

L_c: length of predator

L_p: length of prey

M_c: mass of predator

M_p: mass of prey

m: added mass during acceleration

Q_{app}: energy expended in approach

Q_{cha}: energy expended in chase

Q_{str}: energy expended in strike

Q_e: total energy expended

Q'_e: total metabolic energy expended

Q_i: energy input

ρ: density of water

S_c: maximum depth of section of predator

T_{cha}: time of chase

θ: reaction angle of predator

U_{app}: approach velocity

U_{cha}: chase velocity

U_{str}: strike velocity

U_p: escape velocity of prey

A. INTRODUCTION

Optimal foraging theory is central to modern views of animal energetics in a behavioural, ecological, and evolutionary context. It has been extensively studied (for reviews, see Schoener, 1971; MacArthur, 1972; Emlen, 1973; Pianka, 1974; Krebs *et al.* 1983; Stephens and Krebs, 1986). Theoretical and experimental work has focussed on attempts to find out if there are any general rules about diet choice (e.g., Pulliam, 1974; Charnov, 1976), the responses of predators to changes in their prey density (e.g., Holling, 1965, 1968), and movement in relation to habitat quality (e.g., MacArthur and Pianka, 1966; Emlen, 1973). In these and other areas it is assumed that decision rules have been shaped by natural selection to allow the animal to perform efficiently. Efficiency in this context is often equated with energetic criteria, such as maximization of the net energy intake per unit time spent foraging or maximizing the unit energy gain per unit energy expended.

Simple energy (or intake) maximizing models have been successful in forwarding our understanding of foraging in a variety of animals (e.g., see Krebs *et al.* 1983, Table 6.1). Recently, more complex models have been developed, incorporating trade-offs between foraging and other behaviours (e.g., territorial defense and vigilance). Krebs *et al.* (1983) have argued that it is advisable to take a piecemeal approach to optimal foraging problems, building from simple to complex, rather than attempting to develop all-inclusive models. They justify this view by reference to the success and extension of the simple optimal foraging models outlined above.

This paper is about the energetics of piscivorous predator-prey interactions. A complete understanding of predator-prey interactions is beyond the scope of any single study. Here, aspects of foraging theory are

combined with biomechanical information on swimming performance, to assess the optimal prey size of a piscivorous predator. This issue has been studied previously employing theoretical and experimental approaches (e.g., Dill, 1973; Werner and Hall, 1974; Dunbrack and Dill, 1983; Weihs and Webb, 1983). A number of studies have found that large pelagic marine predators select small prey (e.g., Allen and Aron, 1957; Alverson, 1963). Isaacs and Wick (1973) employed an energy based model to show that, in theory, the optimal prey size for large, steady swimming fish is the smallest available. However, some experimental studies and other observations indicate that many piscivorous fish may take prey as large as 25 to 40% of their own length (Popova, 1967; Nursall, 1973; Gillen *et al.* 1981).

The predator-prey interaction considered here represents a simple, stereotypic system in which a predator stalks, chases, and strikes at a single prey. The interaction consists of three stages (Dill, 1973). As shown in Fig. A1(a), the predator detects the prey at some distance, D_{pred}, and swims towards it at a constant velocity. When the predator reaches distance D_{prey}, the prey identifies the threat and flees. At this point, stage two, the predator increases its velocity and chases the prey until it closes within striking disance, D_{str}. The final stage is a high-powered, accelerative strike at the prey. It is assummed that the predator is always successful and that handling time is zero. It is also assumed that the prey is still, alone, and fully exposed, in non-turbid, fully illuminated water. The optimal prey size is determined employing an energetic benefit/cost approach. The cost to the predator is the sum of the energy outputs in each of the three stages of the interaction. The benefit comes from consumption of the prey.

Figure A1. (*a*) Diagramatic representation of the three-staged predator-prey interaction (adapted from Dill, 1973). A full explanation is given in the text. (*b*) Representation of the geometric relationship between the reaction angle of the predator, θ, the length of the prey, L_p, and D_{pred}, the reaction distance of the predator.

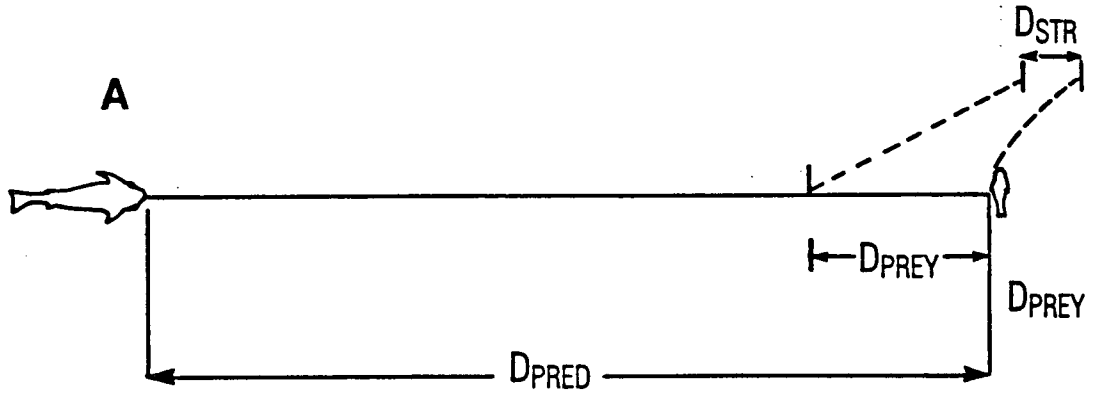
A
D_{STR}
D_{PREY}
D_{PREY}
D_{PRED}

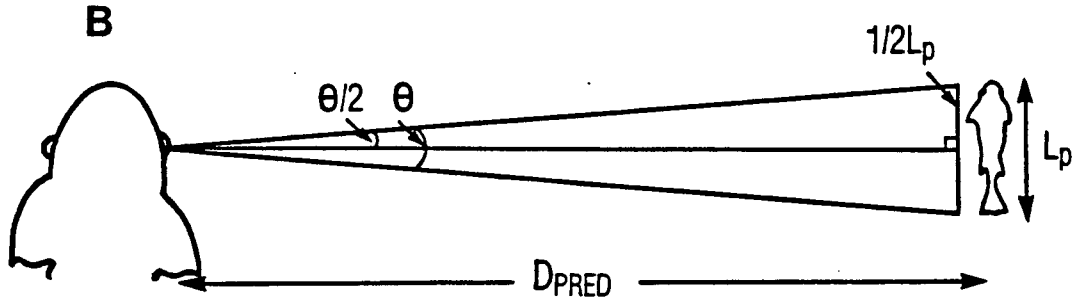
B
1/2L_p
θ/2
θ
L_p
D_{PRED}

B. MODEL

The model determines the ratio of energetic benefit to energetic cost for a single predator capturing a single prey in an open water environment. The energy benefit, Q_i, comes from the consumption and digestion of the prey item. The cost, Q_e, is the energy involved in the pursuit and capture of the prey. This involves three hydrodynamically distinct events and so their energies are considered separately. The ratio of benefit to cost is given by

$$\frac{\text{benefit}}{\text{cost}} = \frac{Q_i}{Q_e} = \frac{Q_i}{Q_{app} + Q_{cha} + Q_{str}} \qquad \text{(A1)}$$

where Q_{app}, Q_{cha}, and Q_{str} represent the energy consumed in the approach, chase, and strike portions of the interaction, respectively.

In the model, fish are considered to be geometrically, physiologically, and hydrodynamically similar. Although most of the emperical relationships used for both predator and prey are taken from studies on salmonids, the model is not specifically intended for any one species. Throughout, an attempt is made to use morphological and performance values for rainbow trout *Oncorhynchus mykiss*. When this is not possible, values for other species are used and noted. All values and relations are given in c.g.s. units.

1. Input energy (Q_i)

The energy gained from a successful interaction is equal to the product of the mass of the prey, M_p, its gram caloric value, e, and a factor which takes digestive losses into account:

$$Q_i = M_p \times e \times \frac{\text{net energy}}{\text{ingested energy}} . \qquad \text{(A2)}$$

The average gram caloric value for twelve *Salmonidae* was found to be 1492 calories per gram wet weight (Cummins and Wuycheck, 1973). This is substituted for *e*. Ware (1975) calculated that the losses in digestion, specific dynamic action, and urine formation for bleak (*Alburnus alburnus*) amounted to about 30% of the ingested energy. Assuming similar digestive losses for other fish and substituting this into equation A2 gives

$$Q_i = 1044\ M_p . \qquad \text{(A3)}$$

The relation of length to mass for *Salmo gardneri* is given by

$$M_p = 0.002\ L_p^{3.29} \qquad \text{(A4)}$$

(Webb, 1977, Table II). Prey length, L_p, is normalized to predator length, L_C. The ratio of prey/predator length $\left(L_p/L_c\right)$ is defined as C, so L_p is equal to $L_c C$. Substituting this into A4 gives

$$M_p = 0.002\ L_c^{3.29}\ C^{3.29} \qquad \text{(A5)}$$

and combining equations A3 and A5 gives

$$Q_i = 2.089\ L_c^{3.29}\ C^{3.29} . \qquad \text{(A6)}$$

2. Energy expended (Q_e)

The energy expended during the three stages of this interaction will be considered separately.

The cost of swimming at constant velocity from the point at which the predator reacts to the prey to the point at which the prey initiates evasive maneuvers, Q_{app}, is given by

$$Q_{app} = F_{app} (D_{pred} - D_{prey}) , \quad \text{(A7)}$$

where F_{app} is the thrust force needed to overcome hydrodynamic drag, D_{pred} is the distance at which the predator detects the prey, and D_{prey} is the distance at which the prey identifies the threat and flees. Since this is a steady swimming phase, F_{app} can be represented by the standard hydrodynamic equation

$$F_{app} = {}^1/_2 \rho C_D A_c U^2_{app} , \quad \text{(A8)}$$

where ρ is the water density, C_D is the coefficient of drag, A_c is the surface area of the fish, and U_{app} is its velocity (further details can be found in introductory fluid mechanics texts, e.g., Binder, 1973, p. 131).

The velocity of approach, U_{app}, is assumed to be the optimal constant speed (as defined by Weihs and Webb, 1983, equation 7) at which the rate of energy expended per unit distance is minimized. In terms of L_c, this is

$$U_{app} = 6.902 L_c^{0.43} . \quad \text{(A9)}$$

Webb (1977) determined the relation between length and wetted surface area for *S. gairdneri*:

$$A_c = 0.28\ L_c^{2.11} . \qquad \text{(A10)}$$

Marchaj (1979, Fig. 29.3) gives drag coefficients for rigid bodies of revolution of varying fineness ratio (length/ maximum depth of section). The drag coefficient for a body of fineness ratio 5 is 0.02. Webb (1977, Fig. 4) found the theoretical C_D for a swimming fish to vary from 0.004 to 0.06 depending on the flow regime. The effects of changes in C_D and other variables on the model will be addressed later. For now C_D is assumed to be 0.02 and water density is taken to be 1 g/cm^3. Substituting these values and equations A9 and A10 into A8 gives

$$F_{app} = 0.1334\ L_c^{2.97} . \qquad \text{(A11)}$$

The distance at which the predator initiates the approach, D_{pred}, is assumed to be proportional to both the length of the prey and predator:

$$D_{pred} = L_p\ L_c\ K = K\ L_c^2\ C . \qquad \text{(A12)}$$

It is assumed that D_{pred} is determined visually, from the size of the prey's image on the predator's retina, which depends on a critical angle, θ, at which the predator reacts. The variable K, is dependent on this angle. From Fig. A1(b),

$$\tan(\theta/2) = \frac{{}^{1}/_{2} L_p}{K L_c L_p} = \frac{1}{2 K L_c} \qquad \text{(A13)}$$

solving for K gives

$$K = \frac{1}{L_c \tan \theta} \qquad \text{(A14)}$$

and substituting for K in equation A13,

$$D_{pred} = \frac{L_c C}{\tan \theta} \qquad \text{(A15)}$$

The reactive distance of the prey, D_{prey}, is described by Dill (1974*a*). Prey react when the rate of change of the visual angle subtended by the predator's image exceeds some threshold, k:

$$D_{prey} = \left(\frac{U_{app} S_c}{k} - \frac{S_c^2}{4} \right)^{1/2} \qquad \text{(A16)}$$

(Dill, 1974*b*, equation 3), where S_c is the maximum depth of section of the predator. The fineness ratio, f_c, is the ratio of length to depth of section $\left(\text{i.e. } f_c = L_c/S_c\right)$. The threshold k, is given by

$$k = 0.2349 + 0.1985\, e^{-(E/2)} \qquad \text{(A17)}$$

(Dill, 1974*b*, equation 5), where E is the number of previous predator exposures to the prey. Substituting equations A9 and A17 into A16 gives

$$D_{prey} = \left(\frac{6.902\ L_c^{1.43}}{f\ (0.2349 + 0.1985\ e^{-(E/2)})} - \frac{L_c^2}{4\ f^2} \right)^{1/2} \qquad \text{(A18)}$$

and combining with equation A11 and substituting into equation A7:

$$Q_{app} = 0.1334\ L_c^{2.97} \left(\frac{L_c\ C}{\tan\ \theta} - \left(\frac{6.902\ L_c^{1.43}}{f(0.2349+0.1985e^{-(E/2)})} - \frac{L_c^2}{4f_c^2} \right)^{1/2} \right). \qquad \text{(A19)}$$

The energy cost of the chase, Q_{cha}, over time, T_{cha}, is

$$Q_{cha} = F_{cha}\ U_{cha}\ T_{cha} \qquad \text{(A20)}$$

The force, F_{cha}, is required to overcome drag at the higher velocity, U_{cha} ($U_{cha} > U_{app}$). U_{cha} is assumed to be the maximum sustainable speed for the predator. Brett and Glass (1973) found that the critical speed, in terms of length of a Sockeye salmon *Oncorhynchus nerka*, swimming for 1 hour at 15°C, was $U = 13.46\ L^{0.63}$. This relation is used for U_{cha}, and substituting into equation A8, F_{cha} becomes:

$$F_{cha} = 0.5073\ L_c^{3.37}\ . \qquad \text{(A21)}$$

Dill (1973) gives the time taken to close the distance between the predator and the prey:

$$T_{cha} = \frac{0.7874\ (D_{prey} - D_{str})}{(U_{cha} - U_p)} . \qquad \text{(A22)}$$

It is assumed that U_p scales with L_p as U_{cha} scales with L_c. This means that the denominator in equation A22 can be divided by U_{cha}, giving

$$U_{cha} T_{cha} = \frac{0.7874\ (D_{prey} - D_{str})}{(1 - C^{0.63})} . \qquad \text{(A23)}$$

The reaction distance of the prey, D_{prey}, is described in equation A18. The predator strike distance, D_{str}, is the distance at which the predator accelerates to seize the prey. From Webb (1978):

$$D_{str} = 0.38\ L_c^{1.01} . \qquad \text{(A24)}$$

Substituting equations A18, A21, A23, and A24 into equation A20 gives

$$Q_{cha} = 0.4008\ L_c^{3.37}\ \frac{\left(\left(\frac{6.902\ L_c^{1.43}}{f(0.2349+0.1985e^{-(E/2)})} - \frac{L_c^2}{4f^2}\right)^{1/2} - 0.38 L_c^{1.01}\right)}{(1 - C^{0.63})} . \qquad \text{(A25)}$$

The energy consumed by the accelerative lunge at the prey, Q_{str}, is given by

$$Q_{str} = F_{str}\ D_{str} . \qquad \text{(A26)}$$

D_{str} is given in equation A24. The accelerative force, F_{str}, is the product of the predator mass, M_c, plus its longitudinal added mass of entrained water, m, and the acceleration from the maximum sustainable speed to the maximum sprint speed, U_{str}. Webb (1982) determined the added mass of an accelerating fish to be equal to about 20% of the body mass. Considering this and equation A4:

$$M_c + m = 0.0024\ L_c^{3.29} . \tag{A27}$$

The average acceleration of the predator, a_c, is given by $\Delta U/T_{str}$, where ΔU is the difference between U_{str} and U_{cha}, and T_{str} is given by Webb (1978, equation 2) as

$$T_{str} = 0.0035\ L_c + 0.43 . \tag{A28}$$

Thus the accelerative force is

$$F_{str} = (M_c + m)\ a_c = 0.0024\ L_c^{3.29} \left(\frac{U_{str} - U_{cha}}{0.0035\ L_c + 0.43} \right) . \tag{A29}$$

U_{str} for *Salmo irideus* was determined by Webb (1977, Table II) to be

$$U_{str} = 22\ L_c^{0.81} . \tag{A30}$$

Substituting this and equations A24 and A29 into A26 gives

$$Q_{str} = 0.0123\ L_c^{4.93} \left(\frac{1.634\ L_c^{0.18} - 1}{0.0035\ L_c + 0.43} \right) . \qquad \text{(A31)}$$

Q_e then, is simply the sum of Q_{app}, Q_{cha}, and Q_{str} (i.e., the sum of equations A19, A26, and A31). The derivation of Q_e gives energy in g f cm. To compare with Q_i, this is converted to calories (i.e., Q_e is multiplied by a factor of 0.00002344 calories/g f cm; Pennycuick, 1975).

The energy needed to meet the hydrodynamic demands, is less than that generated by the swimming muscles. According to Hill (1950) the maximum mechanical efficiency, η_m, of vertebrate striated muscle is about 0.2. The Froude propulsive efficiency, η_p, during steady swimming approaches 0.9 (Chopra and Kambe, 1977; Magnuson, 1978; Yates, 1983), while the efficiency of unsteady swimming is maximally about 0.5 (McCutchen, 1977). The total metabolic energy required for propulsion is given by Q_e', where

$$Q_e' = \frac{(Q_{app} + Q_{cha})}{\eta_m\ x\ \eta_{p_{st}}} + \frac{Q_{unst}}{\eta_m\ x\ \eta_{p_{unst}}} . \qquad \text{(A32)}$$

Therefore, Q_{app} and Q_{cha} are multiplied by 5.6 and Q_{str} by 10.

C. RESULTS

Predator length, fineness ratio, reaction angle, and the level of experience of the prey, can be fixed, or varied independently to illustrate their effect on the benefit/cost curves (see Figs A5-A7). The independent variable in each case is the ratio of predator to prey length. Each figure shows values for net energetic benefit for a range of relative prey sizes. The remaining variables are fixed or varied reflecting realistic biological values. A range of predator length from 5 to 110 cm is considered here. Popova (1967) observed that 5 cm is a practical lower bound for the size at which predation on other fish occurs.

Fineness ratio in fish may vary from about one, for fish with relatively small length and large depth of section, to about twenty for very long slender forms. In this study, fineness ratio is set at 5. Many active piscivorous pelagic fish are characterized by a fineness ratio of this order (Blake, 1983*a*).

Prey experience, E, is varied from one, for the first encounter, to six, for very experienced prey. The seventh encounter results in a change in prey reaction distance of only 0.87%, at any value of C .

The predator reaction angle is set at 1° (= 0.017 rad). A number of studies indicate that many pelagic predators rely exclusively on vision to locate prey (Ivlev, 1961; Brooks and Dodson, 1965; Ware, 1973). Isaacs and Wick (1973), concluded from their model that open ocean, steady-swimming predators use three-dimensional cues to estimate the volume of prey items. Experimental data, however, do not support this. Ware (1973, Fig. 3) shows that the relationship between predator reactive distance and target length is linear. Furthermore, O'Brien *et al.* (1976) found that bluegill *Lepomis macrochirus* selected the prey of largest apparent size, where size is a

linear dimension. The only applicable dimension for cueing in these studies is a linear one. Ware (1971) found reaction distances for naive predators to be about 20 cm for prey 0.5 cm in length, resulting in an angle, θ, of 1.4° (= 0.025 rad). With experience, reaction distances were found to increase; implying a decrease in θ.

Fig. A2 shows the relation between energy input and output, and C for L_c = 30 cm, f_c = 5, $\theta = 1^{\circ}$, and E = 1. Evidently, optimal prey size for the three stage interaction is the largest available. However, few piscivorous fish are capable of consuming extremely large prey, so the remaining figures are presented with values of C ranging only to 0.45. This accounts for the range of prey sizes taken by the majority of piscivorous species (Allen and Aron, 1957; Alverson, 1963; Popova, 1967; Nursall, 1973).

Although energy input remains constant for any given prey size in the model, the energy expended in capture may vary. In Fig. A3, the energy consumed in each stage of the interaction is shown as a percentage of the total metabolic energy expended, for given C. The strike energy, Q_{str} (used in the accelerative burst of stage 3), ranges from about 80%, for small C, to about 50% for large C. Conversely, Q_{app} (the energy used to stalk the prey), ranges from about 5% for small C, to 35% for large C. The energy consumed in the chase remains relatively constant, at about 13% of the total metabolic energy.

Although this model is developed for a three-staged interaction, the expended energy components can be employed to simulate other strategies. Fig. A4 shows benefit/cost curves for a variety of strategies, including the three-staged strategy, shown in Fig. A1(a).

Figure A2. Relative energetic benefit for three-staged prey capture where prey length is normalized to predator length.

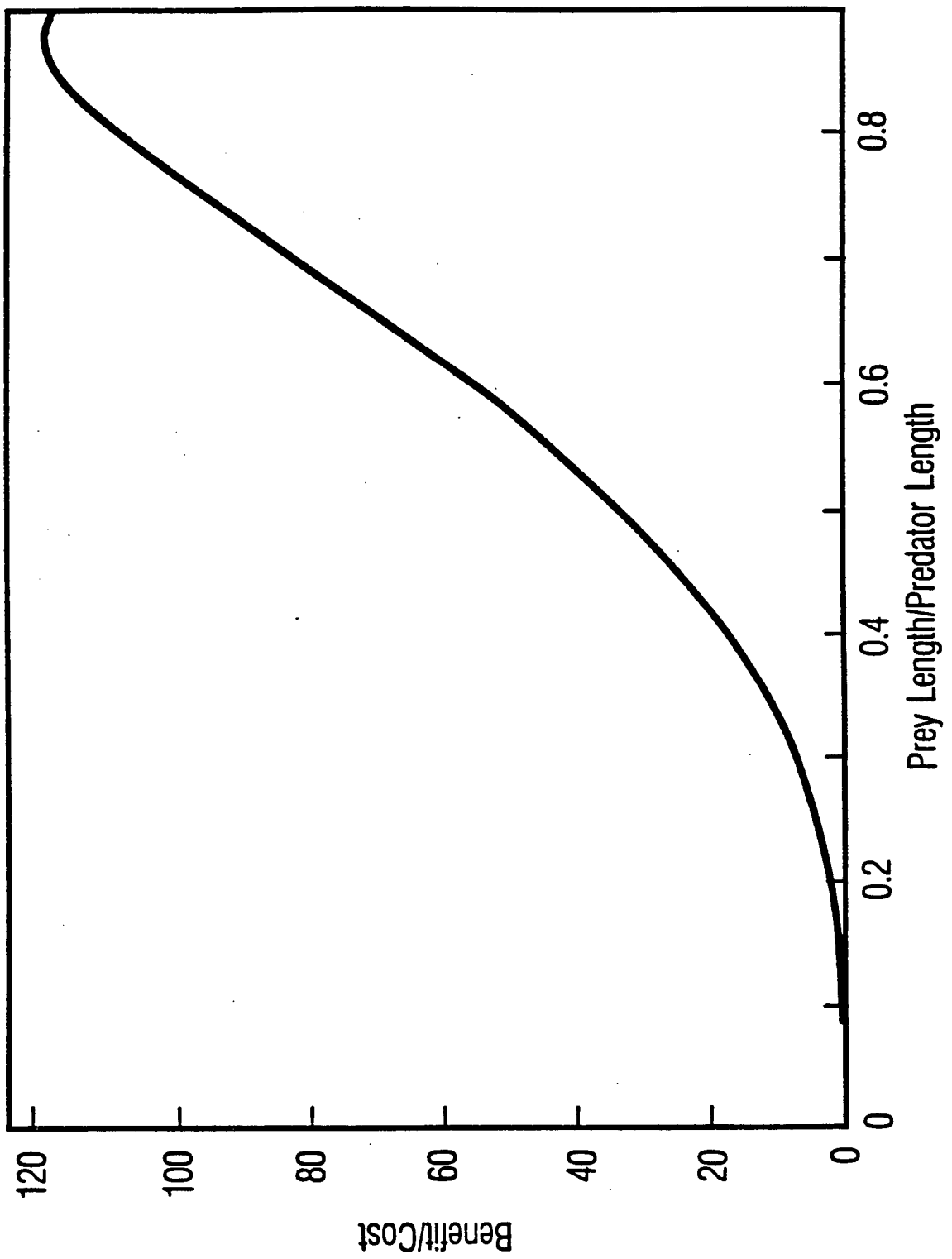
Benefit/Cost
120
100
80
60
40
20
0
0
0.2
0.4
0.6
0.8
Prey Length/Predator Length

Figure A3. Contributions of approach, chase, and strike as a percentage of the total energy expended in the predator-prey interaction.

% Total Energy Expended
0
10
20
30
40
50
60
70
80
90
0
0.2
0.4
Prey Length/Predator Length
Qcha
Qapp
Qstr

Figure A4. Relative energetic benefit of various prey capture strategies considered independently.

Benefit/Cost
0
10
20
30
40
50
60
70
80
0
0.2
0.4
Prey Length/Predator Length
Qapp
Qstr
Qapp+cha
Qtotal

Figure A5. Effect of varying predator length on relative energetic benefit.

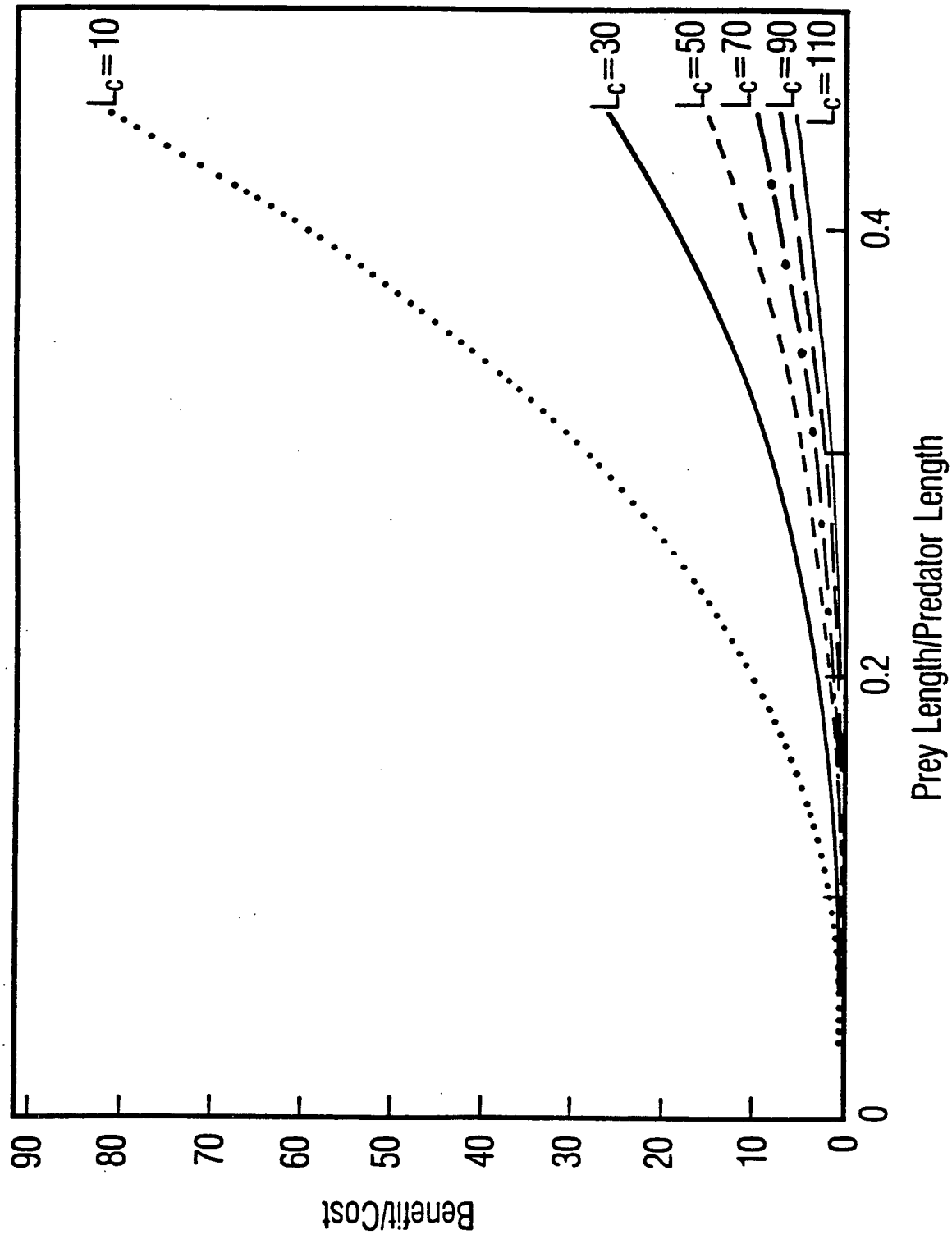
Benefit/Cost
90
80
70
60
50
40
30
20
10
0
0
0.2
0.4
Prey Length/Predator Length
L_c=10
L_c=30
L_c=50
L_c=70
L_c=90
L_c=110

Figure A6. Effect of varying predator fineness ratio on relative energetic benefit.

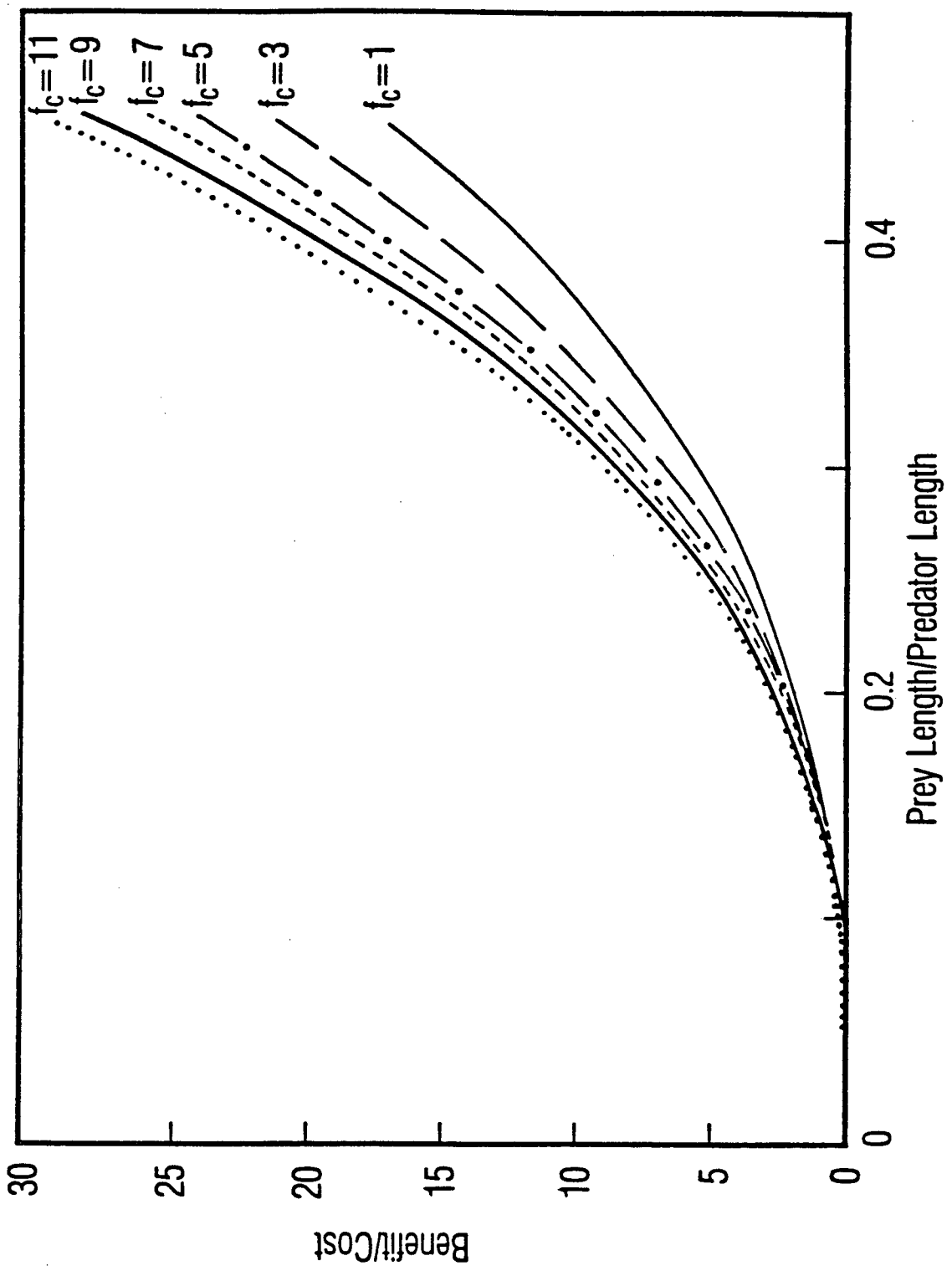
f_c=11
f_c=9
f_c=7
f_c=5
f_c=3
f_c=1
30
25
20
15
10
5
0
Benefit/Cost
0
0.2
0.4
Prey Length/Predator Length

Figure A7. Effect of varying predator reaction angle on relative energetic benefit.

Benefit/Cost
0
10
20
30
0.2
0.4
Prey Length/Predator Length
θ=1.4
θ=1.2
θ=1.0
θ=0.8
θ=0.6
θ=0.4

D. DISCUSSION

1. Assumptions

The model is based on a number of experimentally established relationships and some assumptions about the behaviour of fish during predator-prey interactions. The benefit/cost curves, therefore, should be analyzed with respect to trends and do not necessarily accurately reflect absolute energy gains and losses.

The model does not consider the effects of schooling, water turbidity, handling time, or failure to catch prey. Schooling has been shown to benefit predators by increasing the probability of catching prey (Major, 1973) and may reduce the energetic cost of steady swimming (Weihs, 1974). When prey school, the probability of capture for individual prey is reduced, but the likelihood that one of the school is caught increases (Major, 1973), again benefiting the predator. Water turbidity will tend to reduce the reaction distance of the predator, D_{pred}, which reduces energy expended during the approach, Q_{app}. This increases feeding efficiency, but also reduces the likelihood of an interaction occurring due to the limited visual field (Vinyard and O'Brien, 1976). Werner (1974) found that handling time increased with prey size, and that the optimal prey size, with respect to handling time, occurs at a prey size/predator mouth size of 0.59. Handling time at this optimum is 2.2 seconds. Although handling time would decrease feeding efficiency, it is assumed that the energy expended in handling prey for such short periods is small compared to that expended catching prey. If an interaction is unsuccessful and no prey is captured, there is a net loss of energy equal to that expended. In reference to the model, lost energy would have to be included in the efficiency of the next feeding interaction.

Therefore success rate, defined as the number of successful attempts divided by the total number of attempts, would be multiplied by energy input Q_i.

The velocity values are normalized to length; so some assumptions are made about the relationship between velocity and length for both predator and prey. Equations A9 and A21 describe the relationship of L_c to U_{app} and L_c to U_{cha}, respectively. The empirical relations are not from studies concerned with predation, making them questionable for use in this model. However, data from Morgan and Ritz (1983) lend support to their use; they measured the velocity of the Australian salmon *Arripis trutta* during its approach and chase of prey. In terms of predator length, U_{app} was found to scale as 7.5 $L_c^{0.49}$ and U_{cha} as 11.97 $L_c^{0.63}$. These values compare very favorably with those chosen, falling within 8 and 11% of the model values, respectively, for the range of predator lengths considered in the model.

It is also assumed that U_p scales with L_p as U_{cha} scales with L_c. Webb (1986) measured high- and low-level escape responses of three teleost species: fathead minnow *Pimephales promelas*, largemouth bass *Micropterus salmoides*, and bluegill *Lepomis macrochirus*. Escape velocities during predatory attacks ranged from approximately 20 - 80 cm s^{-1}, depending on the species and level of response. Substituting reported prey lengths into equation A21 gives values of U_p ranging from 37.6 - 43.4 cm s^{-1}. Although these values probably represent low-level responses, they do fall within the range reported by Webb.

2. Sensitivity

Additional simulations of the model were run to determine its sensitivity to variations in model parameter values. From equation A1, it is clear that changes in variables included in the expression for Q_i will have a directly proportional effect on energetic benefit only, and will not

affect the shape of any curve generated by the model. Alterations of variables in Q_e, however, will affect both the magnitude and shape of all curves (Figs A2-A7) because of the differential effects on Q_{app}, Q_{cha}, and Q_{str}. Variations in the magnitude of the ratio of energetic benefit to energetic cost are not addressed, since this magnitude is not expected to reflect accurate values, as discussed earlier.

The sensitivity of the model to changes in Q_e variables can be considered with reference to Figs A3 and A4. Regardless of which variable is altered, the general trend that benefit/cost increases exponentially with C, holds true. In fact, even extreme variations of Q_e parameters have little effect on the nature of the curves. For example, if any variable in the hydrodynamic drag equation (equation A8) were to be made infinitely small, the values of Q_{app} and Q_{cha} would approach zero and the model would approximate the curve Q_{str}, in Fig. A4. Conversely, if any variable in Q_{str} were to be made small, the model would then approximate the curve $Q_{app+cha}$. Therefore, with reference to Fig. A4, reasonable changes in Q_e variables will only slightly affect Q_{total}, the model in question.

With reference to Fig. A3, additional simulations of the model, run with variables halved or doubled, indicate that the relative contributions of the steady (Q_{app} and Q_{cha}) and unsteady (Q_{str}) components may be altered by as much as 15% of the total energy expended. For example, the curve Q_{app} would be as high as 50% of total energy expended at C = 0.4, while Q_{str} would decline to about 35%. It is not likely, however, that any variable is in error by a factor of two, and it is quite possible that an increase in the value of one variable would be offset by a decrease in another. Thus it is reasonable to accept the general trends of the model as true, within biological limits.

3. Optimal prey size

Figure A2 indicates that the optimal prey size is the largest available. A number of cases support this finding. For example, bluegill sunfish *Lepomis macrochirus* and striped surfperch *Embiotoca lateralis* select the largest prey available (O'Brien *et al.* 1976; Schmidt and Holbrook, 1984, respectively). As stated previously many studies indicate a predator preference for prey ranging up to 40% of their own length (Popova, 1967; Nursall, 1973; Gillen *et al.* 1981). There are piscivorous fish that consume prey near to, or greater than their own size. For example, gulpers (*Saccopharyngoidei*), wide-mouths (*Stomiatoidei*), and deep-sea angler-fishes (*Ceratioidei*) (Jordan, 1925; Norman, 1975). The great swallower *Chiasmodon niger* is an extreme example. Museum specimens were found to contain prey fish twice their own length and six to twelve times their own mass (Carte, 1866; Jordan, 1925, respectively).

It is important to re-emphasize that this model predicts optimal prey size on the basis of feeding efficiency alone. The upper limit of prey size is also influenced by other morphological and ecological factors. Werner and Hall (1974) showed that an optimal prey size can be determined in an optimal foraging model if handling time and search time are considered. Schmitt and Holbrook (1984) found that the number of prey taken increases with size and abruptly truncates at a size equal to the mouth gape of the predator. Werner (1974) determined that an optimal prey size occurs at prey to mouth size of 0.59, again due primarily to limitations set by handling time.

4. Consideration of different predatory strategies

The energy expended in each of the three stages of the interaction is presented in Fig. A3, as a percentage of Q_e. Argueably, predators pursuing relatively small prey can best minimize Q_e by reducing the energy expended in stage 3, whilst those pursuing relatively large prey should reduce the energy expended in stage 1. The special case of pike (*Esox*) can be used to illustrate this point. Pike pursue relatively large prey (Gillen *et al.* 1981) and Q_e may be limited by approaching at a very low velocity (see equation A9). Predators such as tuna, which feed on relatively small prey, limit Q_e by reducing or eliminating stage 3 and rely on "running down" prey.

When Q_{app} is the sole component of expended energy, the predator simply swims at its optimal cruising speed; no chases or strikes are involved. Argueably, this simulates the active filter feeding seen in fish such as the northern anchovy *Engraulis mordax* (Leong and O'Connell, 1969) and Pacific mackerel *Scomber japonicus* (O'Connell and Zweifel, 1972). Fig. A4 shows that for any value of *C*, filter feeding is the most energetically beneficial. In a practical sense, the prey must be so small that no chase or strike is necessary (i.e., small *C*). In this case it is very unlikely that a sole prey item would provide a net energetic benefit. Increasing the number of prey consumed per unit time would result in increasing energy gains with no additional cost. For this reason, filter-feeders forage on patches of food where many prey can be taken during each feeding event (Leong and O'Connell, 1969). Even this may not provide enough energy to meet daily requirements. Analysis of the energy budgets of three active filter feeding species, wavyback tuna *Euthynnus affina*, Atlantic menhaden *Brevoortia tyrannus*, and anchovies *Engraulis mordax*, indicate that each of these species must, at times, resort to other feeding strategies, such as particulate feeding and

gulping, to meet daily needs (Walters, 1966, Durbin *et al.* 1981, and Pandian and Vivekanandan, 1985, respectively). In fact, mackerel have been observed consuming fish up to 30% of their own mass (Hatanaka and Takahashi, 1960).

Skipjack tuna *Katsuwonus pelamis* pursue small prey by employing an approach and chase strategy ($Q_{app}+Q_{ch}$) (Kerr, 1982). Again, the energetic returns are greater than for the three-stage model, but are small for prey of such relative proportions ($C \approx 0.1$). However, prey of skipjack tuna travel in large schools, so it is possible to capture many prey on each attack run (Kitchell, 1983). In addition, tuna inhabit open ocean waters and must feed opportunistically (Stevens and Neill, 1978).

Ambush predators (e.g., *Esox*), expend some energy during the "stalk". This is small, however, relative to the strike energy, and the energetics reflect an accelerative strike (stage 3). Figure A4 shows that this strategy is more energetically beneficial than the "$Q_{app}+Q_{cha}$" strategy for $C > 0.4$. In other words, for $C > 0.4$ the more energetically beneficial strategy is to sit and wait. This seems to be what *Esox* does. Dianna (1980) observed that *Esox* in Lac Ste. Anne, Alberta were idle about 80% of the time.

5. Effect of variations in predator size, fineness ratio, reaction angle, and prey experience

Figure A5 shows that as predator size decreases, the relative energetic benefit increases exponentially. This has two biologically important implications. Firstly, it makes the acquisition of proportionally larger prey more energetically beneficial for smaller predators. Popova (1967) showed that for pike *Esox lucius*, perch *Perca fluviatilis*, Chinese perch *Perca chau-tsi*, and zander *Lucioperca lucioperca*, C ranges from 0.4 to 0.5, and 0.2 to 0.25, for juvenile and adult fish, respectively. He argues that

this may be because both small and large predators were feeding on the same prey population. Thus the prey available to smaller predators would necessarily be proportionally larger. However, Gillen *et al.* (1981) determined experimentally that the hybrid tiger muskellunge *Esox* sp. selected relatively larger prey (C_{max} = 0.37 to 0.43) when young than when mature (C_{max} = 0.25 to 0.3).

Secondly, the greater energetic benefit afforded to smaller predators allows faster growth. Ware (1982) defines the scope for growth as dependent on the total reserve of surplus energy, implying that the relatively higher returns for smaller predators increase surplus energy and enhance growth.

Many pelagic fish are characterized by fineness ratios of about five, (e.g., Blake, 1983*b*). However, many piscivorous predators, such as the pike (*Esocidae*), barracuda (*Sphyraenoidei*), gar-fish (*Belonidae*), and gar pike (*Lepisosteus*) have much higher fineness ratios (about ten). This adaptation results in an energetic penalty during steady swimming. However, Fig. A6 shows that energetic benefit in predator-prey interactions increases with fineness ratio, but with diminishing returns. For small C, fineness ratio is less important.

High fineness ratio reduces energetic cost because it reduces the angle that the predator's body depth subtends on the retina of their prey. This means that the prey react to an approach later than they would if attacked by a predator with a higher fineness ratio. This increases the approach distance and decreases the chase distance. Therefore, during the interaction, the predator spends less time and energy on the relatively expensive chase. The energy, Q_{app}, can also be reduced by a slower approach velocity as shown in equations A8 and A9. *Esox* is known to slowly stalk its prey (Webb, 1978; Webb and Skadsen, 1980). By so doing, it may be that *Esox* can close to within strike distance and thereby avoid the chase altogether,

since the distance at which the prey reacts is proportional to the depth of section of the predator, as well as its speed (Dill, 1973).

Figure A7 shows that as the predator reaction angle, θ, decreases, the energetic benefit of the interaction also decreases due to a corresponding increase in D_{pred}. The reduction of the threshold angle is related to predator experience. Ware (1971) found that D_{app} increases as predators become more experienced. Equation A15 shows that for a predator and prey of given length, a decrease in θ accompanies an increase in D_{pred}. Energetically, this seems to be counterproductive. However, it may be that predators compete with one another for the same prey and in maximizing D_{pred} by reacting at smaller values of θ, assuming the energetic return for a given prey is positive, the predator that reacts to the prey first has an advantage.

Figure A7 also shows that the reaction angle becomes more energetically significant as C increases. For smaller, less experienced predators, θ is high and the energetic returns are greater. This supports the concept mentioned earlier, that smaller predators have relatively higher returns.

Dill (1974*b*) showed that the reactive distance of the prey (D_{prey}) is increased by experience. This means that the energy expended during the chase will increase, and that expended during the approach will decrease. However, prey experience has little effect on the energetics of the interaction (not shown). Energetic benefit is only slightly reduced for large C.

Prey experience is more important to the prey because it affords greater lead time and distance in stage 2 (chase). Dill (1974*b*) showed that experience significantly increases prey survival. This model assumes that the predator is always successful, so it does not reflect differences in prey survivability.

6. Summary

The present study indicates that an approach incorporating biomechanics and feeding behaviour can be employed in a quantitative assessment of the feeding efficiency of a simple predator-prey interaction. A more comprehensive piscivorous foraging model would also consider low-performance behaviour, such as search and handling time. The inclusion of these variables in the present model, however, would increase its uncertainty and complexity, making a quantitative analysis impossible.

The general trend is for maximum feeding efficiency when prey size is large. This effect is pronounced for small predators, providing more surplus energy for growth. Predators of high fineness ratio also maximize feeding efficiency, whereas those with small retinal reaction angles may increase feeding opportunities by detecting prey at greater distances.

The model can be used to examine independently the contributions to energy output of both steady and unsteady swimming behaviour. Simulations of various predatory strategies can be generated by manipulating these components, allowing an investigation and discussion of optimal predatory behaviour.

The model could be experimentally tested by observing piscivorous predation in the laboratory. For example, a range of prey sizes could be presented to determine selectivity. Predator length and fineness ratio could be varied and growth rates measured. Reaction distances of both predator and prey and the velocities involved in each stage could be measured from film records and the reaction angle of the predator could be determined. Such experiments would clearly lead to greater insight into piscivorous predator-prey interactions.

REFERENCES

ALLEN, G. and ARON, W. (1957). Food of the salmonid fishes of the western North Pacific Ocean. *U.S. Fish Wildl. Serv. Spec. Sci. Rep. Fish.* **237,** 1-11.

ALVERSON, F.G. (1963). The food of the yellowfin and skipjack tuna in the eastern tropical Pacific Ocean. *Inter-American Tuna Commission Bull.* **7,** 295-396.

BINDER, R.C. (1973). *Fluid Mechanics.* Englewood Cliffs: Prentice Hall.

BLAKE, R.W. (1983*a*). *Fish Locomotion.* Cambridge: Cambridge University Press.

BLAKE, R.W. (1983*b*). Functional design and burst-and-coast swimming in fishes. *Can. J. Zool.* **61,** 2491-2494.

BRETT, J.R. and GLASS, N.R. (1973). Metabolic rates and critical swimming speeds of sockeye salmon *Onchorhynchus nerka* in relation to size and temperature. *J. Fish. Res. Bd. Can.* **30,** 379-387.

BROOKS, J.L. and DODSON, S.I. (1965). Predation, body size, and composition of the plankton. *Science* **150,** 28-35.-35.

CARTE, A. (1866). Notes on the genus *Chiasmodan. Proc. Zool. Soc. Lond.,* 35-39.

CHARNOV, E.L. (1976). Optimal foraging, the marginal value theorem. *Theor. Popul. Biol.* **9,** 129-136.

CHOPRA, M.G. and KAMBE, T. (1977). Hydromechanics of lunate-tail swimming propulsion, Part 2. *J. Fluid Mech.* **79,** 49-60.

CUMMINS, K.W. and WUYCHECK, J.C. (1973). Caloric equivalents for investigations in ecological energetics. *Mitt. Int. Ver. Theor. Angew. Limnol.* No. **18.**

DIANNA, J.S. (1980). Diel activity pattern and swimming speeds of northern pike *Esox lucius*, in Lac St. Anne, Alberta. *Can. J. Aquat. Sci.* **37,** 1454-1458.

DILL, L.M. (1973). An avoidance learning submodel for a general predation model. *Oecologia (Berl.)* **13,** 291-312.

DILL, L.M. (1974*a*). The escape response of the zebra danio *Brachydanio rerio* I. the stimulus for escape. *Anim. Behav.* **22,** 711-722.

DILL, L.M. (1974*b*). The escape response of the zebra danio *Brachydanio rerio* II. the effect of experience. *Anim. Behav.* **22,** 723-730.

DUNBRACK, R.L. and DILL, L.M. (1983). A model of size dependent surface feeding in a stream dwelling salmonid. *Env. Biol. Fish.* **8,** 203-216.

DURBIN, A.D., DURBIN, E.G., VERITY, P.G., and SINAYDA, T.J. (1981). Voluntary swimming speeds and respiration rates of a filter feeding planktivore, the Atlantic menhaden *Brevoortia tyrannus*. *Fish. Bull.* **78,** 877-886.

EMLEN, J.M. (1973). Ecology: an evolutionary approach. Reading: Addison-Wesley.

GILLEN, A.L., STEIN, R.A. and CARLINE, R.F. (1981). Predation by pellet-reared tiger muskellunge on minnows and bluegills in experimental systems. *Trans. Amer. Fish. Soc.* **110,** 197-209.

HATANAKA, M.A. and TAKAHASHI, M. (1960). Studies on the amounts of the anchovy consumed by the mackerel. *Tohoku J. Agric. Res.* **11,** 83-100.

HILL, A.V. (1950). The dimensions of animals and their muscular dynamics. *Sci. Prog.* **38,** 209-230.

HOLLING, C.S. (1965). The functional response of predators to prey density and its role in mimicry and population regulation. *Mem. Entomol. Soc. Can.* **45,** 1-60.

HOLLING, C.S. (1968). The tactics of a predator. In *Insect Abundance* (ed. T.R.E. Southward), Oxford: Blackwell Scientific Publications, pp. 47-58.

ISAACS, J.D. and WICK, G.L. (1973). Optimized tactics for open-water marine predators. In *Marine Biological Association of India Special Publication dedicated to Dr. N.K. Panikar.* Cochin, India: S.T. Reddiar and Sons, pp. 192-199.

IVLEV, V.S. (1961). *Experimental Ecology of the Feeding of Fishes.* New Haven: Yale University Press.

JORDAN, D.S. (1925). *Fishes.* New York: D. Appleton and Co.

KERR, S.J. (1982). Estimating the energy budgets for actively predatory fishes. *Can. J. Fish. Aquat. Sci.* **39,** 371-379.

KITCHELL, J.F. (1983). Energetics. In *Fish Biomechanics* (eds. P.W. Webb and D. Weihs), New York: Praeger, pp. 312-338.

KREBS, J.R., STEPHENS, D.W., and SUTHERLAND, W.J. (1983). Perspectives in optimal foraging. In *Perspectives in Ornithology: Essays Presented for the Centennial of the American Ornithological Union* (eds. A.H. Brush and G.A. Clark Jr.), New York: Cambridge University Press, pp. 165-216.

LEONG, R.J.H. and O'CONNELL, C.P. (1969). A laboratory study of particulate and filter feeding of the Northern anchovy *Engraulis mordax. J. Fish. Res. Bd. Can.* **26,** 557-582.

MACARTHUR, R.H. (1972). *Geographical ecology: patterns in the distribution of species.* Hagerstown: Harper and Row.

MACARTHUR, R.H. and PIANKA, E.R. (1966). On the optimal use of a patchy environment. *Am. Nat.* **100,** 603-609.

MAGNUSON, J.J. (1978). Locomotion by scombrid fishes: hydromechanics, morphology, and behaviour. In *Fish Physiology VII Locomotion* (eds. W.S. Hoar and D.J. Randall),New York: Academic Press, pp. 240-315.

MAJOR, P.W. (1973). Predator-prey interaction in two schooling fishes, *Caranx ignobilis* and *Stolephorus purpureus. Anim. Behav.* **26,** 760-777.

MARCHAJ, C.A. (1979). Aero-hydrodynamics of sailing. New York: Dodd, Mead and Company.

McCutchen, C.W. (1977). Froude efficiency of a small fish, measured by wake visualization. In *Scale Effects in Animal Locomotion* (ed. T.J. Pedley), London: Academic Press, pp. 339-353.

Morgan, W.L. and Ritz, D.A. (1983). Sensory cues and mechanisms involved in the capture of euphausiids by the Australian salmon *Arripis trutta*. *J. Fish. Biol.* **23,** 489-493.

Norman, J.R. (1975). *A History of Fishes*, 3rd edition. London: Ernest Benn Ltd.

Nursall, J.R. (1973). Some behavioural interactions of spottail shiners *Notropis hudsonius*, yellow perch *Perca flavescens*, and northern pike *Esox lucius*. *J. Fish. Res. Bd. Can.* **30,** 1161-1178.

O'Brien, W.J., Slade, N.A. and Vinyard, G.L. (1976). Apparent size as the determinant of prey selection by bluegill sunfish *Lepomis macrochirus*. *Ecology*. **57,** 1304-1310.

O'Connell, C.P. and Zweifel, J.R. (1972). A laboratory study of particulate and filter feeding of the Pacific mackerel *Scomber japonicus*. *Fish. Bull.* **70,** 973-981.

Pandian, T.J. and Vivekanandan, E. (1985). Energetics of feeding and digestion. In *Fish Energetics: New Perspectives* (eds. P. Tytler and T. Calow), London: Croom Helm, pp. 99-124.

Pennycuick, C. (1975). *Handy Matrices*. London: Edward Arnold.

Pianka, E.R. (1974). *Evolutionary Ecology*. Hagerstown: Harper and Row.

Popova, O.A. (1967). The predator-prey relationship among fish. In *Biological Basis of Freshwater Fish Production* (ed. S.D. Gerking), Oxford: Blackwell Scientific Publications, pp. 359-376.

Pulliam, H.R. (1974). On the theory of optimal diets. *Am. Nat.* **108,** 59-74.

Schmitt, R.J. and Holbrook, S.J. (1984). Gape-limitation, foraging tactics and prey selectivity of two microcarnivorous species of fish. *Oecologia* **63,** 6-12.

SCHOENER, T.W. (1971). Theory of feeding strategies. *Ann. Rev. Ecol. Syst.* **2,** 369-404.

STEPHENS, D.W. and KREBS, J.R. (1986). *Foraging Theory.* Princeton: Princeton University Press.

STEVENS, E.D. and NEILL, W.E. (1978). Body temperature relations of tunas, especially skipjacks. In *Fish Physiology* Vol. 7 (eds. W. Hoar and D.J. Randall), New York: Academic Press, pp. 316-360.

VINYARD, G.L and O'BRIEN, W.J. (1976). Effects of light and turbidity on the reactive distance of bluegill *Lepomis macrochirus. J. Fish. Res. Board Can.* **33,** 2845-2849.

WALTERS, V. (1966). On the dynamics of filter feeding by the wavyback tuna *Euthynnus affinis. Bull. Mar. Sci.* **16,** 209-221.

WARE, D.M. (1971). Predation by rainbow trout *Salmo gairdneri*: the effect of experience *J. Fish. Res. Bd. Can.* **28,** 1847-1852.

WARE, D.M. (1973). Risk of epibenthic prey to predation by rainbow trout *Salmo gairdneri. J. Fish. Res. Bd. Can.* **30,** 787-797.

WARE, D.M. (1975). Growth, metabolism, and optimal swimming speed of a pelagic fish. *J. Fish. Res. Bd. Can.* **32,** 33-41.

WARE, D.M. (1982). Power and evolutionary fitness of teleosts. *Can. J. Fish. Aquat. Sci.* **39,** 3-13.

WEBB, P.W. (1977). Effects of size on performance and energetics of fish. In *Scale Effects in Animal Locomotion* (ed. T.J. Pedley), London: Academic Press, pp. 315-331.

WEBB, P.W. (1978). Fast-start performance and body form of seven species of teleost fish *J. exp. Biol.* **74,** 211-226.

WEBB, P.W. (1982). Fast-start resistance of trout. *J. exp. Biol.* **96,** 93-106.

WEBB, P.W. (1986). Effect of body form and response threshold on the vulnerability of four species of teleost prey attacked by largemouth bass *Micropterus salmoides. Can. J. Fish. Aquat. Sci.* **43,** 763-771.

WEBB, P.W. and SKADSEN, J.M. (1980). Strike tactics of *Esox*. *Can. J. Zool.* **58,** 1462-1469.

WEIHS, D. (1974). Some hydromechanical aspects of fish schooling. In *Swimming and flying in nature* Vol.2 (eds. T.Y. Wu, C.J. Brokaw, and C. Brennen), New York: Praeger, pp. 203-218.

WEIHS, D. and WEBB, P.W. (1983). Optimization of Locomotion. in predator-prey interactions. In *Fish Biomechanics* (eds. P.W. Webb and D. Weihs), New York: Praeger, pp. 339-371.

WERNER, E.E. (1974). The fish size, prey size, handling time relation in several sunfishes and some implications. *J. Fish. Res. Bd. Can.* **31,** 1531-1536.

WERNER, E.E. and HALL, D.J. (1974) Optimal foraging and the size selection of prey by the bluegill sunfish *Lepomis macrochirus*. *Ecology* **55,** 1042-1052.

YATES, G.T. (1983). Hydromechanics of body and caudal fin production. In *Fish Biomechanics* (eds. P.W. Webb and D. Weihs), New York: Praeger, pp. 177-213.